Departamento de Engenharia Mecânica

Load carrying capacity of polymer-metal hybrid gears

Mário Ricardo Costa Moutinho
2020

Mário Ricardo Costa Moutinho

Load carrying capacity of polymer-metal hybrid gears

A Dissertation submitted to
Faculdade de Engenharia da Universidade do Porto
For the degree of

Mestre em Engenharia Mecânica

Supervisor: Doctor Carlos M. C. G. Fernandes
Co-Supervisor: Professor Jorge H. O. Seabra

Departamento de Engenharia Mecânica
Faculdade de Engenharia
Universidade do Porto

Abstract

In this work a study of polymer gears and hybrid polymer gears with metallic inserts is conducted.

The growing use of polymer gears and the difficulties presented when in operation justify the several different ways that have been attempted to improve their performance. Polymer gears with metallic insert is one of hypothesis to improve polymer gears and so there is a need to further develop and study this type of gear.

In order to do this, it is validated and used a Finite element mechanical and thermo-mechanical model. It is presented methods for evaluating load carrying capacity that will then serve to compare between solutions of hybrid gears and between the hybrid gear and the standard polymer gear. Along with stress, the respective temperatures are also quantified.

Resumo

Neste trabalho é realizado um estudo de engrenagens poliméricas e engrenagens poliméricas híbridas com insertos metálicos.

O crescente uso de engrenagens poliméricas e as dificuldades que apresentam em operação justificam as várias formas diferentes que foram tentadas de melhorar a sua performance. As engrenagens poliméricas com inserto metálico são uma dessas hipóteses de melhorar as engrenagens poliméricas standard e por isso existe uma necessidade de desenvolver mais e estudar este tipo de engrenagem.

Por forma a se conseguir realizar este estudo, é validado e usado um modelo mecânico e termo-mecânico de Elementos Finitos. São apresentados métodos para avaliar a capacidade de carga das engrenagens que irão servir para comparar entre soluções de engrenagens híbridas e entre a engrenagem híbrida e a engrenagem polímerica standard. A par da análise de tensões, as respectivas temperaturas também são quantificadas.

Keywords

Polymer gears
Hybrid gears
Load carrying capacity
Stress
Temperature

Acknowledgements

For the words of advisement and encouragement, but also for the shared attention to detail, perfectionism and general wisdom, I would like to thank my supervisor Carlos Fernandes for helping me throughout the making of this present work. To the professor Jorge Seabra I thank for teaching me Contact Mechanics and more about gears.

To the faculty Faculdade de Engenharia Universidade Porto I also have to thank for being a second home to me, and for providing the opportunity to meet all the professors with whom I learned so much, but also for the opportunity to meet all the good friends that accompanied me through these times and with whom I also had great moments and learnt a lot from.

I also have to thank all my extended family and parents for all the love and support, and especially my mother for always being there for me and for making me grow as person everyday.

In loving memory of
my grandfather Manuel

Contents

List of Figures

List of Tables

List of Symbols

α	Gear pressure angle	$[^\circ]$
$\bar{q}_{VZP}$	Meshing gears heat flux per unit area averaged over one revolution	$[W/m^2]$
γ_p	Boundary rotation of the hub pinion in Step 3	$[rad]$
γ_t	Rotation twist value for the delay of the wheel in Step 3	$[rad]$
γ_w	Boundary rotation of the hub wheel in Step 3	$[rad]$
γ_{BL}	Boundary rotation for the approach of the pinion to the wheel	$[rad]$
μ	Coefficient of tooth friction	$[-]$
ν	Poisson's ratio	$[cST]$
ν_{air}	Kinematic viscosity of the air	$[cSt]$
ω	Rotational speed	$[rad/s]$
ρ	Density	$[kg/m^3]$
σ_1	Maximum Principal Stress	$[Pa]$
σ_3	Minimum Principal Stress	$[Pa]$
σ_{FlimN}	Fatigue strength under pulsating stress	$[Pa]$
$\tau_{shear\ max}$	Maximum shear stress	$[Pa]$
$\tau_{shear\ oct}$	Normal octahedral shear stress	$[Pa]$
θ	Boundary rotation of the hub	$[rad]$
a	Hertzian contact semi-width	$[m]$
B	Boundary torque	$[N \cdot m]$
b	Gear face width	$[m]$
c_p	Heat capacity	$[J/kg \cdot K]$
D	Gear's diameter	$[m]$
d_i	Pitch circle diameter	$[m]$
d_i	Pitch circle diameter	$[m]$
E	Elastic Young's Modulus	$[Pa]$
g_r	Gear ratio	$[-]$
h_n	Heat transfer coefficient	$[W/m^2 \cdot K$
k	Thermal Conductivity	$[W\ /m \cdot K]$

m	Module	$[m]$
p_0	Hertz contact pressure	$[Pa]$
Pr	Prandtl number	$[-]$
q_{VZP}	Instantaneous meshing gears heat flux per unit area	$[W/m^2]$
Re	Reynolds number	$[-]$
T	Absolute temperature	$[K]$
T	Boundary torque of the hub	$[N \cdot m]$
T_B	Absolute bulk temperature	$[K]$
T_{air}	Temperature of the air	$[^\circ C]$
T_{air}	Temperature of the air	$[^\circ C]$
T_{root}	Temperature at tooth root	$[Pa]$
z_i	Number of teeth in pinion/wheel	$[-]$
β_{ki}	Heat thermal distribution partition between pinion and wheel	$[-]$

Chapter 1

Introduction

Polymer gears are known for having low density, good tribological performance and good resistance to corrosion. This makes them ideal candidates for some specific applications such as food industry, precision instruments, office appliances, mechatronic devices and household facilities that don't require high mechanical resistance but instead require chemical inertness and materials that can be compact and inexpensive to produce.

In spite of the growing demand for this type of gears, there are difficulties in designing them for applications since they require a study of temperature in conjugation with a mechanical analysis. This is due to the fact that its mechanical properties are essentially temperature dependent but also dependent on other factors as humidity and deformation cycles.

Temperature is a determinant factor and even more so because polymer gears have low temperature resistance and have low thermal conductivity which makes them highly temperature sensitive and some specific modes of failure related to this dependence can occur.

Because of this several attempts to improve the performance of polymer gears have been tested and simulated including a hybrid gear concept of a polymer gear matrix with metallic inserts. This hybrid gear showed in these studies improvement by managing to lower bulk temperature of the gear. The metallic inserts were then effective on helping the polymer gear evacuate heat thanks to a higher thermal conductivity of metals.

As metals have higher mechanical resistance and better mechanical properties compared to the polymer gears, it is also predicted an increase of load carrying capacity of the hybrid gears. It is therefore necessary a study of this hybrid gear using a Finite Element Thermo-Mechanical analysis that considers temperature dependent mechanical properties to verify this prediction.

In this manner, the purpose of this thesis is to study and understand the load carrying capacity of polymer gears and polymer gears with metallic inserts, using for this a Finite Element Method. In the end, it is intend to show a decrease in temperature and increase in load carrying capacity using the hybrid gears.

1.1 Thesis Outline

Chapter 2, entitled **Literature Review of Polymer Gear**, summarizes polymer gear's materials, advantages and disadvantages, modes of failure, attempts to improve polymer gears, the standards that verse this gears and FEM models used to study them.

Chapter 3, entitled **Finite Element Models for Gears**, defines the Finite Element methods necessary to the analysis of hybrid gears and describes the implementation that is done for these models.

Chapter 4, entitled **Model Validation**, validates the models described in the previous Chapter comparing the results obtained with the standards and literature. It also introduces concepts for evaluating load carrying capacity of gears.

Chapter 5, entitled **FEM of the Hybrid Gear Pair**, studies polymer gears with metallic inserts, using the concepts for evaluating load carrying capacity and the models validated in the previous Chapter. It describes the influence of geometric variables and material of inserts for varying applied loads. A study of equivalent stress and strain on the interface, an optimization of the positioning of the insert and a proposed solution are also included in this Chapter.

Chapter 2

Literature Review of Polymer Gears

2.1 Introduction

In this chapter it is reviewed for polymer gears which materials are commonly used and what are the advantages and disadvantages of using this type of material in a gear set.

Following the disadvantages, it is going to be studied the types of failures associated with this type of gear and what has been done to improve upon its use.

Finally it is going to be discussed the guidelines that approach polymer gears and the Finite Element Methods that have been employed to study this type of gear.

2.2 Polymer Gear's Materials

The most common polymer gear materials are POM (polyacetals/polyoxymethylene) and PA (polyamide/nylon), but other plastics are used such as: PEEK (polyetherether ketone), PP (polypropylene), PE-HD (high-density polyethylene), PUR (polyurethane), PC (polycarbonate), PET (polyetherether ketone), PBT (polybutylene terephthalate) [1; 2].

The material POM is a thermoplastic that is highly crystalline, being used in essentially two different forms, either copolymer or homopolymer. The homopolymer has better mechanical properties than the copolymer in stiffness, strength and coefficient of friction. On the other hand the copolymer has better dimensional tolerances than the homopolymer, shrinking less on molding.

Moreover, this thermoplastic can cost up to 3.00€/kg, with a density of around 1410 kg/m^3 and being more expensive for the homopolymer. Other advantages of POM are good abrasion resistance, easy to process and to fabricate, low coefficient of friction, good surface hardness and good fatigue resistance.

The material PA, is a thermoplastic that has two main sub groups, PA6 and PA66. This group of materials PA, are known for having low coefficient of friction, good slip and wear properties, good fatigue resistance and for being more receptive to improvements than POM when additives are added to the polymer.

However, PA materials have higher water absorption being more susceptible to dimensional instability and properties changing with relative humidity present, leading to a decrease in the tensile strength and modulus, but also to an increase in toughness and flexibility.

As for the subgroups of PA, PA66 has fiber glass reinforcements in the PA matrix, having slightly better mechanical properties, abrasion resistance and lower water absorption than PA6 but also worse impact strength an flex-fatigue life. In contrast, PA6 has lower processing temperature and mold shrinkage than PA66. These two subgroups can cost up to 4.70€/kg, with a density of around 1080 kg/m^3, which compared to POM translates to about 20% more expensive, also corroborated by Figure 2.1.

Compared to PA, POM is more creep resistant, has greater high stress heat distortion temperature (temperature at which a the polymers deforms under load), it is more resistant to corrosion, has higher processing temperature and has lower moisture absorption. In spite of this, POM has worse lower temperature toughness than PA, Figure 2.1.

2.3 Advantages

Polymer gears have been finding more and more applications in several areas, standing a growing presence and even replacing metallic gears in some cases especially for low to medium power transmissions [3]. In this section it is going to be detailed more of the advantages of polymer gears.

Because polymers have lower density, polymer gears have in terms of the dynamic response lower inertia and have good noise damping properties. [4]

As already being said, polymer gears have low coefficients of friction, but they also have in general good tribological properties including wear resistance. This characteristic is the reason for the dry running ability of these type of gears which is much explored. [3; 5]

The resistance to solvents and general chemical inertness is also known for polymer gears. This also means that they are better resistant to corrosion which makes them good candidates for usage in food processing or other chemically more demanding environments. The ability to dry run in these types of usages also favour its usage, since special oils or sealants aren't needed. [3; 5]

Finally, polymer gears are inexpensive as a raw material, Figure 2.1, but at the same time are very easy to process, melting at lower temperature, and easy and cheap to manufacture being able to adjust to every manufacturing process available. It is possible for example to 3D print, machine, injection mold and laser based additive manufacturing.[3; 6]

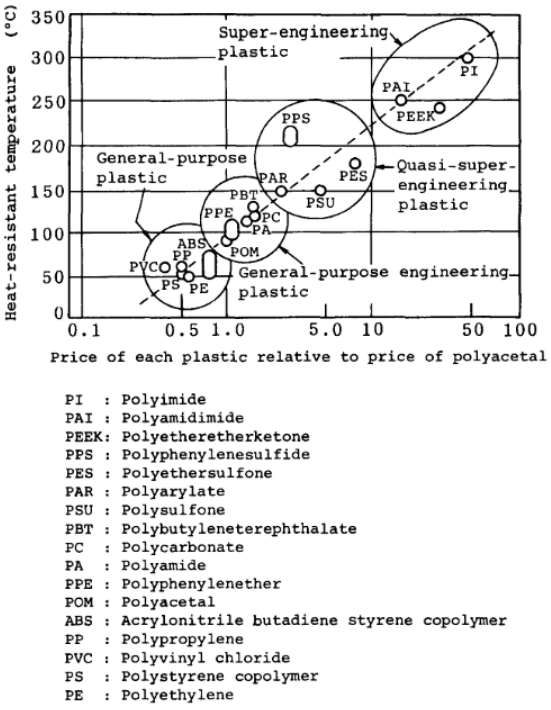

Figure 2.1: Polymer gear prices (Yen/kg) compared to the polyacetal (POM) and heat resistant temperature (1995) [6]

- Good noise damping properties [4]
- Good tribological properties, are able to run dry [3; 5]

- Chemical inertness, good resistance to corrosion [3; 5]
- Low density and low inertia, leading to better dynamic response [3; 4]
- Relative low cost, easy and fast to manufacture [3]

2.4 Disadvantages

However, the mechanical and some of the thermal properties of polymer gears are generally lower compared to those of metallic gears and its mechanical properties are mostly temperature dependent. In this section it is going to be detailed more of the disadvantages of polymer gears.

Polymer gears have high water absorption and are sensitive to the humidity present, especially PA. This can lead to dimensional instability and changes in its properties, lowering the modulus and tensile strength. [3]

Temperature is also a factor, since polymer gear tend to have low conductibility leading to an increase in the temperature of the gear, lower modulus, tensile strength and higher linear thermal expansion. Therefore, the resistance to heat is poor [5]. This higher thermal expansion could make the gears increase in size, closing the gap of the backlash and if this increase in size continues it could even result in the gears stop running and jamming [7].

The mechanical response also varies, existing an hysteresis on strain for a stress cycle but it also depends on the loading time application [6; 8].

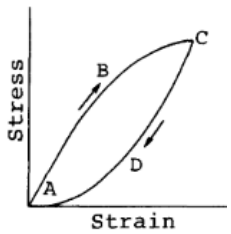

Figure 2.2: Hysteresis loop of polymers [6]

- High water absorption [3]
- Low heat resistance [5]
- Poor thermal conductibility
- Dependence of mechanical response, stress and deformation, on loading time [8]
- Lower mechanical resistance

2.5 Modes of failure

The thermal properties of polymer gears and the temperature on these gears when in operation are very important for the design. Usually it is due to temperature that some specific modes of failure, typical on polymer gears, occur. In this section it is going to be detailed more this modes of failure.

The failure on polymer gears are mostly due to a decrease of the tooth thickness because of wear, melting because of thermal overload or tooth root and pitch fracture because of mechanical overload [5]. The standard VDI 2736, also points to melting, fracture from pitting, tooth flank fracture, pitting and deformation as typical modes of failure [1]. In the following pictures the main modes of failure are presented, Figure 2.3.

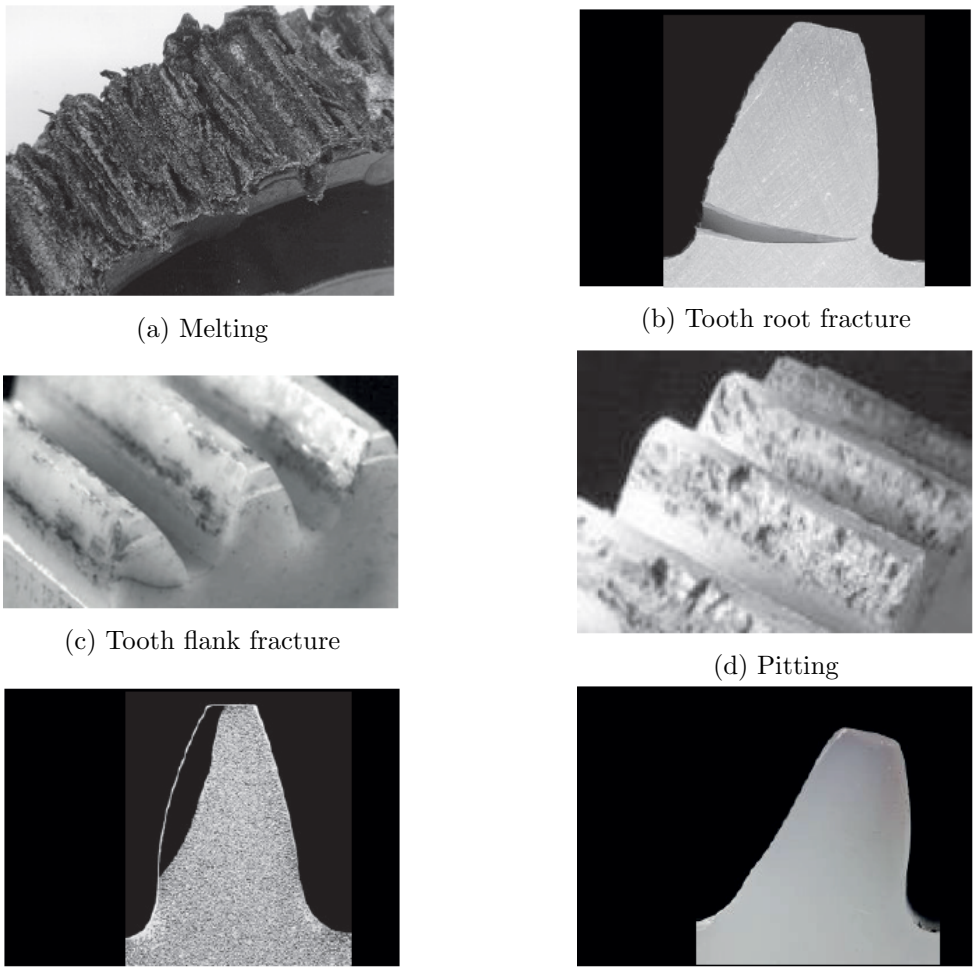

(a) Melting

(b) Tooth root fracture

(c) Tooth flank fracture

(d) Pitting

(e) Tooth Wear

(f) Plastic Deformation

Figure 2.3: Modes of failure in polymer gears [1]

The authors Pogačnik and Tavčar [7] further describe the failure modes in polymer gears, stating that after surpassing an initial run and thermal and mechanical overload don't occur, polymer gears fail due to fatigue. Furthermore, the wear damage mechanism is said to only occur in some gears pairs for some specific combinations of materials for the driving and driven gears where the coefficient of friction and running conditions play a role.

Since polymer gears present lower thermal properties, a higher temperature occurs during operation. Consequently, the mechanical properties of the gears decreases, due to temperature dependence, and even melting could occur. Therefore, polymer gears are very temperature sensitive, and this sensitivity is the cause of most of the failures mentioned. In order to mitigate and control this effect, different methods that can decrease the surface temperatures were attempted, being successful in improving the performance of the polymer gears [5].

2.6 Methods for improving polymer gears' performance

2.6.1 Different material combination in the gear pair

The authors Pogačnik and Tavčar [7] studied the tooth root stress at failure and bulk temperature at different loads for the following material combination: PA6/PA6, POM/PA6, POM/POM, PA6/PA6-30, POM/PA6-30, PA6-30/PA6-30.

It was concluded that (POM/PA6) and (POM/PA6-30) were the most suitable to reach a higher load level followed by the (PA6-30/PA6-30) pair. This suggests that using different material combination for the gear can improve its performance, compared to using only one material for the driven/driving pair (for example (POM/POM)).

In order to prevent sudden temperature increases, that could result in the jamming of the gears, it was recommended that the (PA6-30/PA6-30) gear pair should be avoided.

This jamming was described has a restriction of movement of the gears, since an increase of temperature causes the increase of the thermal expansion which makes the gears increase in size, lose the backlash and with some more increase in temperature stop running and jamming.

The guideline [1] also describes the improvement of behaviour in dry running conditions when pairing different polymers in a gear. For this the guideline presents the results of experimental work where the wear and friction coefficients were tested for different material pairs, Figure 2.4.

The results of this experimental work showed lower wear and friction coefficients for the gear pairs using different materials (PBT/PA66, POM/PBT, POM/PA66, PBT/POM and PA66/POM) compared to the gear pairs using the same type of material (PA66/PA66 and POM/POM). This corroborates the conclusions withdrawn with the results of Pogačnik and Tavčar [7].

With this experimental results of Figure 2.4, the guideline [1] also indicates that when the higher friction material is used in the pinion, the wear and friction coefficients are lower compared to when the higher friction material is used in the wheel (PBT/POM has less wear coefficient than POM/PBT; and PA66/POM has less wear and friction coefficients than POM/PA66).

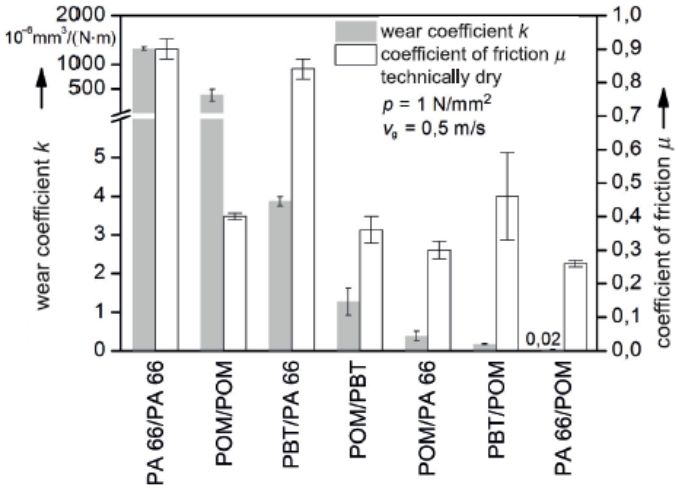

Figure 2.4: Wear and friction coefficients for different pairing materials from pin-and-disk tests [1]

2.6.2 Composite gears, polymer gears with fillers and reinforcing materials

Also known as internal lubrication, they intend to improve the tribological properties of the polymers such as friction, since higher friction leads to higher temperature and possible failure of the gear set. On the other hand the improvement on tribological properties can result in lower mechanical properties, withstanding lower load. The most common fillers and reinforcing materials are glass, carbon and aramid fibres, PTFE, PE, graphite, boron nitride, silicon oil and mineral fillers [1].

The authors Wright and Kukureka [9] tested a PA-66 with varying short glass, short carbon and long glass fibres coupled with or without PTFE. It was concluded that the reinforcement and filler can change the wear rate, especially the carbon fibre reinforcement with PTFE filler with lower wear ratio.

As already been said, PA66 and PA in general are more susceptible to improvements with additives in its matrix compared to POM.

2.6.3 Coatings

The authors Nozawa et al. [10] proposed to test a steel gear with a PA 66 sheet coating of 0.2 mm thickness adhered onto its teeth. It was studied the noise levels of operation and measured torque output for a set of loading conditions and for a thousand cycles each set. The results showed that noise level is reduced and a smoother torque output and smoother contact pairing is achieved for the steel gear with PA66 sheet coating compared to the steel gear without sheet coating. However, the adhesion of the polymer to the steel turned out to be weak and so only a few cycles were conducted.

The study of the influence of coatings on tooth tip deflection was performed in [11]. In this paper the gear is made of 42CrMo4 steel with a polymer coating, and the pinion is either made of POM or PA, for dry running conditions. The coatings used had four different thicknesses and the materials for the polymer coating were: PTFE, aluminium, boron nitride and molybdenum disulphide. The higher the thickness of the coating and the higher the Young Modulus of the coating material, the lower the tooth tip deformation

observed.

2.6.4 External lubrication

The guideline [1] refers the use of external lubrication on polymer gear via synthetic or mineral oil, but also via greases. However, it indicates that precautions should be taken to make sure the lubricant used adheres completely to the sliding face especially at higher temperatures.

The authors Mertens and Senthilvelan [12] explored the effects of compressed air cooling on PP polymer gear. The parameters tested for this gear pair with and without this cooling method were: transmission efficiency, wear and surface temperature. The results suggest an improvement of transmission efficiency and a decrease in tooth thickness loss and surface temperature for the tests using cooling, regardless of load conditions after 10^5 cycles.

2.6.5 Gear geometry

Several methods have been implemented to reach the best gear geometry for a certain application, keeping in mind life span, temperature, load and tangential speed. An example of this is the multilevel test and design procedure proposed in [7]. Through an iterative algorithm, the best geometry was successfully determined once the design constrain was met. In this algorithm it was considered life span and temperature of the polymer gears in test.

Moreover, the effects of the teeth profile shape on the properties of polymers was also seen for instance in [13], having concluded that material shrinkage after cooling in injection moulding should be taken into account in gear design, since it interferes significantly on stress and stress calculation.

The teeth profiles studied included S-gears and involute gears. The S-gears showed better resistance for higher loads but lower life span. On the other hand involute gears showed lower resistance for higher load, but higher life span. It was also verified that for gears with higher life span, fatigue effects would occur, and that at higher loads temperature related defects and modes of failure occurred.

2.6.6 Metallic Inserts

Metallic inserts impregnated in the polymer matrix were studied in [14; 15]. The variables tested were: the position of the insert relative to the tooth tip, geometry and material of the insert.

The objective was to study the effect of these variables on tooth temperature using Finite Element Method. It was concluded that the best compromise between an increase in total mass of the gear and the minimum and maximum temperature was for a simple plate insert using aluminum as material of the insert.

As this solution is the subject of this thesis, further developments and more detailed descriptions of this solution are presented further on.

2.7 Guideline and standards

There are two major polymer gear german guidelines, VDI 2545 and VDI 2736 that consider the strength calculation of plastic gears. The VDI 2545 was withdrawn in 1996, being the most current guideline for the strength calculation the VDI 2736. [7]

As for geometry of the polymer gears, AGMA 909-A06, ANSI/AGMA 1006-A97, and ANSI/AGMA 1106-A97 are pointed as reference for this subject [7; 13]. It is also noted in [13] that the comparisons made between the several different standards and the numerical results obtained through individual software as KISSsoft, can show significant differences.

The VDI 2736 guideline contemplates the properties of some polymer gears and their temperature dependence, as well a guide for the selection and use of polymer gears and what manufacturing processes, accuracy and gear design should be used [1]. The second part of this guideline contemplates the equations and considerations for the calculation of the load carrying capacity for thermoplastic cylindrical gears [16].

The JIS B 1759 was created to develop equations for the tooth bending strength of thermoplastic gears, basing on the equations of the standard for the calculation of load carrying for cylindrical gears ISO 6336 [17].

Both the guideline VDI 2736 part 2, its predecessor VDI 2545 and the JIS B 1759 needed to create specific equations for the load carrying capacity of thermoplastic gears since the other standards, ISO 6336 and VDI 3990, with generic equations for load carrying capacity don't take in consideration factors that are prevalent in polymer gears.

As such this generic equations overestimate the results and there is in fact a need for different equations of the load carrying capacity. However, this guideline VDI 2736, VDI 2545 and JIS B 1759 only make the needed alterations of the ISO 6336 and VDI 3990, referring the general aspects to them.

2.8 FEM models

For studying other polymer gear geometries such as the attempts to improve thermoplastic gears described in Section 2.6, or for further studying polymer gear Finite Element Methods are implemented and in this section it is described some of the example of usage of these methods.

A thermo-mechanical analysis of a polymer gear was conducted by Roda-Casanova et al. [3] considering a coupled and uncoupled thermo-mechanical analysis, in which the thermal part consisted on thermal transient analysis. The material properties were tested as being hyperelastic and temperature dependent.

A thermal model of polymer gears with metallic inserts and standard polymer gear considering a thermal transient and steady state analysis was conducted by Rocha [15].

In all the works of [3; 15; 18] for the thermal part, considered a gear power loss model in which most of this loss is converted to heat so that a friction heat flux occurs.

Chapter 3

Finite Element Models for Gears

3.1 Introduction

The previous chapter focused on describing polymer gears in general, detailing its advantages and problems. This was then followed by analysing the several attempts to improve upon its disadvantages, including a listing of the finite element methods that were employed to study this type of gears.

In this chapter, it is going to carried out a more detailed description of the finite element models that are going to be used, starting with a thermal model, followed by the mechanical and thermo mechanical models, and finally an implementation procedure of these models for the validation cases and for the studying of polymer gears with metallic inserts.

3.2 Thermal Model

The equation that describes the thermal behaviour for an Elasto-hydrodynamic contact, can be rewritten considering a transient problem and a steady state problem. In the case to be applied for the present model, it is considered a fully established regime and for this reason the thermal behaviour can be described as steady state and is as in equation (3.1) [15].

$$k \cdot \left(\frac{\partial^2 T_B}{\partial x^2} + \frac{\partial^2 T_B}{\partial y^2} + \frac{\partial^2 T_B}{\partial z^2} \right) = 0 \tag{3.1}$$

The boundary conditions for the thermal model must be set so that the differential equation (3.1) can be solved. For this the different surfaces of a single tooth are going to be used as in Figure 3.1.

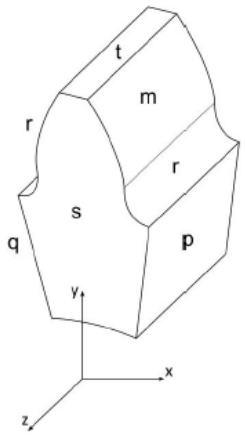

Figure 3.1: Surfaces used as boundary conditions for the thermal model [15]

Despite the fact that in Figure 3.1, a single tooth makes reference to the boundary condition surfaces, and the model used is of either a gear set or only the pinion, for simplicity in describing the boundary conditions it should be considered that when referencing

a surface of the single tooth, every such surface of every tooth of the pinion or wheel are also referenced. To this extent, the surfaces **p** and **q** are disregarded.

Since dry contact is to be modelled the surfaces **s**, **r**, **t** and **m** are subjected to a convective heat transfer, in which the surrounding temperature is the air temperature (T_{air}). The boundary equation is as follows in (3.2). The heat transfer coefficient of air (h_n) is calculated from equation 3.3

$$-k \cdot \frac{\partial T}{\partial n} = h_n \left(T - T_{air}\right) \tag{3.2}$$

$$h_n = 0.36 \cdot \frac{k_{air}}{D} \left(\frac{\omega \cdot D^2}{\nu_{air}}\right)^{0.2} \tag{3.3}$$

The meshing surface **m** is not only subjected to a convective heat transfer, as displayed in (3.2) but also to the gear power loss ($\bar{q}_{VZP}$) caused by friction in the interaction between pinion and wheel.

The gear power loss is assumed to be converted for the most part into heat, so that this friction heat flux is as in (3.5). For this it is needed the β_k of equation (3.4) that is the distribution coefficient of friction heat flux between the contacting bodies (the pinion and the wheel) and the γ_k that is the amount of heat generated that is transferred for the solids, which generally has its value in the range between 0.9 and 0.95.

Also, the coefficient of friction in equation (3.5) is equal to 0.280 for a POM/POM contact according to VDI 2736, and assuming constant along the path of contact.

The heat transfer coefficient (h_n) of equation (3.7) is calculated from equation (3.3). The resulting boundary condition in the meshing surface **m** is then in equation (3.7). [15]

$$\beta_{ki} = \frac{b_i}{b_1 + b_2}, \text{ with } b_i = \sqrt{k_i \cdot c_{p_i} \cdot \rho_i \cdot \nu_{ri}} \tag{3.4}$$

$$q_{VZP_i}(x) = \gamma_k \cdot \beta_{ki} \cdot p_o(x) \cdot \mu(x) \cdot \nu_g(x) \tag{3.5}$$

$$\bar{q}_{VZP_i}(x) = \frac{a(x) \cdot \omega_i}{\pi \cdot \nu_{ri}} \cdot q_{VZP_i}(x) \tag{3.6}$$

$$-k \cdot \frac{\partial T}{\partial n} = h_n \left(T - T_{air}\right) - \bar{q}_{VZP} \tag{3.7}$$

The implementation of the thermal model is in the Fortran code that is read by the CCX solver (Calculix) in Appendix A.

The inner hole of the pinion and, or the wheel is considered to be adiabatic and so the heat conduction in this area is neglected. Other authors, such as Černe et al. [18] considered conduction in the hub and found similar results compared to not considering conduction in the hub.

The resulting temperatures using this thermal model for the standard polymer gear are displayed in the Figure 3.2.

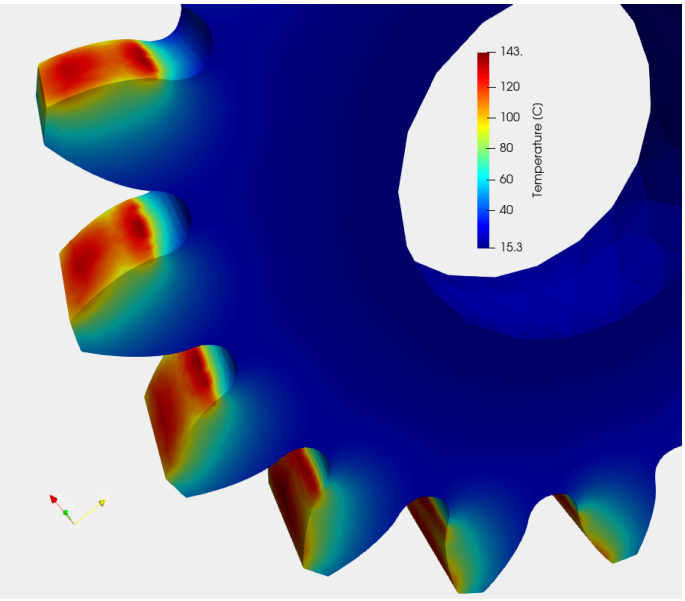

Figure 3.2: Example of temperatures obtained with thermal model, using standard polymer gear

3.3 Mechanical Models

The mechanical models that are going to be described detail a contact model where the whole gear set (pinion and wheel) is simulated and a contactless model where only the pinion is simulated.

3.3.1 Contact model

For the contact model it is going to be needed to describe the finite element methods for contact problems, and as the penalty method and the lagrange multipliers' method are the most commonly used methods, these are the ones to be detailed.

Penalty Method

There are two main methods for finite element contact problems, the lagrange multipliers method and the penalty method. The lagrange multipliers method uses an additional term to the energy of the system that emulates a constraint that can be considered as the reaction force on the contact. The penalty method refers to a pairwise interaction of slave and master bodies by adding a penalty term to the energy. This term can be interpreted as the energy of a spring which connects between the point mass of one body and the rigid support of another body, and thus ensuring the contact interface [19], as shown in Figure 3.3.

This also means that non-physical penetration will always occur, and the higher the constant stiffness of the spring in the contact the lower the penetration will be. In the limit the constant stiffness tends to infinity, a hard contact will occur and this method will result the same as the lagrange multipliers' method. [19]

The author Dhondt [20] recommends that this constant stiffness should be in the range of five to fifty times the value of the Young's modulus of the surfaces in the contact. This constant stiffness will also dictate the rate of convergence of the solution.

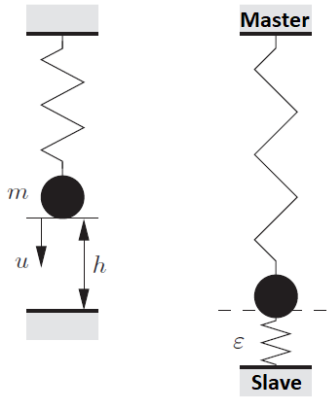

Figure 3.3: Interaction in the contact area using the penalty method [19]

As stated above a spring between the contacting bodies will be enforced and the surface that is considered for the point mass will be defined as the master body. The opposing surface is defined as the slave body. Since only the point mass of the master is considered, it is recommended that the master body is the one with higher rigidity. In this manner, the present model will consider the contact areas in the wheel to be the master and the contact areas in the pinion to be the slave.

The penalty method so far has been described as with a master and slave body, but in fact the body can be referred to a node to node, node to surface and surface to surface contact interactions each one with its specific contact algorithms.

There are also specific methods when for instance the master surface is misaligned with the slave surface and the spring is need to be enforced. The surface to surface contact algorithm is considered to be the most accurate and it is the one to be used in the present model. The creation of a face to face penalty contact element is displayed in Figure 3.4.

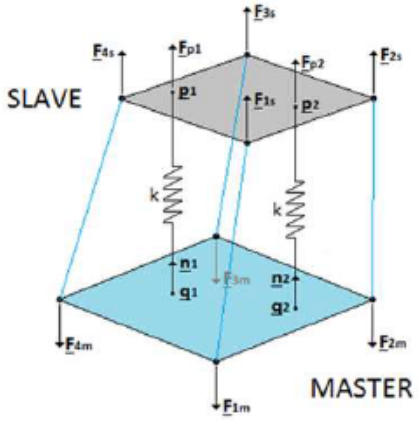

Figure 3.4: Creation of a face-to-face penalty contact element

Loading and rotational Steps

The contact model needs additional steps in order to be possible to apply torque to the hub of the pinion with the wheel fixed. This is due to the fact that for the contact problem this torque is equivalent to applying a force in the teeth of the wheel with an origin of application being the teeth of the pinion, with a spring for contact between them.

However, the algorithm that is going to be used only considers a spring between surfaces (effective contact) when the distance between slave and master surfaces is zero and as such the force being applied only is applied when master and slave surfaces touch, but the gear to be studied has backlash. Therefore, an initial rotational approach is needed.

The steps conceived for this FEM model intend to study the load carrying capacity of the gears and were based on the works published by [21; 22]. The summary of this simulation is as displayed in Table 3.1.

Table 3.1: Simulation steps for the contact model

Simulation steps	Wheel		Pinion	
	θ	T	θ	T
Step 1 Rotational Approach	0	-	γ_{BL}	-
Step 2 Loading	0	-	Free	B
Step 3 Rotation	γ_w	-	γ_p	-

Step 1, Figure 3.5a, involves a rotation of the pinion, γ_{BL}, of at least the value of the backlash present in the gear pair, maintaining the wheel fixed. This will ensure that when Step 2 is done, it can be accurately calculated and the step converges [21].

Step 2, Figure 3.5b, intends to impose a torque in the hub of the pinion, maintaining the wheel fixed, so that contact pressure and the stresses present in the gear pair can be calculated.

Step 3, Figure 3.6, is the last step and intends to calculate the gear mesh stiffness, represented by the torsional stiffness calculated according to equation (3.8) and (3.9). The variable g_r represents the gear ratio of the gear pair and the variable γ_t stands for twist.

The twist is a prescribed rotation on the pinion hub, because a prescribed displacement assures better convergence than a prescribed load. In this way, applying to the model a rotational boundary condition with the twist ensures that the step converges. In this sense, an alternative to this test could consist of one or two of the following scenarios: γ_w is zero and substituted for a torque in the wheel; γ_p is zero and substituted for a torque in the pinion.

$$\gamma_w = -\frac{\gamma_p}{g_r} + \gamma_t \tag{3.8}$$

$$k_g = \frac{4\,T}{\gamma_t\,(d_2\,cos\,\alpha)^2} \tag{3.9}$$

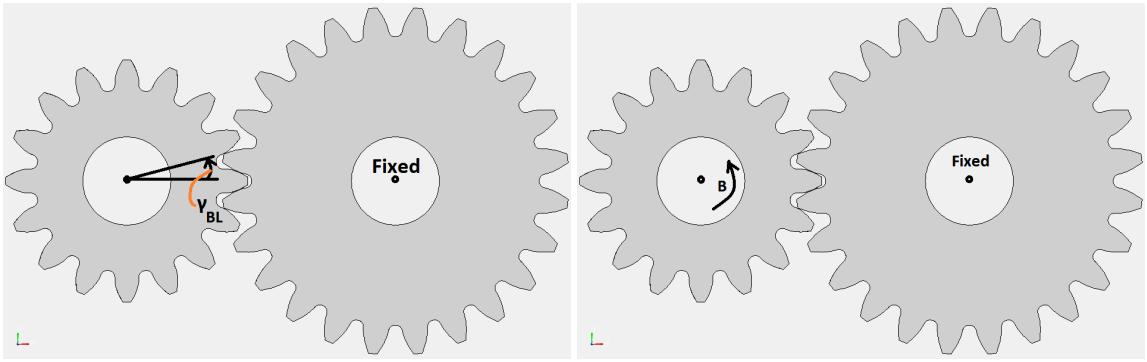

(a) Step 1 (b) Step 2

Figure 3.5: Rotational and loading steps 1 and 2

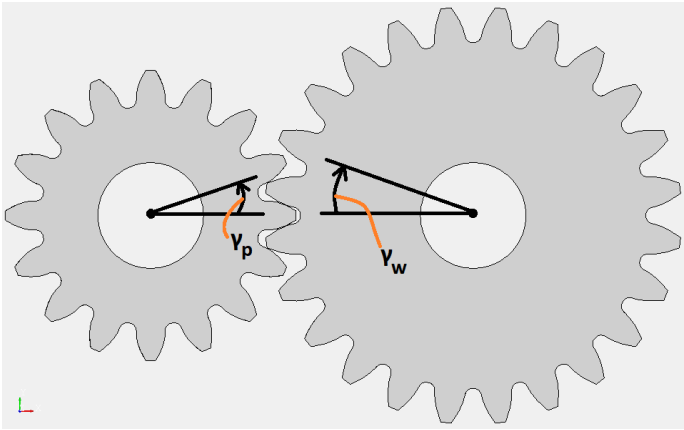

Figure 3.6: Rotation steps in the wheel and pinion for meshing Step 3

Rotational degrees of freedom are the only ones active, being translation degrees of freedom restricted. This is valid assuming that the deflection of supporting elements is small compared to teeth deflection.

3.3.2 Contactless Model

Due to limited capacity of computational resources and time, a contactless model that only considers the pinion could be a viable possibility to study the gear. The reason for a Finite Element model that only studies the pinion and not the wheel, is due to the fact that preliminary results of the validation cases presented in the following chapter, indicate that the pinion has higher stress, deformations and temperatures compared to the wheel.

This model contemplates a similar simulation Step 2 and considerations as those of section 3.3.1, being displayed in Table 3.2 the step for this model.

This Step 1 no longer requires a first Step with a rotational boundary since the step emulates the wheel by creating lines in the meshing teeth through the division of the surface **m** of the pinion and forcing those lines in the boundary conditions to be fixed in space. This essentially means that the step is already applying force to a fixed point and so the step converges. The lines described are represented in Figure 3.7 below.

Table 3.2: Simulation steps for the contactless model

Simulation steps	Pinion	
	θ	T
Step 1 Loading	Free	B

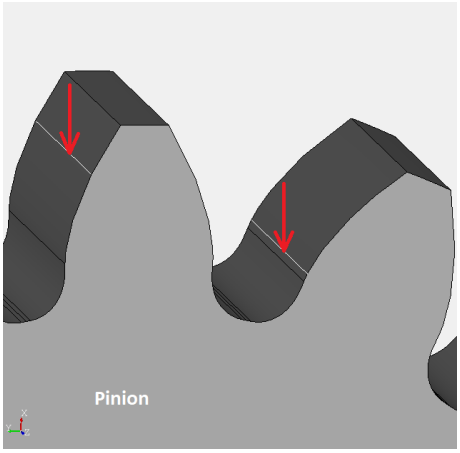

Figure 3.7: Line over pinion used for Step 1 and 2 in the contactless model

3.4 Thermo-mechanical Model

The thermo-mechanical model couples the thermal model and mechanical models already discussed. This thermal model can either be coupled with the contact model or with the contactless model.

When the thermal model is solved independently of the mechanical model, i.e. the mechanical and thermal equations are not dependent, the thermo-mechanical model is called an uncoupled. Notwithstanding, the thermal model is firstly solved and after that with the resulting temperature the mechanical properties that are going to be used in the following mechanical model are also defined.

However, when the deformations in the mechanical part interact with the temperature in the thermal part via dissipative mechanisms such as plastic deformations and frictional forces, the uncoupled thermo-mechanical model isn't valid [19]. In case either of this mechanisms should be considered a coupled thermo-mechanical model must be used instead of the uncoupled thermo-mechanical model considered and in this model the thermal and mechanical equations are dependent.

In spite of this annotation the authors Roda-Casanova et al. [3], who tested for several loadings conditions various material combination of gears using a coupled and uncoupled thermo-mechanical model, concluded that the loss in accuracy isn't significant and that the computational times were reduced. For this reason, even though the coupled thermo-mechanical analysis could be performed it is going to be preferred the uncoupled thermo-mechanical analysis which is the only one used.

3.5 Implementation of the FEM Models

Regarding the implementation of the FEM model, an explanation of the steps performed in the several software packages used will be provided. Such implementation followed an algorithm as described in the flowchart of figure 3.8. After its implementation the results obtained are compared with standards or literature results.

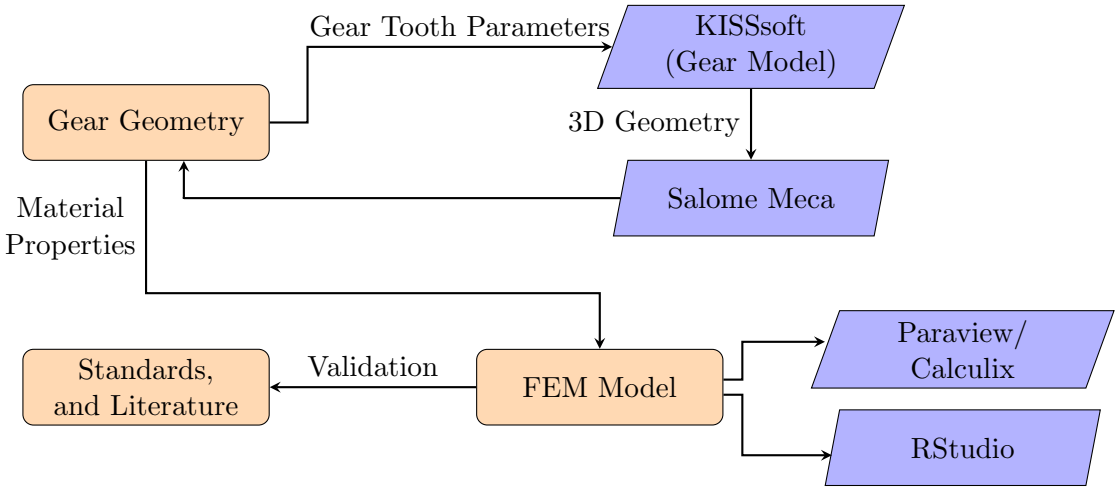

Figure 3.8: Methodology used for the validation cases

3.5.1 Geometry - Pre processor

KISSsoft

In order to obtain the gear geometry, the software KISSsoft is used. This software enables the selection of several different standards that are then used as reference for the calculation of the machine element's geometry, in this case a gear set, and the calculation method for many different choosing outputs such as stress, temperature, safety factors and contact analysis. It can also be used optimize geometries according to some constraints.

In this way, a standard is chosen for KISSsoft to calculate the gear set geometry, and the gear's parameters are inputted. The resulting geometry is then exported into a STEP file, that is a universal file type created by ISO for exchanging geometries between different CAD software.

Salome Meca

This STEP file is then imported into the Salome platform that is an open source software and includes every stage for a successful implementation of a FEM model. It includes a CAD software for geometry manipulation; a meshing software very similar to GMSH software; a pre processor for Code Aster for introducing boundary, step and material conditions; a solver that is the Code Aster software; a pos processor for analysing the FEM results using the software Paraview. It must be noted that every single software can be used separately.

The CAD software has every function and some more for geometry manipulation as its equivalents and paid versions, for example the Solidworks software. The meshing software enables meshing of geometries with an unlimited number of nodes and elements.

As Salome has a CAD and a meshing software incorporated into one single platform, a second conversion to a STEP file in order to mesh in a different software is no longer needed. This second conversion could implicate eventual loss of quality or other. In this manner, the Salome platform has been chosen.

3.5.2 Mesh Generation - FEM model

The meshing generation in the Salome platform is based on structured (regular volumes) and unstructured (free volumes) mesh algorithms. The structured mesh algorithms includes Hexahedron (i,j,k) and Body fitting, while the unstructured mesh algorithms includes NETGEN, MG-Tetra and MG-Hexa.

In Hexahedron (i,j,k) the solid is split into hexahedral elements and that 2D mesh generated on a solid could be considered as a mesh of a box. In body fitting the solids are also split into hexahedral elements but a Cartesian grid must be specified since the intersection of the geometry boundary with the Cartesian cells determines the generation of elements.

All the algorithms for the free volumes spawn elements in the solid that best fit its geometry constrains. The NETGEN offers NETGEN 1D-2D-3D that first discretize the lines of the solid, then from this it spawns elements to mesh the surfaces and finally from this spawns elements to mesh the volume of the solid, resulting in tetrahedron 3D elements (four face pyramid with triangular faces). As the gear set has a high degree of geometric complexity and tolerance, the best fitting algorithm is the NETGEN 1D-2D-3D despite the fact that it is an unstructured mesh.

The NETGEN 1D-2D-3D also enables the inclusion of the Delaunay algorithm to prevent steep or very small angles between the edges of the tetrahedron elements, the size of the mesh with the minimum and maximum size of the elements, the specification of local sizes in the mesh and the type of element of either first or second order element.

To mesh the gear the Delaunay algorithm was used, the size of the mesh was specified as suggested by the algorithm, the size was limited by surface curvature and first order elements were chosen because the time of computation is reduced compared to using second order elements and so more elements can be used in the mesh. A generic mesh using this procedure is in Figure 3.9.

A mesh refinement study was performed, where the total number of elements was successively increased till the results for each of the simulations converged. While increasing the total number of elements, the local mesh refinements where also adjusted accordingly in order to obtain more precise results in the contact areas. It was also tested second order elements, having concluded that the computation times outweighed the difference in the results obtained with each element type.

Local mesh refinements were then specified according to this mesh convergence study, and reflected the simulation steps described in the subsection 3.3.1. Step 1 and Step 2 required a refinement in the contact zone after the rotation of the pinion and the resulting mesh is displayed in Figure 3.10.

Several surfaces and node groups were imported into the mesh by selecting surfaces groups in the geometry. These surface and node groups allow to establish boundary conditions in the solver. The master and slave surfaces for the contact specification, must be defined ensuring that as for its local sizes the slave surfaces should always be at least as fine as the master surfaces. The mesh is then exported as UNV file that is a mesh file that the solver recognizes.

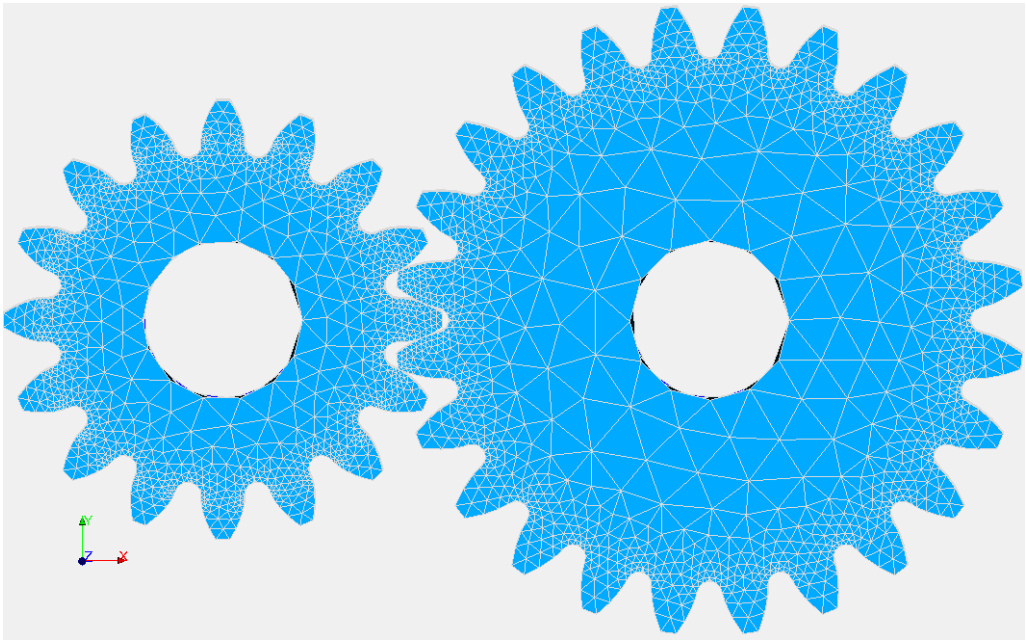

Figure 3.9: Generic Mesh, with 105 037 elements, 11 728 nodes, 4 node tetrahedron elements (C3D4)

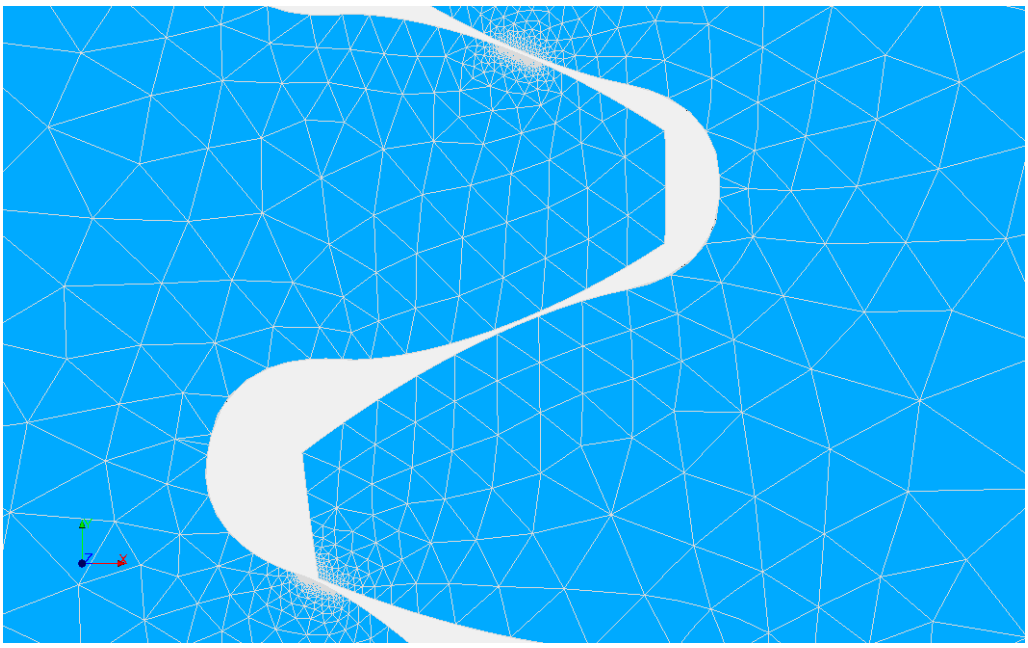

Figure 3.10: Mesh refinement used for fixed gear simulations, local size of 3×10^{-5} on slave surface and 9×10^{-5} on master surface

The surface groups of the geometry that were used are described (green) in Figure 3.11. The master and slave surfaces are used to define the contact interaction in the code.

The hub surfaces are used to define a rigid body, enabling to associate each hub surface to a fictitious node for translation and another for rotation, both located in its respective centre hub. With the rotational node, both loading and rotational boundaries

are imposed causing the hub surface to respond accordingly, either with an imposed rotation or torque. The same goes for the translation node where it is defined that the hub surface doesn't move laterally, fixing these three degrees of freedom.

For the thermal model, the dflux code is activated for the **ar** surfaces. This code embodies the equations described for the thermal model, with the non meshing surfaces (all but the hub that is considered to be adiabatic). It is also defined the groups for the meshing surfaces with **fl_p** and **fl_w** surface groups that are going to be need to calculate in the code dfilm.

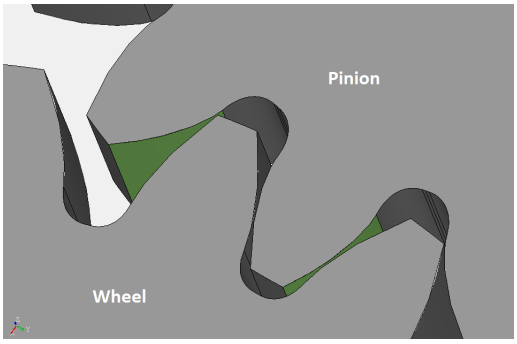

(a) Slave surface

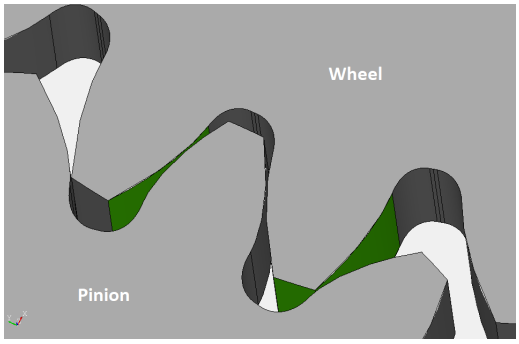

(b) Master surface

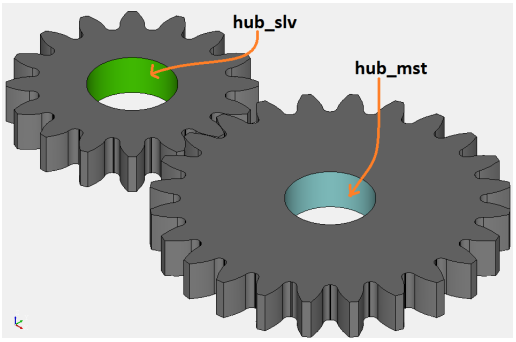

(c) Hub surfaces

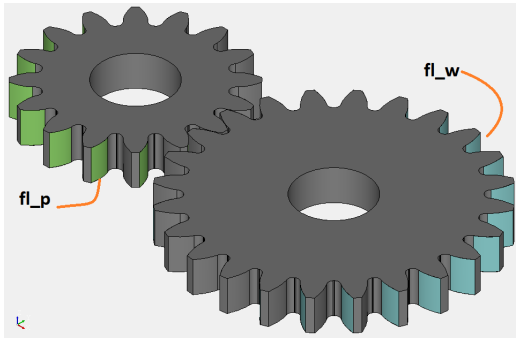

(d) Every Meshing surface **m**, *DFLUX

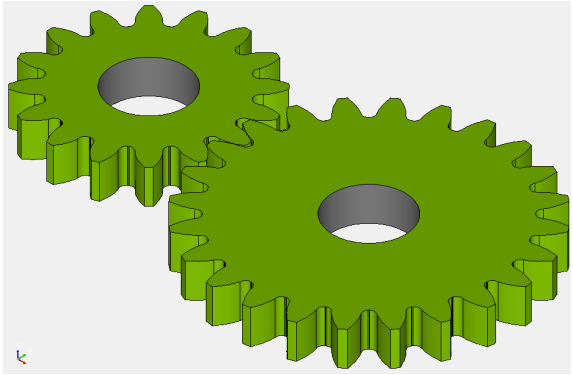

(e) Every surface except hub, *FILM

Figure 3.11: Groups of surfaces created and imported to the mesh to establish boundary conditions

3.5.3 Calculix solver - FEM model

The authors Rajaprabakaran and Ashokraj [23], used successfully Calculix to calculate stress and displacements in a gear pair. The capabilities of implicit and explicit solver, field problems, linear and non-linear calculations, static, dynamic and thermal solutions, and the ability of custom configurability of the code of the solver are among the advantages of Calculix pointed out.

Calculix includes pre processor and post processor, and solver (CCX) capabilities with an interactive 3D tool (CGX) for displaying the results. It is able to solve contact and thermo-mechanical problems.

The custom configurability of the code is used since part of the code was altered to include the thermal Fortran routine described in Appendix A and afterwards the program was recompiled to recognise this alteration.

Calculix has the advantage to have similar input files of those used by ABAQUS CAE software, but being an open source and free software. The developers of the Calculix software recognize that naming conventions and input style formats are based in the ABAQUS software, with the required permissions. So, an input file of Calculix is in some cases compatible with ABAQUS.

The UNV file with the mesh created is imported in Calculix, and it converts this file to the INP file that can be read by CCX solver, recognizing the coordinates of the nodes, the type of elements, and the groups of nodes and surfaces of the mesh file. Another INP file is then created with the definition of the initial conditions and the steps to simulate with the system. This INP file consists of the following:

- Reading the INP with the mesh definition
- Definition of the properties of the material and the elements that constitute it
- Definition of the contact interaction and which surfaces, master and slave, make this contact pair
- Definition of the virtual nodes and corresponding node sets that are going to command the rigid body of the inner hole surface in order to apply rotation and torque in this surface
- Initial boundary conditions
- Steps definition for the simulation either with boundary or load conditions
- Request in the step for what is going to be the output of the simulation

The description of the user defined subroutine for the non linear solver that is used is in Figure 3.12.

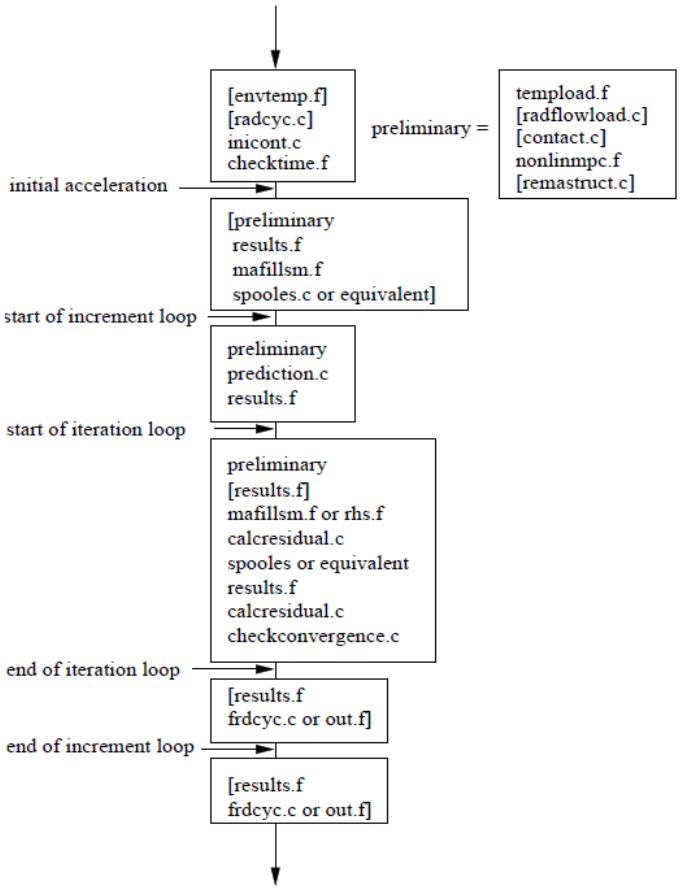

Figure 3.12: Flow diagram of the subroutine for the non linear calculations of the CCX

3.5.4 Post processor

The results of the simulation can either be written to a DAT file that can be read as a text file, or as a FRD file that works with the 3D visualization tool CGX to display the results.

The DAT file is used with Python programming language to process its information and create the plots displayed in the following chapters. The FRD file is used for a preliminary analysis of the results of the FEM simulation, but for a more detailed analysis this file is converted as a VTU file through the CCX2PARAVIEW program available online. This VTU file can be read in the Paraview software, also included in the Salome platform.

The python code of the CCX2PARAVIEW can also be modified to extract the dictionaries with the information of the stress of nodes, when the stress is outputted in the integration points of the elements by the DAT file which saves a processing step.

Other python code was made in order to process information and to run various simulations in a parametric way integrating also with the CCX2PARAVIEW for a later analysis on the Paraview software.

Paraview is a very versatile and complete way to extract data from a simulation geometry, being also able to plot data, and extract data from specific regions.

RStudio software is also used to study the influence of some geometry variants in different parameters further on. This could be accomplished through Pareto plots.

Chapter 4

FEM Model Validation

4.1 Introduction

In the previous chapter 3 the finite element models and its implementation methodology were described. It was discussed the governing equations and boundary conditions for the mechanical and thermo-mechanical models.

In this chapter the mechanical and thermo-mechanical models are used to predict the gear temperature, calculate the local material properties and predict the load carrying capacity of gears.

These FEM results are then compared to the results from standards, using KISSsoft, and results from the literature, to validate the models and ensure accurate results when applied to hybrid gears concepts.

4.2 Steel Gears

To validate the mechanical models with penalty contact type as described in subsection 3.3.1 and without contact in sub subsection 3.3.2, a steel gear pair is going to be simulated using the load carrying capacity of spur gears described ISO 6336.

The geometry of this gear pair was based on the FZG back-to-back gear test rig, C-type 14 gear [24], displayed on Table 4.1. With this input it was obtained the geometry represented in Figure 4.1. The mechanical properties of the material 16MnCr5 were assumed to be in the elastic domain, and its values are as follows in the Table 4.2 [14]. For the standard calculation the spur steel gear was lubricated with an oil bath lubricant of ISO-VG220.

In this validation case the steel gears were simulated for the operating conditions described in Table 4.3. Using the procedure for mesh generation detailed in Chapter 3, it was obtained the meshes in Figures 4.2 and 4.3.

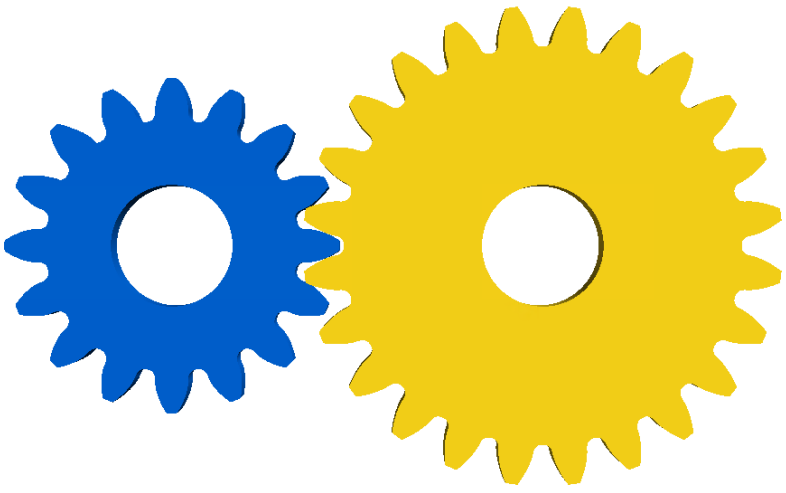

Figure 4.1: Geometry Results

Table 4.1: FZG back-to-back gear test rig, C-type geometry

Geometry Data	**Steel Gear**	
	Pinion 1	Wheel 2
Number of Teeth, z [-]	16	24
Module, m [mm]	4.5	
Center Distance, a [mm]	91.5	
Pressure angle, α [°]	20	
Face Width, b [mm]	14	
Addendum Modification, x [-]	+0.1817	+0.1715
Bore Hole [mm]	30	
Normal Backlash [mm]	0.224	
Material	16MnCr5	

Table 4.2: Mechanical properties of 16MnCr5 for the steel gears [14]

Mechanical Properties	Steel - **16MnCr5**
Young's Modulus, E [GPa]	206
Poisson's ratio, ν [-]	0.30
Density, ρ [kg/m^3]	7830

Table 4.3: Loading conditions tested with the FEM simulation

Loading conditions	**Torque** of the pinion hub [N·m]
A	180.000
B	215.513
C	250.000

The loading conditions were chosen around the k9 testing torque 215.513 $N \cdot m$, with a variation of torque of 35 $N \cdot m$ of torque.

The boundary conditions surfaces for the mesh groups are described in Figure 4.5.

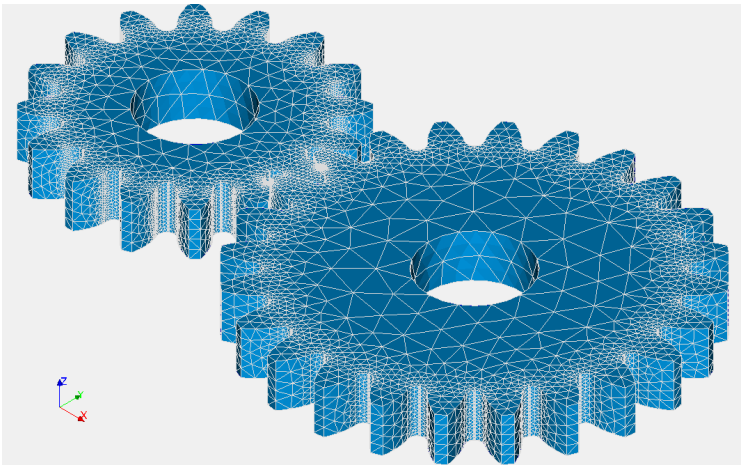

(a) Isometric view

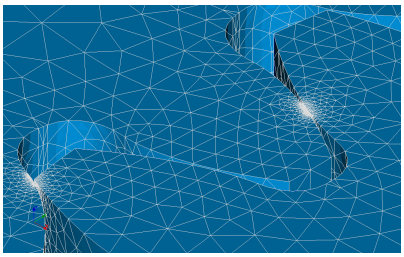

(b) Detail of the mesh in the contact area

Figure 4.2: Mesh obtained with Salome, with 245 937 elements, 26 823 nodes, 4-node tetrahedron elements (C3D4). For simulation 3, contact model

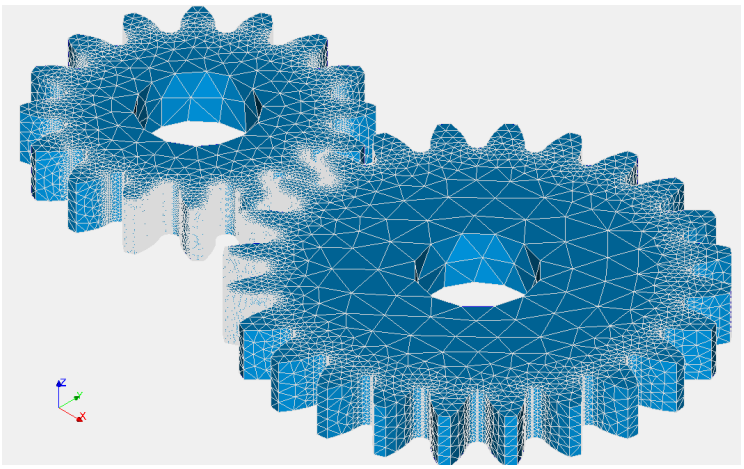

(a) Isometric view

(b) Detail of the mesh in the contact area

Figure 4.3: Mesh obtained with Salome, with 487 923 elements, 107 734 nodes, 4-node tetrahedron elements (C3D4). For simulation 3, contact model

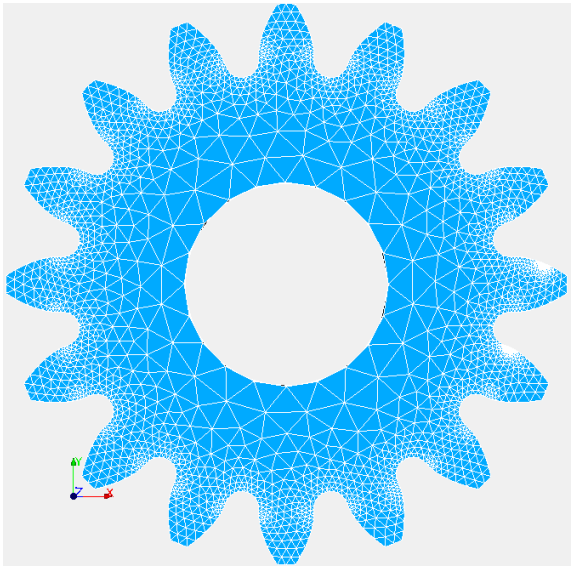

Figure 4.4: Mesh for the contactless model, 318 871 elements, 44 688 nodes, 4-node tetrahedron elements (C3D4). For simulation 1 and 2

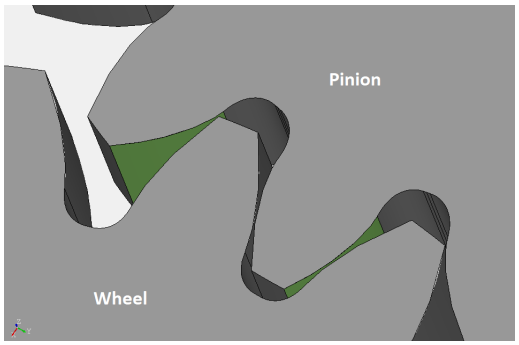

(a) Slave surface

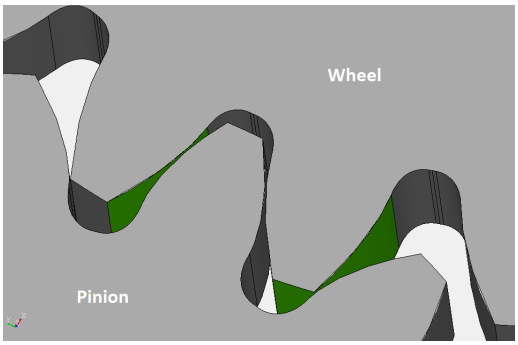

(b) Master surface

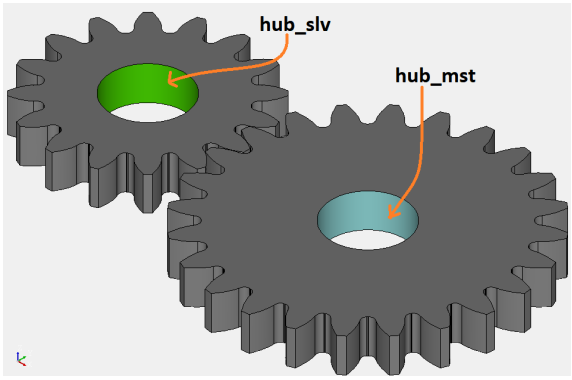

(c) Hub surfaces

Figure 4.5: Groups of surfaces for the boundary conditions

Table 4.4: FEM Mesh detail

Mesh Parameter	Step 1 and 2 Contact model	Step 3 Contact model	Contactless Model
Maximum size [m]$\times 10^{-2}$	2.25259	2.25259	1.17422
Minimum size [m]$\times 10^{-4}$	2.49936	2.49936	0.111522
Mesh Fineness	Moderate	Moderate	Fine
Local size master surface [m]$\times 10^{-4}$	0.35	3.6	0.65
Local size slave surface [m]$\times 10^{-4}$	0.34	3.5	0.65
Total number elements	487 923	245 937	318 871
Total number nodes	107 734	26 823	44 688
Figure	4.2	4.3	4.4

4.2.1 Tooth root Stress

The tooth bending strength stands for the permissible bending stress and it represents an important part of the characterization of the load carrying capacity of gears since the stress occurring in the tooth fillets can lead to cracks in the root and propagate to failure. The tooth root stress present in the gear should be less than permissible bending stress being that it represents the load capacity of that gear [25].

For unidirectional loading, gears tend to crack on the side of the working tooth flank where tension occurs. In this manner, tooth root stress is the maximum principal stress (σ_1 or σ_{max}) present in the working tooth flank side, in the surface of the root. The location of this maximum in the fillet, using method B from ISO 6336, which considers that the load is applied in the outer most point of a single pair gear tooth contact (D), is given by the standard and is represented in Figure 4.6.

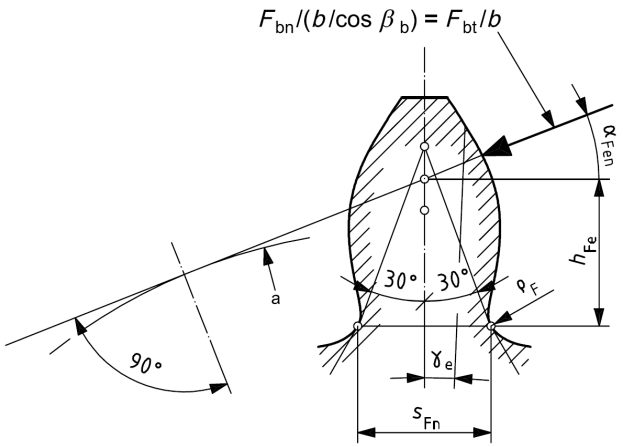

Figure 4.6: Tooth root Critical section point according to ISO 6336-3 Method B [25]

As for the geometry described in Section 4.1, the exact coordinates for this point must be determined. To this effect, the initial STEP file from KISSsoft was imported into the software Solidworks, and a 2D sketch was done to determine this point's coordinates. Besides the geometric restrictions followed by Figure 4.6, the standard also indicates that the line that lies on the tooth root fillet is tangent to it. With this, the sketch represented on Figure 4.7, taken from Solidworks, enabled the calculation of the following coordinates of this tooth root stress critical point.

- x = 4.4066 mm
- y = 31.5502 mm

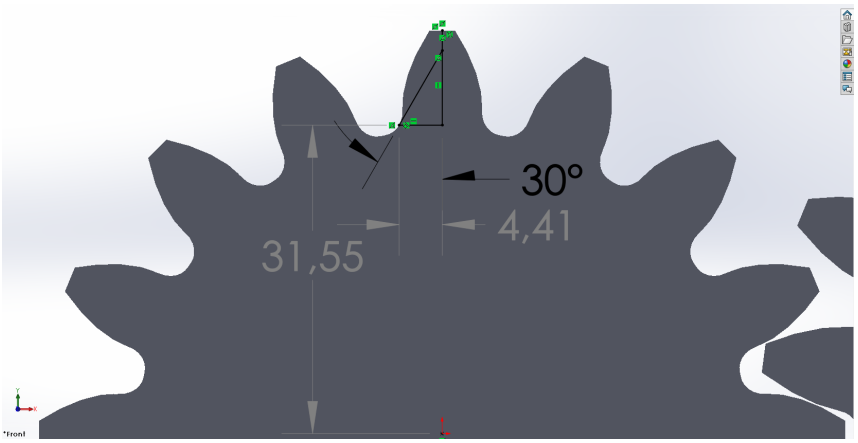

Figure 4.7: Critical Tooth root stress point coordinates

Because in the outer most point of single pair gear tooth contact, the pinion suffers higher tooth root stress, only the pinion is considered for this parameter and its coordinates. Both mechanical models consider contact in two teeth, one tooth in the outer most point (D) and the other the inner most point (A).

For the results file it was asked that an input and output torque were print. The input torque is the torque measured on the fictitious rotational node where the torque was

applied in the simulation code and that is defined as a rigid body with the hub surface, and the output torque measured is the moment about the centre of gravity of the surface of the hub.

The torque in the pinion for the contactless had to be adjusted because of the discrepancy between the input torque and the output torque read in this resulting file of the simulation. It was then increased the input torque so that the output torque measured was the desired operating conditions. This is considered to be valid since in the contact model both the input and the output torque measured values didn't differ significantly.

The penalty coefficient was adjusted to five thousand times the Young's modulus (10300000 [GPa]) for the contact model. It was adjusted based on incrementing this parameter by a factor of 10 till the tooth root stress stabilized and its change with increasing the penalty coefficient had no more difference than one unit value of [MPa]. The penalty coefficient was only adjusted for the loading conditions with torque value of 215.513 [N·m].

Using this concept of evaluation of the tooth root stress, the implementation of the simulation as described in Table 4.5 and for the operating conditions described in 4.3, results in Figure 4.8. The CCX code used for this FEM model implementation is described in Appendix B.1 and B.3.

Table 4.5: Simulation for evaluation of the tooth root stress, contact stress and tooth flank stress for steel

	Contact Model	**Contactless Model**
Boundary	Wheel Fixed Pinion with Torque	Lines in Pinion fixed (Outer and Inner points of contact fixed) Pinion with Torque
Mesh	Step 1 and 2 Contact model Fig. 4.2	Contactless model Fig. 4.4
Penalty coefficient [GPa]	10300000 (5000*E)	-
Coefficient of friction, μ [-]	0	-

All of the tooth root stress values increase with the increase of torque value, but still remain below the endurance limit for root stress pointed by the standard AGMA refered to in KISSsoft. In Table 4.6 the errors of each simulation compared to the standard ISO 6336 are described.

The percentage of error is more stable in the contactless model, presenting higher percentage of error for the torque values of 180 [N·m] and 215.513 [N·m]. The error value tends to decrease with the increase of torque.

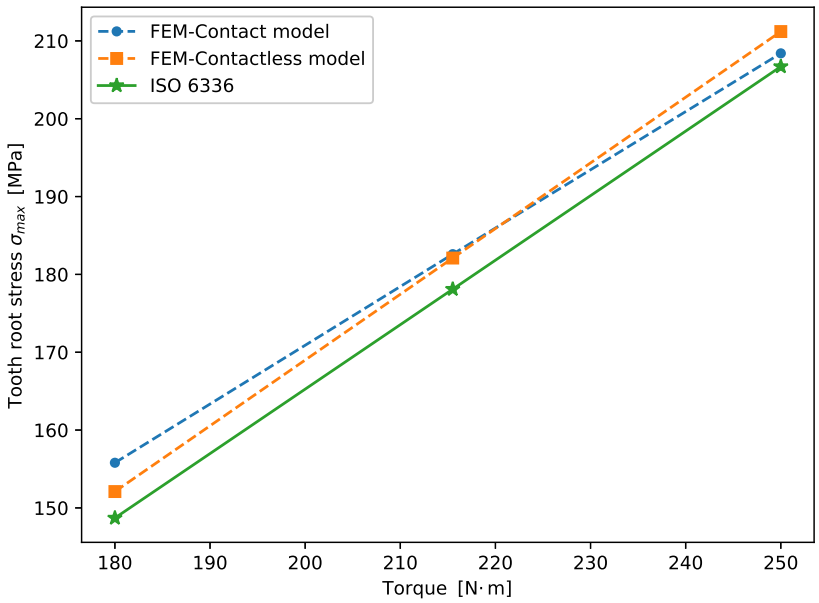

Figure 4.8: Tooth root stress for the mechanical models and standard ISO 6336

Table 4.6: Errors in [%] of the results of tooth root stress comparing with ISO 6336

Loading conditions	**Contact Model**	**Contactless Model**
180.000 N·m	4.77	2.29
215.513 N·m	2.56	2.25
250.000 N·m	0.82	2.18

4.2.2 Contact Stress

Contact stress calculation is based on the Hertzian theory and serves to assess the surface durability of cylindrical gears. This parameter can indicate the stresses that are going to be present on the gear. The highest value of contact stress in either the inner point of contact for the pinion or the pitch point for the wheel, determines the load capacity [26].

As already been said in subsection 4.2.3, there isn't a true contact area on the FEM without contact model, and for this reason only the contact stress for the FEM with contact model is going to be considered.

The FEM model with contact is used to predict the contact pressure at the contact area for point D of the pinion. Despite the fact that the contact stress isn't measured at the pitch point or inner most point (A), and that its value isn't as high as that of load capacity of the standard ISO 6336, this same standard also indicates the contact stresses along the path of contact.

The results were obtained using the same FEM implementation as in Table 4.6 and loading conditions of Table 4.3, which resulted in the Figure 4.9. The CCX code used for this FEM model implementation is described in Appendix B.1.

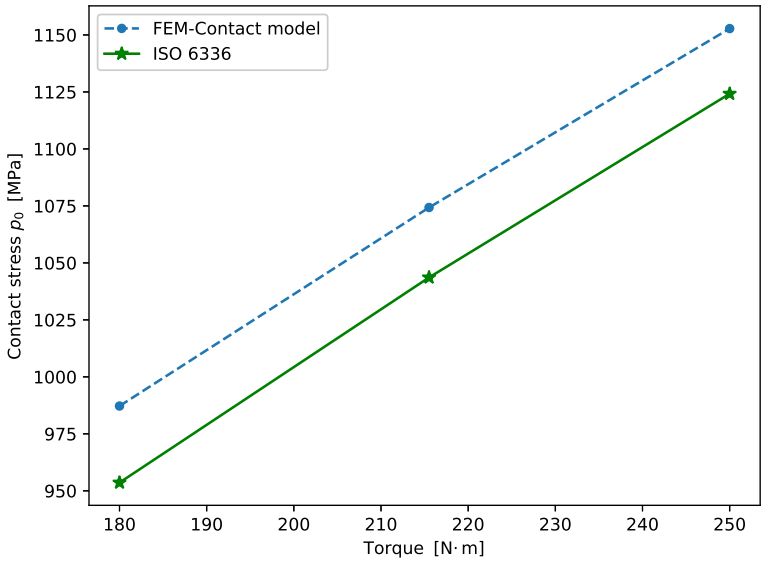

Figure 4.9: Contact stress at point D of contact path for the pinion

The error between the FEM model with contact and the ISO 6336 standard are 3.52%, 2.94% and 2.54% for the torque of 180, 215.513 and 250 N·m, respectively. As seen before, the error decreases with the increase of torque.

With the contact pressure obtained with the FEM model with contact, the maximum and octahedral shear stress can be calculated in equation (4.1).

$$\begin{aligned} \tau_{shear\ max} &= 0.3\, p_0\,, \text{ with } \mu = 0 \\ \tau_{shear\ oct} &= 0.272\, p_0\,, \text{ with } \mu = 0 \end{aligned} \tag{4.1}$$

4.2.3 Tooth flank Stress

The load carrying capacity can be characterized by the tooth flank stress. The resulting fracture caused by this stress is a primary fatigue crack in the region of the active contact area. Values for this tooth flank fracture are usually located at the pitch point beneath the active contact area and are the result of shear stress as indicated by the standard ISO 6336 [27]. The equation that was used to calculate maximum shear stress is in (4.2).

$$\tau_{shear\ max} = 0.5 \times (\sigma_1 - \sigma_3) \tag{4.2}$$

Seeing that the FEM model without contact hasn't an actual contact area simulated, the tooth flank stress is expected not to agree with the FEM with contact model.

Moreover, the tooth flank shear stress isn't evaluated at the pitch point but at the outer most point of single pair gear tooth contact (D) and the standard only gives values for the tooth flank stress for surface hardened gears.

However, it is possible to compare the tooth flank stress of the FEM with contact model and the calculated value for maximum shear stress using the FEM contact pressure evaluated in Figure 4.9. The results were obtained using the same FEM implementation as in Table 4.6 and loading conditions of Table 4.3, which resulted in the Figure 4.10. The CCX code used for this FEM model implementation is described in Appendix B.1 and B.3.

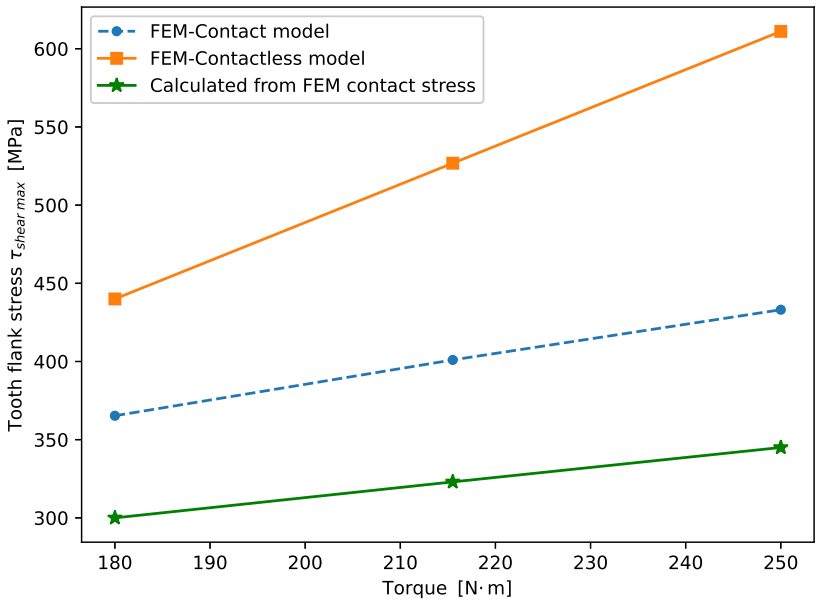

Figure 4.10: Tooth flank stress for the mechanical models

Comparing the results of the FEM-Contact model with the calculated values, it produced values of 22%, 24% and 26% more for the torque values of 180, 215.513 and 250 N·m, respectively.

4.2.4 Mesh Stiffness

Mesh stiffness translates the rigidity of the gears when meshing, being calculated by the torque output by the gears as in equation (4.3). As detailed in 3.3.1, a constant opposing force in the contact area is enforced by means of a constant rotational angular twist (γ_t), that represents a delayed rotation of the wheel. As stated above, since this parameter implies contact only the FEM model with contact is use.

The summary of the implementation of this FEM model is displayed in Table 4.7 and was simulated for the twist values and rotation of the pinion as in Table 4.8. The CCX code used for this FEM model implementation is described in Appendix B.2.

$$\begin{aligned} \gamma_w &= -\frac{\gamma_p}{g_r} + \gamma_t \\ k_g &= \frac{4\,T}{\gamma_t\,(d_2\,cos\,\alpha)^2} \end{aligned} \tag{4.3}$$

Table 4.7: Simulation for evaluation of the mesh stiffness for steel

	Contact Model
Boundary	Wheel Rotating with γ_w Pinion Rotating with γ_p
Mesh	Step 3 Contact model Figure 4.3
Penalty coefficient [GPa]	103000 (500*E)
Coefficient of friction, μ [-]	0

Table 4.8: Rotational boundary conditions simulated with the FEM simulation

Rotational Boundary Conditions	**Rotation twist value,** γ_t [°]	**Pinion Rotation Interval**
A	0.4	from 0° to 40°
B	0.5	from 0° to 40°
C	0.6	from 0° to 40°

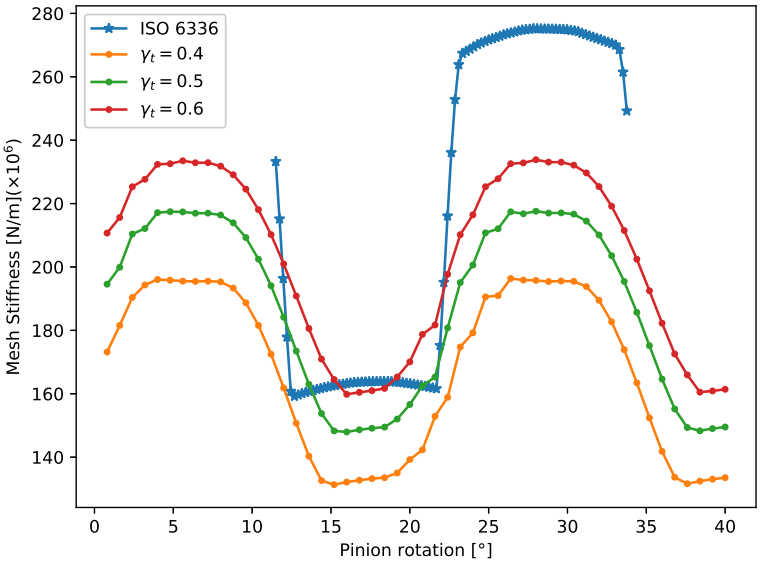

Figure 4.11: Mesh stiffness for the mechanical model with contact and standard

The resulting mesh stiffness depends on the angular twist imposed increasing with increase of the value of the angular twist. Despite the fact that the angular twist that fits best the standard is of 0.6°, the torque values with this twist are too high, in the order of 3000 Nm, and so the results may not be predicting effectively the mesh stiffness value. The penalty method used had to be decreased to (500*E), since higher penalty values would create unstable torque output.

4.3 Polymer Gears

In this section a type C14 polymer gear is considered as in Table 4.9, but using POM as material. The standard for polymer gears is as discussed in Chapter 2, VDI 2736. The thermo-mechanical models simulated in this Section are detailed in Section 3.4, and will integrate either the Contact or the Contactless model for the mechanical part.

Table 4.9: FZG back-to-back gear test rig, C-type geometry

Geometry Data	**Gear**	
	Pinion 1	Wheel 2
Number of Teeth, z [-]	16	24
Module, m [mm]	4.5	
Center Distance, a [mm]	91.5	
Pressure angle, α [°]	20	
Face Width, b [mm]	14	
Addendum Modification, x [-]	+0.1817	+0.1715
Bore Hole [mm]	30	
Normal Backlash [mm]	0.224	
Material	POM	

The standard VDI 2736, only makes some changes in the equations for calculating the load carrying capacity referring the ISO 6336 and DIN 3990 for the general aspects of the load carrying capacity. In this manner, this section can use the considerations and evaluation methods of Section 4.2.

The FEM mesh used for the simulations is in Table 4.11, but more groups are added to represent the boundary conditions needed for the thermal model implementation. These groups are resumed in Figure 3.11.

For simplification in naming the FEM models used, and since in the thermo-mechanical model, the thermal model can be coupled with two different mechanical model it is adopted the following references:

- The thermo-mechanical model that couples the thermal model with the mechanical contact model is named Thermo-Contact model
- The thermo-mechanical model that couples the thermal model with the mechanical contactless model is named Thermo-Contactless model

Mesh Convergence

In order to study the best mesh for the Thermo-Contactless the tooth root stress was evaluated for a set of meshes, as follows in Table 4.10. It was considered a torque value of 10 Nm.

Table 4.10: FEM Mesh refinement convergence

Mesh	Tooth root Stress [MPa]	Maximum Temperature [°C]
Elements 85 691 Nodes 21 006	3.6	140.5
Elements 148 339 Nodes 32 892	3.6	143.5
Elements 318 871 Nodes 44 688	5.4	142.8
Elements 465 847 Nodes 94 111	5.2	142.0

It is then concluded that the mesh with 318 871 elements can be used to access load carrying capacity for this simulation.

Table 4.11: FEM Mesh detail

Mesh Parameter	Step 1 and 2 Thermo-Contact model	Step 3 Thermo-Contact model	Thermo-Contactless model
Maximum size [m]$\times 10^{-2}$	2.25259	2.25259	1.17422
Minimum size [m]$\times 10^{-4}$	2.49936	2.49936	0.111522
Mesh Fineness	Moderate	Moderate	Fine
Local size master surface [m]$\times 10^{-4}$	0.35	3.6	0.65
Local size slave surface [m]$\times 10^{-4}$	0.34	3.5	0.65
Total number elements	487 923	245 937	318 871
Total number nodes	107 734	26 823	44 688
Figure	4.2	4.3	4.4

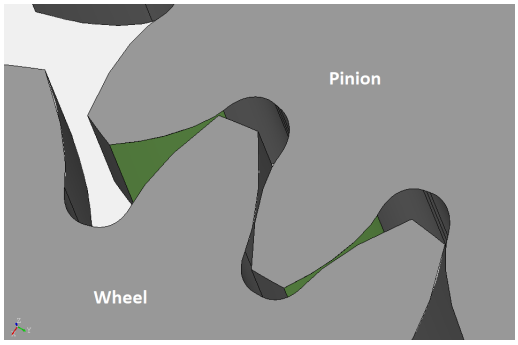

(a) Slave surface

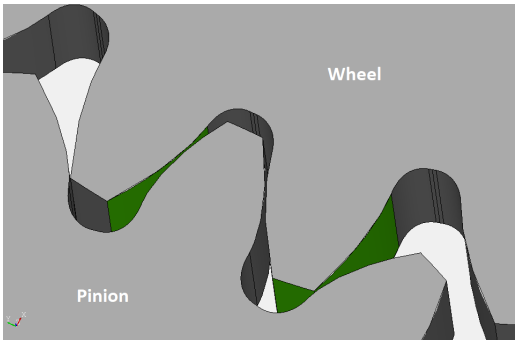

(b) Master surface

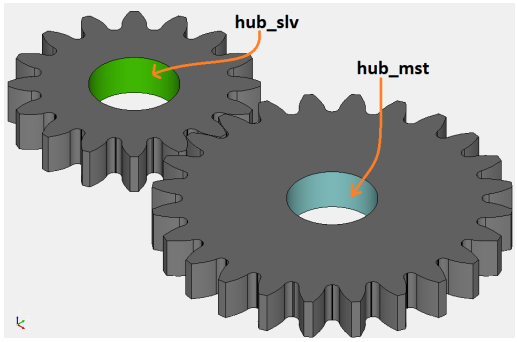

(c) Hub surfaces

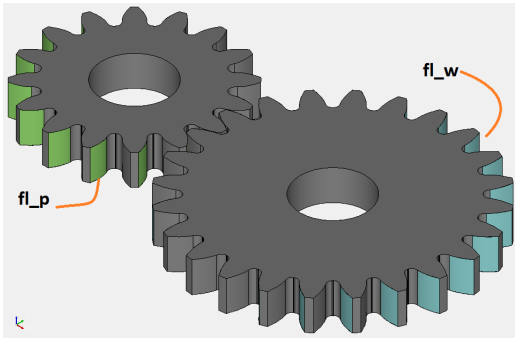

(d) Every Meshing surface **m**, *DFLUX

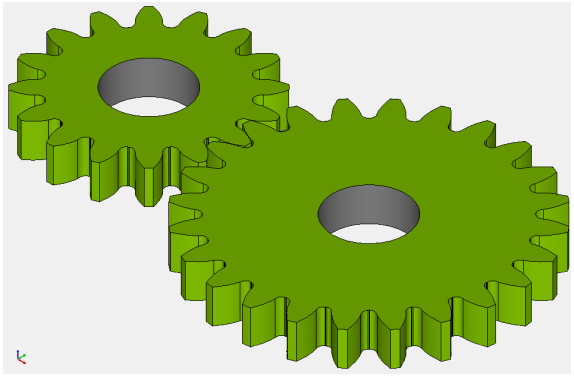

(e) Every surface except hub, *FILM

Figure 4.12: Groups of surfaces for the boundary conditions

The Young modulus and Poisson's ratio were essentially the only parameters considered as mechanical properties with temperature dependence, and the standard details this dependence with the graph provided in figure 4.13 and the equation used for the calculation of the Poisson's ratio in (4.4). The mechanical and thermal properties used are resumed in Table 4.12. The loading and testing conditions are described in Table 4.13.

Table 4.12: Mechanical and thermal properties of POM gears

Mechanical, Thermal Properties	**POM**
Young's Modulus, E [GPa]	Temperature dependent Fig.4.13
Young's Modulus at 23°C, E_0 [GPa]	2.9
Poisson's ratio, ν [-]	Temperature dependent Eq.(4.4)
Poisson's ratio at 23°C, ν_0 [-]	0.435
Density, ρ [kg/m^3]	1410
Thermal conductivity, K [$W\,/\,(m\,K)$]	0.3
Specific Heat, c_p [$J\,/\,(kg\,K)$]	1470
Coefficient of thermal expansion [$°C^{-1}$]	$13.8{\times}10^{-5}$

Table 4.13: Operating conditions tested with the FEM simulation

Loading conditions	**Torque** of the pinion hub [N·m]	**Rotational Speed**, ω [rpm]	**Ambient Temperature** [°C]
A	7.5	1000	15
B	10.0	1000	15
C	10.75	1000	15

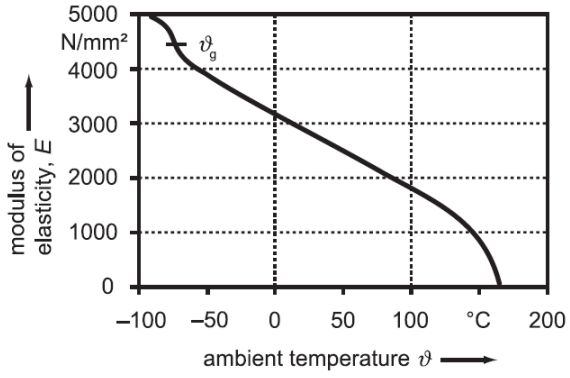

Figure 4.13: Young Modulus dependence of temperature in POM [1]

$$\nu = \nu_0 + (0.5 - \nu_0)\left(1 - \frac{E}{E_0}\right) \quad [1] \tag{4.4}$$

For the FEM model only a few temperature points were taken from Figure 4.13 and thus also those in equation (4.4). The temperature points are read in the Calculix CCX,

and for intermediate temperature points, the software considers a linear interpolation between two points. In this manner, the temperature points considered and their respective Young's Modulus and Poisson's ratio are displayed in Table 4.14.

Table 4.14: Temperature points with different Young Modulus and Poisson ratio considered

	T_1	T_2	T_3	T_4	T_5	T_6	T_7	T_8	T_9
Temperature [°C]	0	20	40	60	80	100	120	140	160
Young Modulus [GPa]	3.1	2.9	2.6	2.4	2.1	1.8	1.5	1.1	0.5
Poisson ratio [-]	0.43	0.44	0.44	0.45	0.45	0.46	0.47	0.48	0.49

4.3.1 Tooth root Stress

It is used the same method for evaluating the tooth root stress as described in Section 4.2.1.

However, regarding the Thermo-Conctacless model, evaluating the tooth root stress with the outer and inner point of contact of two teeth resulted in significant error. To emend this error, instead of considering two teeth in contact, it was considered only one tooth in contact in the outer most point (D), increasing tooth root stress value evaluated.

The penalty coefficient was adjusted in the same manner as before in 4.2.1, but adjusted for the torque value of 10 $N \cdot m$ and resulted in the same five thousand times the Young Modulus (5000*E), using as a reference the lower value of the Young's Modulus presented in Table 4.14.

Using the concept of evaluation of the tooth root stress, the implementation of the simulation as described in Table 4.15 and for the operating conditions described in 4.13, results in Figure 4.14. The CCX code used for this FEM model implementation is described in Appendix C.1 and C.3.

Table 4.15: Simulation for evaluation of the tooth root stress, contact stress and tooth flank stress for POM

	Thermo-Contact Model	**Thermo-Contactless Model**
Boundary	Wheel Fixed Pinion with Torque	Line in Pinion fixed (Outer point of contact fixed) Pinion with Torque
Mesh	Step 1 and 2 Thermo-Contact model Fig. 4.2	Thermo-Contactless model Fig. 4.4
Penalty coefficient [GPa]	2500 (5000*E)	-
Coefficient of friction, μ [-]	0	-

The results obtained also include temperature measurements compared to the works of [15] and [24], and are as follows in the following Figure 4.14 and table 4.16, and with its respective differences in percentages in Table 4.17.

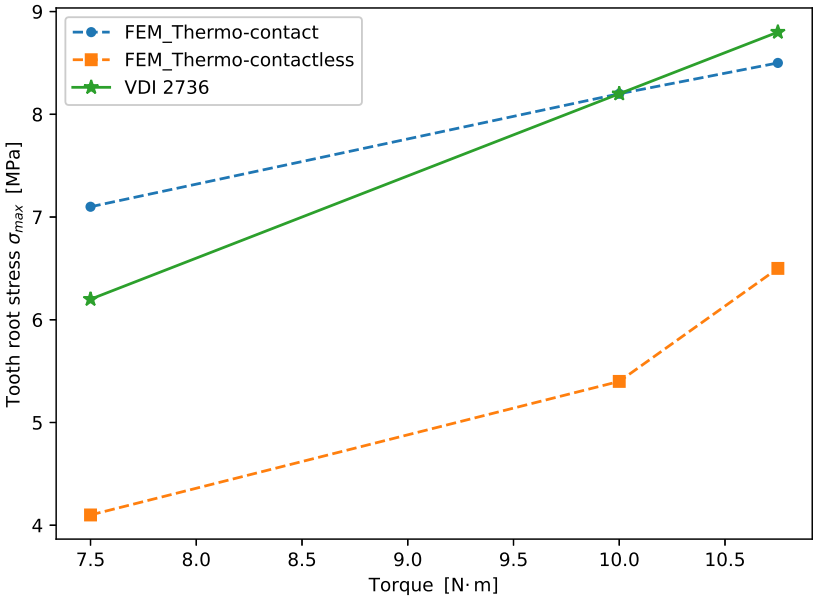

Figure 4.14: Tooth root stress for the mechanical models and standard

The error that is seen for the Thermo-Contactless and the Thermo-Contact models, can also be the result of the mesh that isn't as fine as that of paper [24].

Table 4.16: Temperature results for torque = 10 Nm

T [°C]	**FEM Thermo-Contact**	**FEM Thermo-Contactless**	**Paper** [24]
Maximum temperature	145.1	142.8	139.4
Temperature at maximum tooth root stress	53.6	42.8	-

Table 4.17: Errors in [%] of the results of tooth root stress comparing with VDI 2736

Loading conditions	**FEM Thermo-Contact**	**FEM Thermo-Contactless**
7.5 N·m	14.5	33.9
10 N·m	0.0	34.1
10.75 N·m	3.4	26.14

4.3.2 Contact Stress

Using the same simulation description of Table 4.15, and considerations for the evaluation of contact stress of Subsection 4.2.2, it was obtained the following results of Figure 4.16. The CCX code used for this FEM model implementation is described in Appendix C.1.

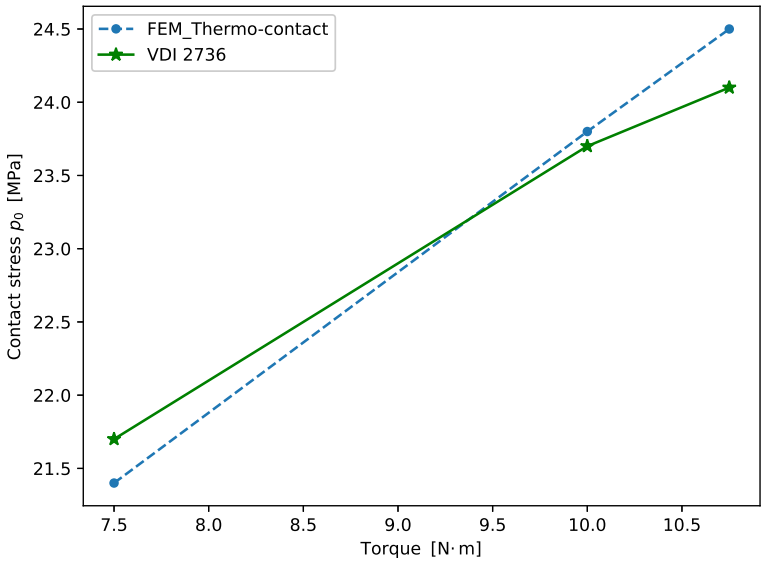

Figure 4.15: Contact stress at point D of contact path for the pinion

With the contact pressure obtained with the FEM model with contact, the maximum and octahedral shear stress can be calculated in equation (4.5).

$$\begin{aligned} \tau_{shear\ max} &= 0.3\, p_0\,, \text{ with } \mu = 0 \\ \tau_{shear\ oct} &= 0.272\, p_0\,, \text{ with } \mu = 0 \end{aligned} \tag{4.5}$$

The errors using the FEM with contact model and comparing with the standard VDI 2736 are 2.38%, 0.42% and 1.66% for the torque values of 7.5, 10 and 10.75 N·m, respectively.

4.3.3 Tooth flank Stress

Using the same simulation description of Table 4.15, and considerations for the evaluation of tooth flank stress of Subsection 4.2.3, it was obtained the following results of Figure 4.16. It is also plotted the calculated values of tooth flank stress using the contact stress values obtained from the previous section and equation (4.5).

The CCX code used for this FEM model implementation is described in Appendix C.1. The equation that was used to calculate maximum shear stress is in (4.6).

$$\tau_{shear\ max} = 0.5 \times (\sigma_1 - \sigma_3) \tag{4.6}$$

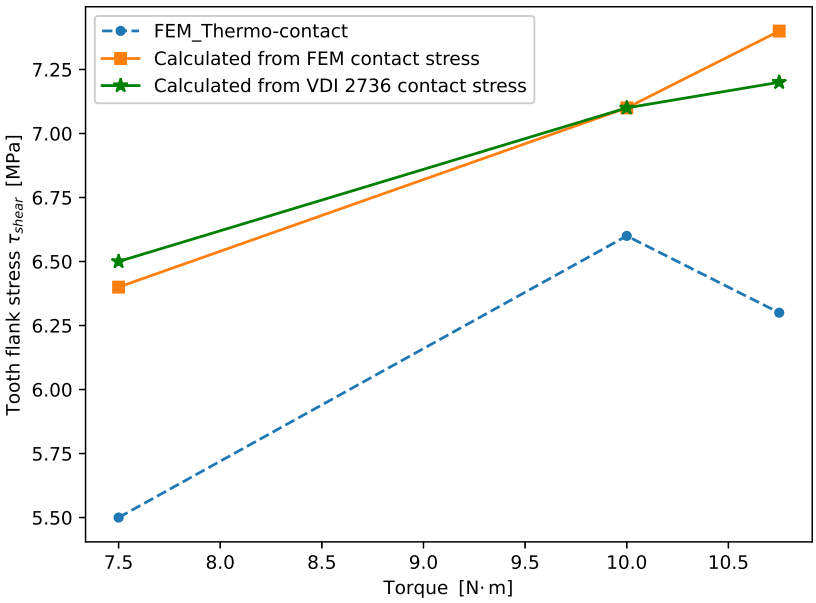

Figure 4.16: Tooth flank stress for the mechanical models

The results show a lower error for the torque value that the penalty coefficient was adjusted to. It also demonstrates that it is more reliable to measure contact stress and obtain from it tooth flank stress than using equation (4.6) and then measuring directly.

Table 4.18: Errors in [%] of the results of tooth flank stress comparing with the calculated value of tooth flank stress using VDI 2736

Loading conditions	**Calculated value FEM**	**FEM Thermo-Contact**
7.5 N·m	1.5	1.5
10 N·m	0.0	7.0
10.75 N·m	2.8	12.5

4.3.4 Mesh Stiffness

Using the simulation that is summarized in Table 4.19, considerations for the evaluation of mesh stiffness of Subsection 4.2.4, and the twist values and rotation of the pinion as in Table 4.20, it was obtained the results of Figure 4.17.

The equation that was used for calculation the mesh stiffness is described in (4.7). The CCX code used for this FEM model implementation is described in Appendix C.2.

$$\begin{aligned} \gamma_w &= -\frac{\gamma_p}{g_r} + \gamma_t \\ k_g &= \frac{4\,T}{\gamma_t\,(d_2\,cos\,\alpha)^2} \end{aligned} \tag{4.7}$$

Table 4.19: Simulation for evaluation of the mesh stiffness for POM

	Thermo-Contact Model
Boundary	Wheel Rotating with γ_w Pinion Rotating with γ_p
Mesh	Step 3 Thermo-Contact model Fig. 4.3
Penalty coefficient [GPa]	250 (500*E)
Coefficient of friction, μ [-]	0

Table 4.20: Rotational boundary conditions simulated with the FEM simulation

Rotational Boundary Conditions	**Rotation twist value, γ_t [°]**	**Pinion Rotation Interval**
A	0.4	from 0° to 40°
B	0.5	from 0° to 40°
C	0.6	from 0° to 40°

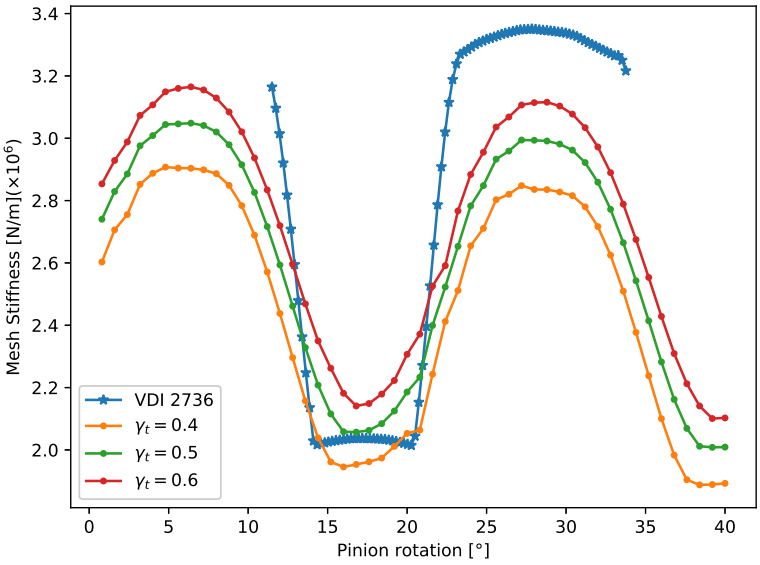

Figure 4.17: Mesh stiffness for the mechanical model with contact and standardn

As seen before, the increase in the angular twist leads to a higher mesh stiffness, and for an angular twist that agrees with the standard the resulting torque torque range is still high, in the range of 30 Nm. The penalty value for this test was the same 500*E, for the lower Young modulus value presented in Table 4.14.

4.4 Conclusion

The FEM models for steel were simulated using mechanical FEM models. Both the contact and contactless mechanical models presented after evaluation of the results low error when compared to the standard ISO 6336. The error tended to be less for the torque value that was used for adjusting the penalty coefficient. For the parameters of load carrying capacity that required evaluation of the contact area the Contactless model couldn't produce comparable results. It is concluded that the mechanical models are well adjusted and validate the Standard ISO 6336.

The FEM models for polymer gears were simulated using thermo-mechanical models, having been used the thermal model coupled the Contact model (thermo-contact model) and the thermal model coupled the Contactless model (thermo-contactless model). It was also verified lower error for the torque value that was used for adjusting the penalty coefficient. Despite the fact that the error with the Thermo-Contactless model compared to the guideline VDI 2736 was relatively high, it is believed to be because of the refinement of the mesh that couldn't be bettered (due to limited computational resources). This refinement of the mesh was determinant, because the result value varied a lot and is very sensitive to the refinement. Hence, it is concluded that the thermo-mechanical model are validated and agree with the guideline VDI 2736.

In general, the mechanical models produced lower error compared to the standard-/guideline and were less sensitive to penalty coefficient adjustments than the thermo-mechanical models. A more detailed analysis of the thermo-contactless model comparing its results with other standards' results could produce other conclusions, since there is still a slight divergence of results between the different standards and guidelines. It is then concluded that all the models discussed are in this manner validated and fit for simulating other polymer gear's solutions.

Chapter 5

FEM of the Hybrid Gear Pair

5.1 Introduction

In this chapter further development of the polymer gears with metallic inserts will be conducted in what regards thermo-mechanical behaviour. Several geometries of metallic inserts are going to be studied, evaluating for each one stress and temperature and comparing solutions.

Temperature is going to be an important factor to consider when comparing load carrying capacity of the tooth root stress, since maximum yield stress also varies with temperature and so, a solution with lower tooth root stress than another, if having with it higher temperature (and lower yield strength), can result in the worst solution.

A better way for comparison should be with safety factors (the tooth root stress divided by the yield strength), but the dependence of the temperature with the yield strength must be also known. This equation hasn't been found, since very few to no studies regarding this topics were published and even the standard VDI 2736 just presents fatigue strength under pulsating stress, noting that this yield strength doesn't depend only on temperature but also with other parameters such as deformation hysteresis and others.

This chapter will focus on firstly introducing the concept of a type of hybrid gears and the geometries and materials to be studied, followed by describing the influence of geometry variances on the tooth root stress and loading, the influence of material's thermal conductivity on tooth root stress, fully characterizing the deformations and tensions in the loaded tooth and insert interface and finally the optimization process and proposed solution.

5.2 Hybrid gear concept

This type of hybrid gear consists of a polymeric gear, with a metallic insert within the polymeric matrix, see Figure 5.2. The main objective is to combine in a gear set the main advantages of a polymer gear like low weight or good tribological behaviour under dry run with the thermal and mechanical properties of metallic insert. In this manner, the metallic inserts will help the polymer evacuate heat from the meshing surface and lowering the operating temperature. However, the structural behaviour of the gear set should be studied.

Metallic inserts are distributed equally for each tooth, being symmetrical in each tooth and in the gear set. An example of this gear set, is represented by the pinion, in Figure 5.2. This Figure displays simple plate concept and a T plate concept inserts with both fixed inserts and floating inserts.

The influence on temperature of some geometric parameters such as width of the insert (w), gap between insert and polymer body (e) and distance between tooth tip and insert (t) were studied in [15]. These parameters are displayed in Figure 5.1.

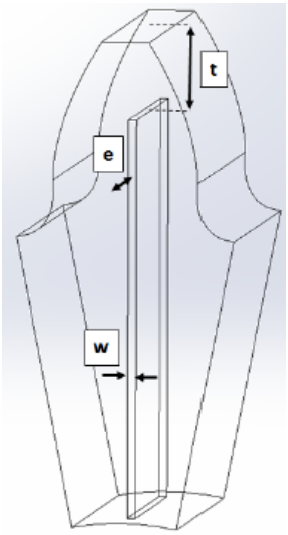

Figure 5.1: Hybrid gear geometric variables [15]

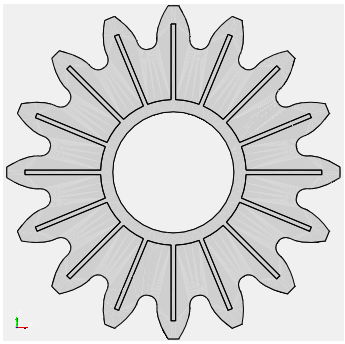

(a) Simple plate, fixed inserts

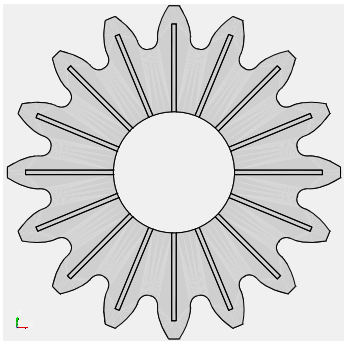

(b) Simple plate, with floating inserts

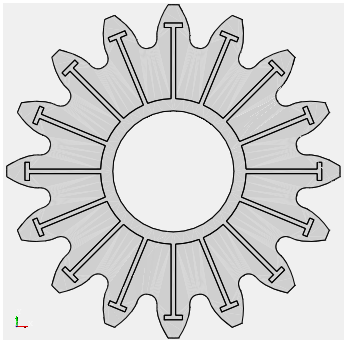

(c) T plate, with fixed inserts

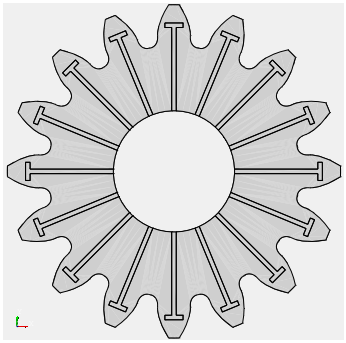

(d) T plate, with floating inserts

Figure 5.2: Example of hybrid gear

5.3 Hybrid gear geometries

In this chapter the following geometric parameters are studied: width of the insert (w); filleting of the edges of the insert in contact with the polymer gear and also fixed and floating inserts. Then, the following variables for the geometry of the inserts are studied throughout the next sections:

- The distance (t), Figure 5.1 and 5.3 between the tooth tip and the insert is constant and equal to the module of gear
- The width of the vertical plate and the width of the horizontal plate in the T shape insert is the same, when T plate inserts are used. (w=w) Figure 5.3
- The width (w) can be equal to 1/4 or 1/2 of the module of the gear Figure 5.1 and 5.3
- The length of the horizontal plate for the T shaped inserts is constant and equal to the module of the gear (L=m) Figure 5.3
- When fixed inserts are used, the bore hole is the same as the with the other geometries.
- The thickness of the ring when called for is constant and equal to 3mm, Figure 5.3
- The gap between insert and polymer (e) is zero Figure 5.1
- The junction between the horizontal plate and vertical plate in the T shaped insert is never filleted. The junction between insert (whichever) and ring can be filleted Figure 5.3
- The plate type can either be simple plate or T plate Figure 5.2
- The corners of the insert in contact with the polymer are either filleted or not
- The radius of the fillet is either equal to 1mm for width of plate of 1/2module or equal to 0.5mm for width of plate of 1/4module (Rd) Figure 5.3

The gear tooth parameters are based in a C14 type polymer gear as described in Table 5.1. From the variables described above, there can be listed four different geometric variants of the gear. These consist of the plate type, the type of insert, the type of corners and the thickness of the insert.

Since each attribute will have two values, it adds up to sixteen different geometries as described in Figure 5.4. This Figure also presents a code system to identify each insert geometry.

It is displayed only one tooth in Figures 5.5 and 5.6, as detail of the geometry of the insert in display for better comprehension of the resulting geometries, considering Figure 5.4 and what was described above.

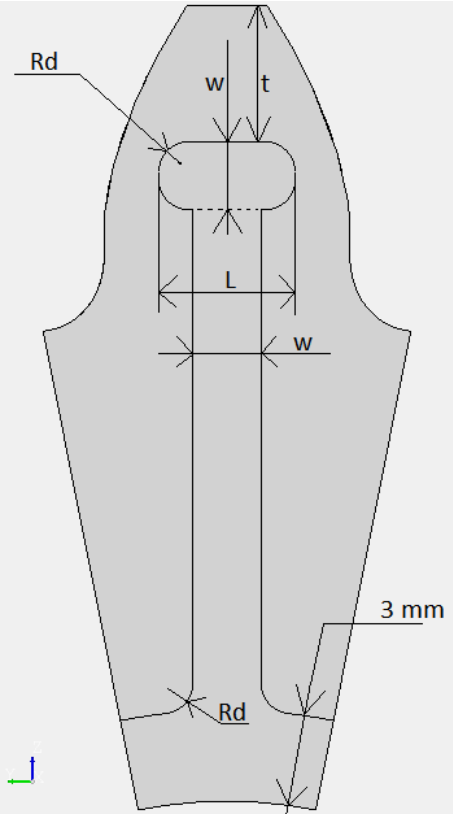

Figure 5.3: Measures for the Geometric variables

Table 5.1: FZG back-to-back gear test rig, C-type, Geometry

Geometry Data	**Hybrid Gear**	
	Pinion 1	Wheel 2
Number of Teeth,z [-]	16	24
Module, m [mm]	4.5	
Center Distance, a [mm]	91.5	
Pressure angle, α [°]	20	
Face Width, b [mm]	14	
Addendum Modification, x [-]	+0.1817	+0.1715
Bore Hole [mm]	30	

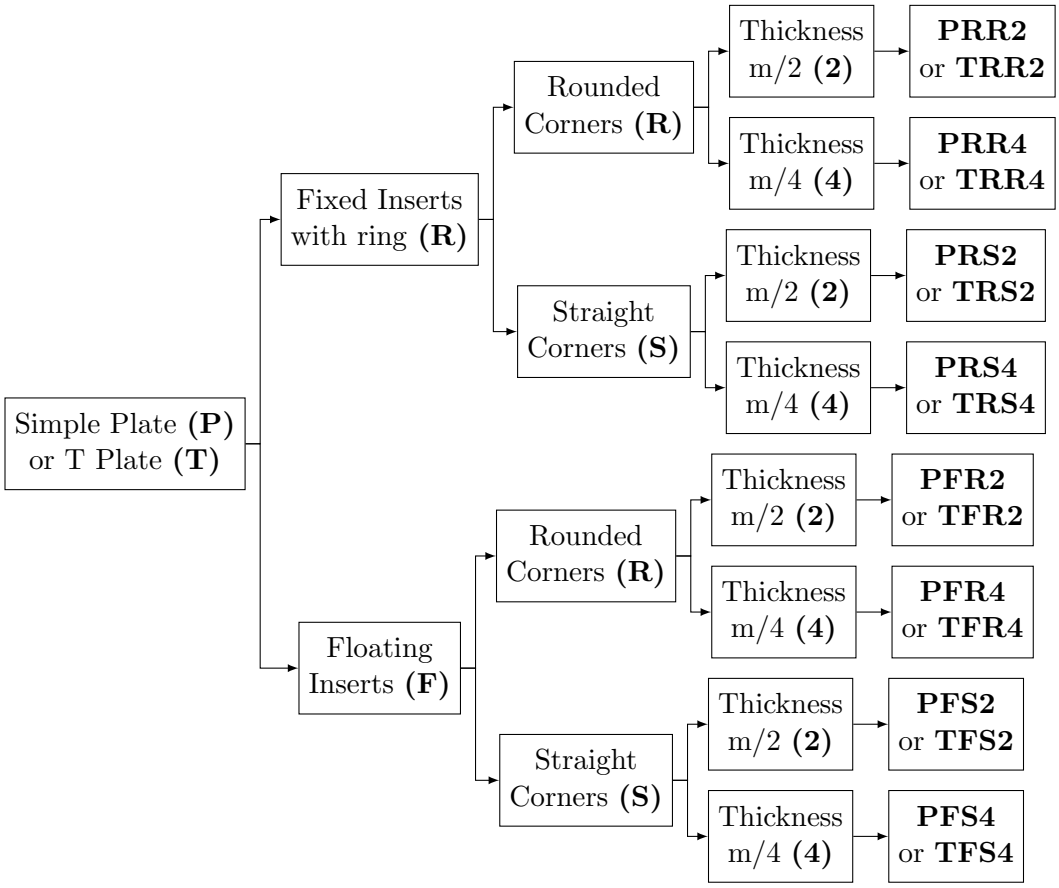

Figure 5.4: Geometric variances

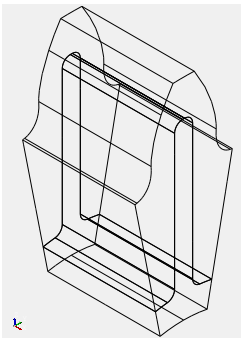

(a) Geometry PRR2

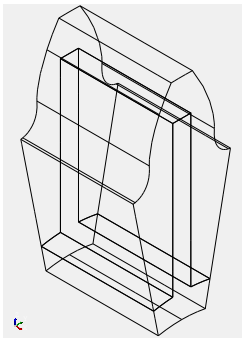

(b) Geometry PRS2

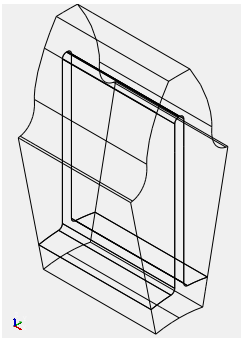

(c) Geometry PRR4

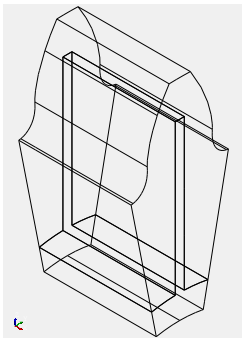

(d) Geometry PRS4

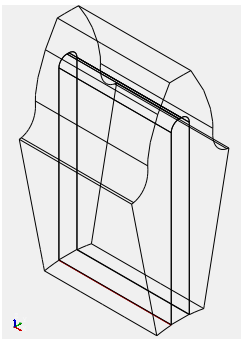

(e) Geometry PFR2

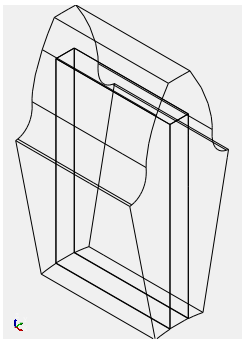

(f) Geometry PFS2

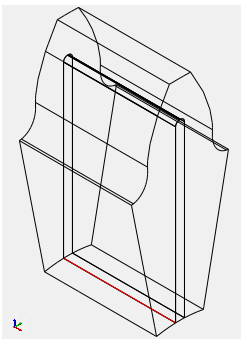

(g) Geometry PFR4

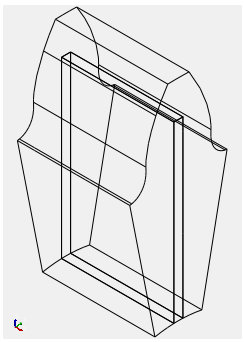

(h) Geometry PFS4

Figure 5.5: Detail of the simple plate inserts

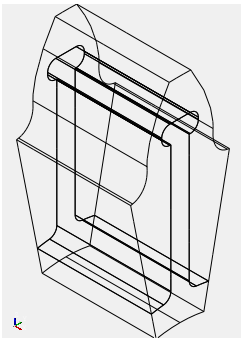

(a) Geometry TRR2

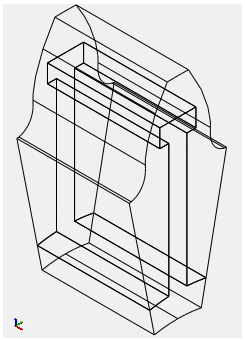

(b) Geometry TRS2

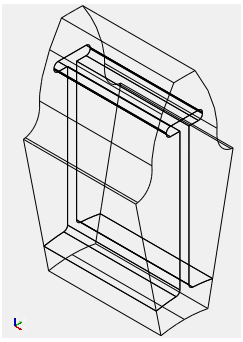

(c) Geometry TRR4

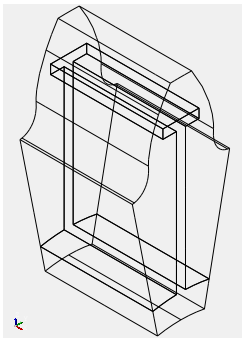

(d) Geometry TRS4

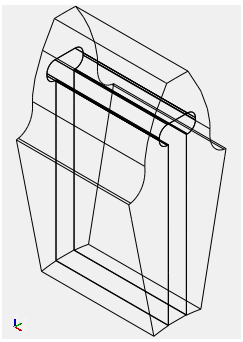

(e) Geometry TFR2

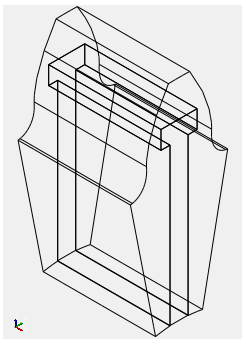

(f) Geometry TFS2

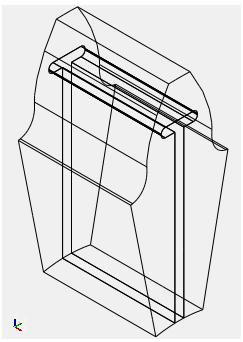

(g) Geometry TFR4

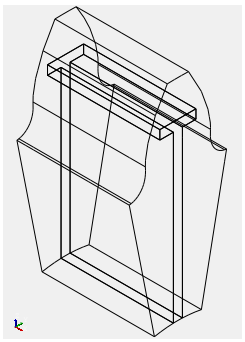

(h) Geometry TFS4

Figure 5.6: Detail of the T plate inserts

5.4 FEM model

For the simulation of the hybrid gears a new type of contact must be defined, and it takes place in the interface between the polymer body and the metallic insert. It's represent by the CCX code *Tied, and it ties the surfaces together with a surface to surface contact algorithm, essentially bonding them.

It must be used with friction, but it referred in the book [20] that its value is irrelevant in the result. For this FEM model it also had be to defined what is called the gap conductance, which stands for the conductance coefficient or ability to conduct heat between two bodies in contact.

This parameter can be defined for certain values of contact pressure and temperature in the contact interaction. The conductance coefficient was defined in this FEM model for a material interface of POM/Aluminium and for a contact pressure of 25 [MPa], which results in a coefficient equal to 17563.08 $[W/m^2K]$ [15].

The CCX code that was used for simulating the hybrid gears and follows what is described in this section is in Appendix D.1.

5.4.1 Boundary Conditions

The boundary conditions are established based on what was already discussed in the validation Chapter 4, for polymer gears using the Thermo-Contactless. In this Chapter for hybrid gears, this Thermo-Contactless model is going to be the only used and as such it follows the boundary conditions described in Table 5.2 and the groups of surfaces in the mesh used for boundary conditions in Figure 5.7.

Table 5.2: Boundary conditions

	Thermo-Contactless Model
Boundary	Line in Pinion fixed (Outer point of contact fixed) Pinion with Torque

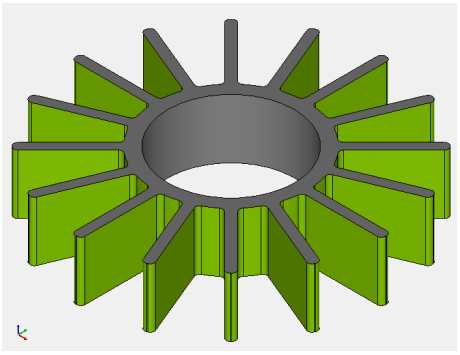

(a) All of the surfaces insert in contact, master

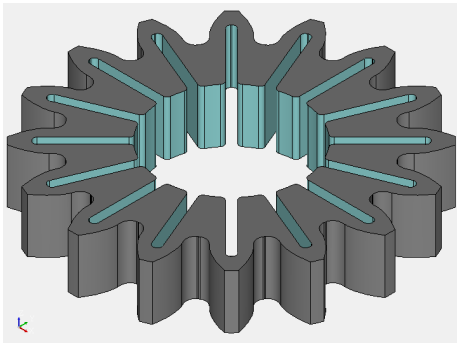

(b) All of the surfaces pinion in contact, slave

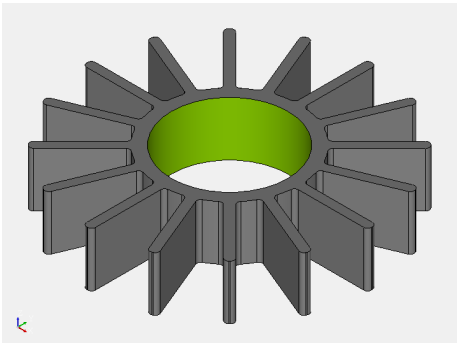

(c) Hub surface, for fixed inserts

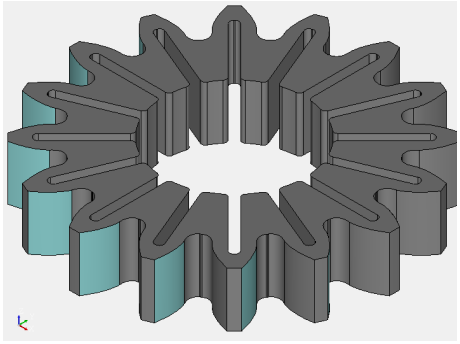

(d) Every Meshing surface **m**, *DFLUX

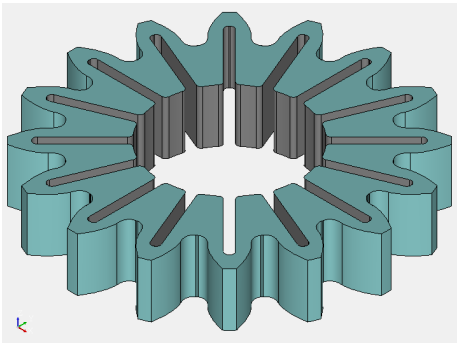

(e) Every surface except contact elements, *FILM

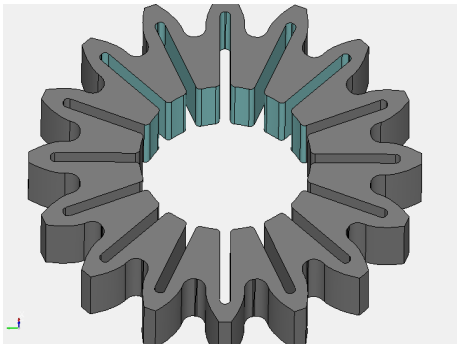

(f) Local size for the mesh in the pinion

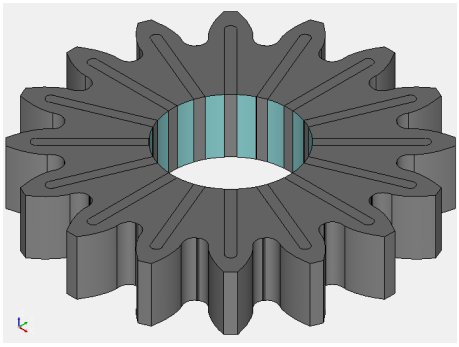

(g) Hub surface, for floating inserts

Figure 5.7: Groups of surfaces in the mesh for the boundary conditions

5.4.2 Mesh

The mesh generation process for the hybrid gears is based in the mesh used in the Chapter 4 and follows what is described in Chapter 3, but this time besides the local mesh in the contact area, a local refinement in the five inserts closest to the contact area was done. The intention is to refine those inserts since it is expected to be those with higher stress and deformations.

An example of the mesh obtained for the geometry PRR2, with its element distribution and its local sizes are presented in Figure 5.8. The values for the number of elements and nodes obtained with each mesh generated is displayed on Table 5.3.

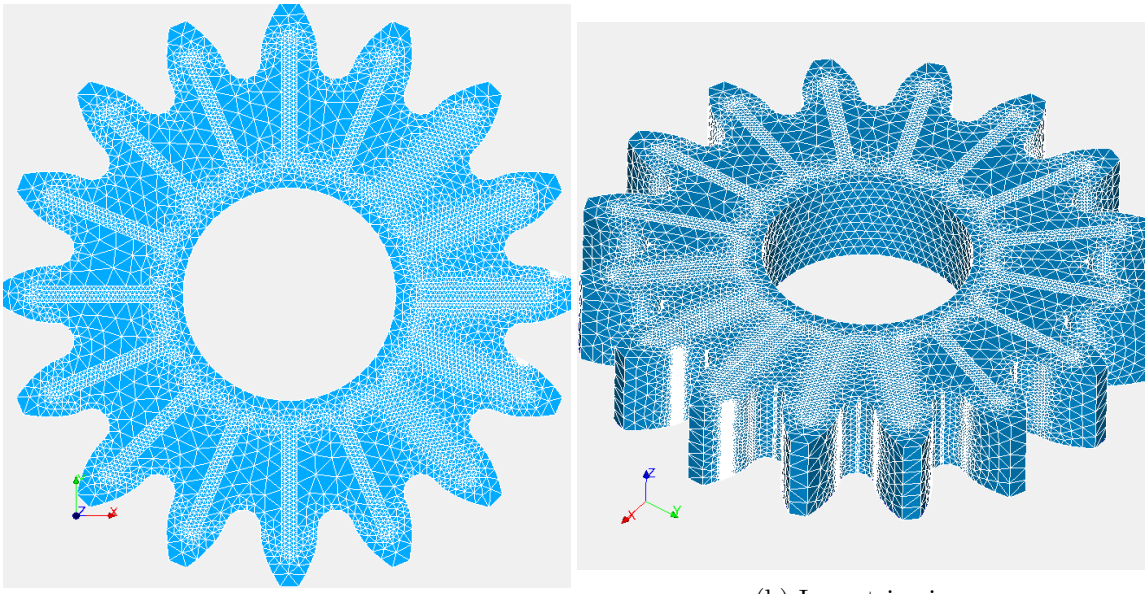

(a) Front view

(b) Isometric view

Figure 5.8: Hybrid Mesh example, using the PRR2 geometry

Table 5.3: Number of Elements and nodes of the resulting mesh for the hybrid geometries, using 4-node tetrahedron elements (C3D4)

Elements and nodes in the mesh		
Geometry reference	**Elements**	**Nodes**
PRR2	457 621	102 099
PRR4	648 505	158 088
PRS2	234 223	60 281
PRS4	256 527	67 012
PFR2	294 682	75 135
PFR4	445 882	110 528
PFS2	242 600	61 897
PFS4	346 582	89 807
TRR2	456 436	101 861
TRR4	798 230	195 109
TRS2	245 750	63 875
TRS4	267 315	70 995
TFR2	424 498	97 429
TFR4	656 015	166 303
TFS2	246 826	64 927
TFS4	265 841	71 976

5.4.3 Material Properties

The material for the polymer body of the gear is going to be POM and its properties are the same as those used in Section 4.3 and they are in Table 5.4. That also describes the properties of the material considered for the inserts which is aluminum.

For the temperature dependent properties it was used the same values displayed in Table 5.5.

The weight was calculated for each gear geometry, using the density provided in Table 5.4 and the volume predicted using the capabilities of the CAD software Salome, for each geometry is displayed in Table 5.6.

Table 5.4: Mechanical and thermal properties of hybrid gears

Mechanical, Thermal Properties	**POM Gear**	**Aluminum Insert**
Young's Modulus, E [GPa]	Temperature dependent	69
Young's Modulus at 23°C, E_0 [GPa]	2.9	69
Poisson's ratio, ν [-]	Temperature dependent	0.33
Poisson's ratio at 23°C, ν_0 [-]	0.435	0.33
Density, ρ [kg/m^3]	1410	2702
Thermal conductivity, K [$W\,/\,(m\,K)$]	0.3	237.0
Specific Heat, c [$J\,/\,(kg\,K)$]	1470	903
Coefficient of thermal expansion [$^{\circ}C^{-1}$]	13.8×10^{-5}	22.5×10^{-6}

Table 5.5: Temperature points with different Young Modulus and Poisson ratio considered

	T_1	T_2	T_3	T_4	T_5	T_6	T_7	T_8	T_9
Temperature [°C]	0	20	40	60	80	100	120	140	160
Young Modulus [GPa]	3.1	2.9	2.6	2.4	2.1	1.8	1.5	1.1	0.5
Poisson ratio [-]	0.43	0.44	0.44	0.45	0.45	0.46	0.47	0.48	0.49

In Table 5.6, the geometries that presented an increase in weight compared to the standard polymer superior to 25% are underlined, and the geometries that weigh 15% or less are in bold. Has it can be seen, five geometries exceeded the 25% mark, PRR2, PRS2, PFR2, TRR2 and TRS2 and four geometries weigh less than 15%, PFR4, PFS4, TFR4 and TFS4.

Table 5.6: Total weight of hybrid gears geometries and its difference compared to standard polymer gears

Weight evaluation [g]				
Geometry reference	Polymer Weight	Insert Weight	Total Weight	Difference in Weight [%]
PRR2	48.495	37.220	85.715	+26.2
PRR4	55.130	24.506	79.636	+17.3
PRS2	48.468	37.273	85.741	+26.2
PRS4	55.126	24.513	79.639	+17.3
PFR2	52.609	29.317	81.926	+29.5
PFR4	60.319	14.559	74.878	**+10.2**
PFS2	52.474	29.577	82.051	+20.8
PFS4	60.199	14.789	74.988	**+10.4**
TRR2	47.032	40.024	87.056	+28.2
TRR4	53.965	26.739	80.704	+18.8
TRS2	46.869	40.337	87.206	+28.4
TRS4	53.927	26.811	80.738	+18.9
TFR2	51.146	32.122	83.268	+22.6
TFR4	59.150	16.801	75.151	**+11.8**
TFS2	50.875	32.641	83.516	+23.0
TFS4	59.000	17.087	79.087	**+12.0**

5.5 Influence of geometry

The geometry of the gear pair is presented in Table 5.1, and the geometries here studied are the ones described in Section 5.3. The FEM model applied for the hybrid gears is described in Section 5.4.

The results for the tooth root stress and respective temperature evaluated for the loading conditions of Table 5.7, produces what is displayed in Figures 5.9 and 5.10.

Table 5.7: Operating conditions tested

Loading conditions	**Torque** of the pinion hub [N·m]	**Rotational Speed**, ω [rpm]	**Ambient Temperature** [°C]
A	10.0	1000	15

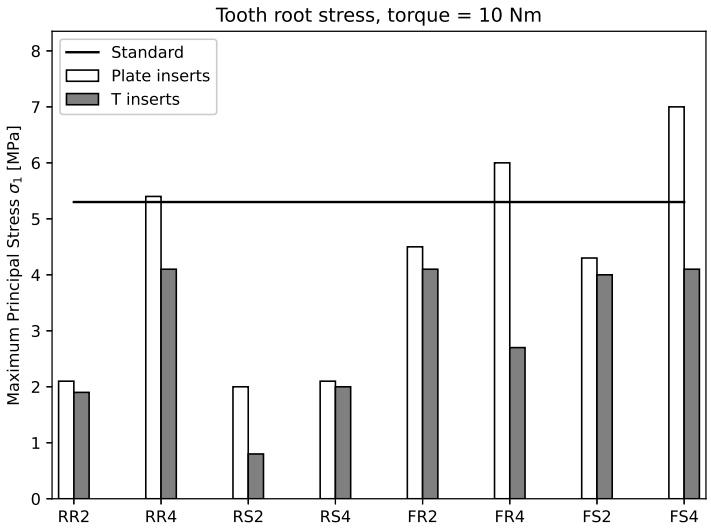

Figure 5.9: Tooth root stress for hybrid gears

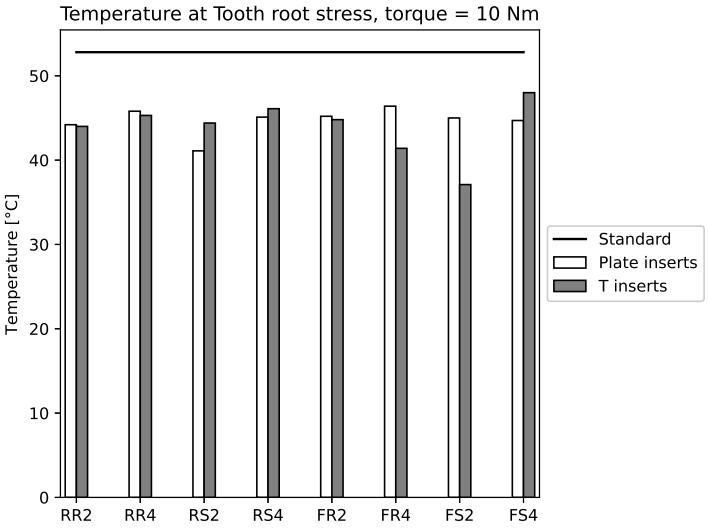

Figure 5.10: Temperature at maximum Tooth root stress for hybrid gears

The temperature values for the lowest tooth root stress geometries (PRR2*, PRS2*, PRS4, TRR2*, TRS2* and TRS4) don't vary much, and in this manner these can be considered the best geometries solution. The geometry TRS2 had the lowest tooth root stress, but this geometry has an increase in weight compared to the standard gear of over 25%. In the same way, considering weigh comparison with standard polymer gear only the PRS4 and TRS4 can be considered good overall options.

Every temperature value is lower than what was found in subsection 4.3.1 for the standard polymer gear, but for the simple plate geometries PRR4, PFR4 and PFS4 the tooth root stress is higher than that of the polymer gear. However, these solutions can't be ruled out since a lower temperature at maximum tooth root stress could still make them better options.

Pareto plot is a type of chart that measures frequency of occurrence of a set of attributes for a unit of measure. It is going to be used to study the magnitude of effect of the different types of geometric variants already described in 5.3, using the tooth root stress results for evaluation.

The variables used in the Pareto Plots are, **plate type** (x_P), **thickness** (x_T), **Fixed (with ring)** (x_R) and **radius** (x_{Rd}) and have to be defined, by giving for each geometry a variable value of either a positive one (+1) or negative one (-1). Using a full factorial design for the simulations, $2^4 = 16$ simulations are presented in Table 5.8, following a standard order. It also results in the following attributions:

- Plate type: simple plate, $x_P = -1$; T plate, $x_P = +1$
- Ring: Floating, $x_R = -1$; Fixed, $x_R = +1$
- Radius: without filleting (straight corners), $x_{Rd} = -1$; with filleting (rounded corners), $x_{Rd} = +1$
- Thickness: equal to a quarter of the module, $x_T = -1$; equal to half of the module, $x_T = +1$

Table 5.8: Variable values of the hybrid geometries

Geometric variables				
Geometry reference	x_T	x_{Rd}	x_R	x_P
PRR2	+1	+1	+1	-1
PRR4	-1	+1	+1	-1
PRS2	+1	-1	+1	-1
PRS4	-1	-1	+1	-1
PFR2	+1	+1	-1	-1
PFR4	-1	+1	-1	-1
PFS2	+1	-1	-1	-1
PFS4	-1	-1	-1	-1
TRR2	+1	+1	+1	+1
TRR4	-1	+1	+1	+1
TRS2	+1	-1	+1	+1
TRS4	-1	-1	+1	+1
TFR2	+1	+1	-1	+1
TFR4	-1	+1	-1	+1
TFS2	+1	-1	-1	+1
TFS4	-1	-1	-1	+1

Using the values of the tooth root stress of Figure 5.9, the definition of variables in Table 5.8 and the R code of Appendix D.2, as input in RStudio it was obtained the following Pareto plot in Figure 5.11.

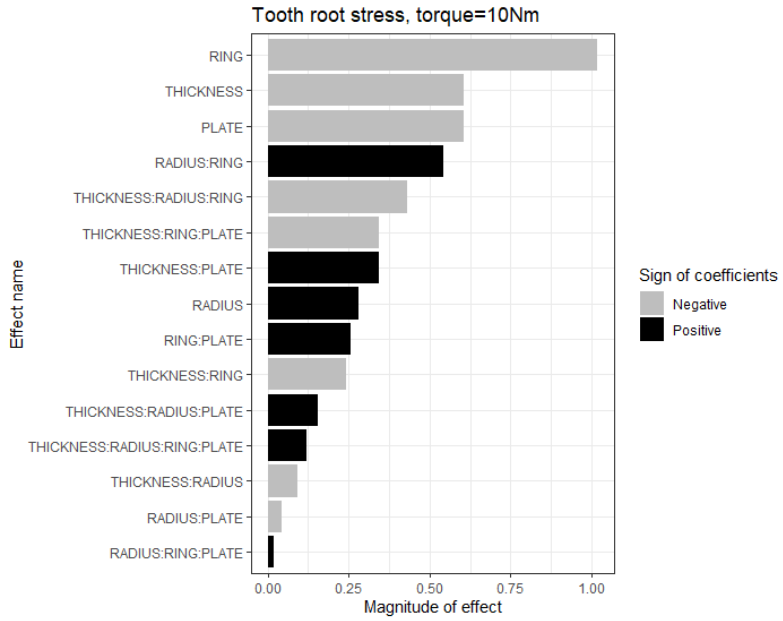

Figure 5.11: Magnitude of effect of plate type, thickness of plate, insert type and filleting of corners on the tooth root stress

In Figure 5.11, the equation that was calculated by RStudio and enabled the plotting of this graph is displayed in (5.1).

$$\begin{aligned}\text{Tooth Root Stress} = 3.57 &- 0.61\,x_T + 0.28\,x_{Rd} - 1.02\,x_R - 0.61\,x_P \\ &- 0.09\,x_T\,x_{Rd} - 0.24\,x_T\,x_R + 0.54\,x_{Rd}\,x_R + 0.34\,x_T\,x_P \\ &- 0.04 x_{Rd}\,x_P + 0.26\,x_R\,x_P - 0.43\,x_T\,x_{Rd}\,x_R \\ &+ 0.16\,x_T\,x_{Rd}\,x_P - 0.34\,x_T\,x_R\,x_P + 0.02\,x_{Rd}\,x_R\,x_P + 0.12\,x_T\,x_{Rd}\,x_R\,x_P \quad (5.1)\end{aligned}$$

As can be seen, to the exception of the first independent term, it was plotted in Figure 5.11 the coefficients of equation (5.1) by order of its absolute value. This means that the biggest influencing factor for a higher tooth root stress value is a floating insert (without ring). The second biggest influencing factors are the thickness of the plate insert and insert type. A simple plate with lower thickness increases tooth root stress.

The biggest advantage of using this type of plot is that a combined influence of two or more geometry attributes can be verified. For instance, the combined positive effect of radius and ring, that occurs when a geometry has both fixed inserts and rounded corners ($x_R \cdot x_{Rd} = (+1) \cdot (+1) = +1$) or when a geometry has both floating inserts and straight corners ($x_R \cdot x_{Rd} = (-1) \cdot (-1) = +1$), has the potential to increase twice as much the tooth root stress as a geometry with only rounded corners.

However, every single effect must be accounted for when analysing the magnitude of effects because it was concluded that the best geometry could be the PRS4 and this geometry verifies some of the biggest influencing factors on a higher tooth root stress (Effects: Thickness, Plate), but at the same time doesn't verify ten of the fifteen effects listed.

For a better understanding of the geometry attributes that influence the geometries with simple plate inserts and T shaped plate inserts individually, it was plotted a Pareto

plot for each eight pair of tooth root stress measures. These plots are represented in Figure 5.12 and 5.13, with its respective equations in (5.2) and (5.3). It was used the R code in Appendix D.3.

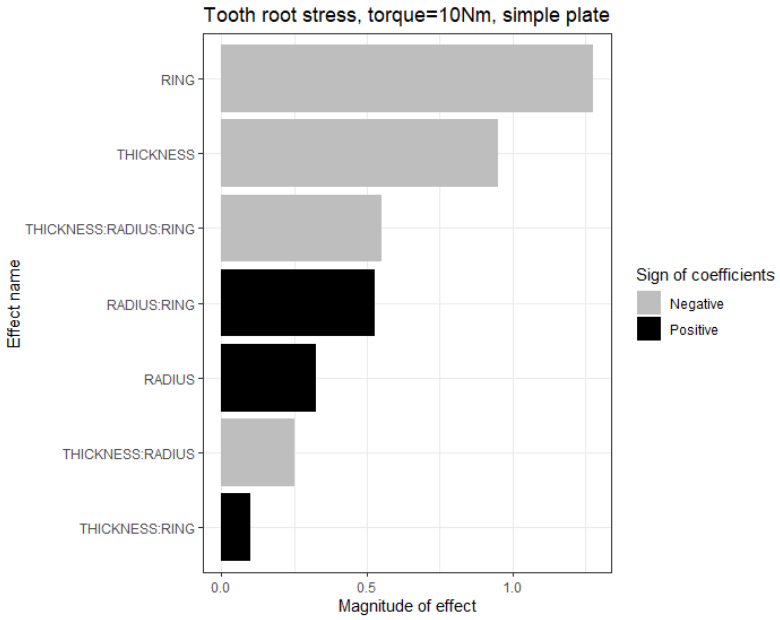

Figure 5.12: Magnitude of effect of geometric variables with simple plate type inserts

$$\begin{aligned}\text{Tooth Root Stress} = 4.18 - 0.95\,x_T + 0.33\,x_{Rd} - 1.28\,x_R - 0.25\,x_T\,x_{Rd} \\ + 0.10\,x_T\,x_R + 0.53\,x_{Rd}\,x_R - 0.55\,x_T\,x_{Rd}\,x_R \end{aligned} \quad (5.2)$$

For the simple plate insert, Figure 5.12, the ring and thickness continue to be the biggest factors of a higher tooth root stress. The combined effect of thickness, radius and ring has in the simple plate almost the same effect as the radius:ring.

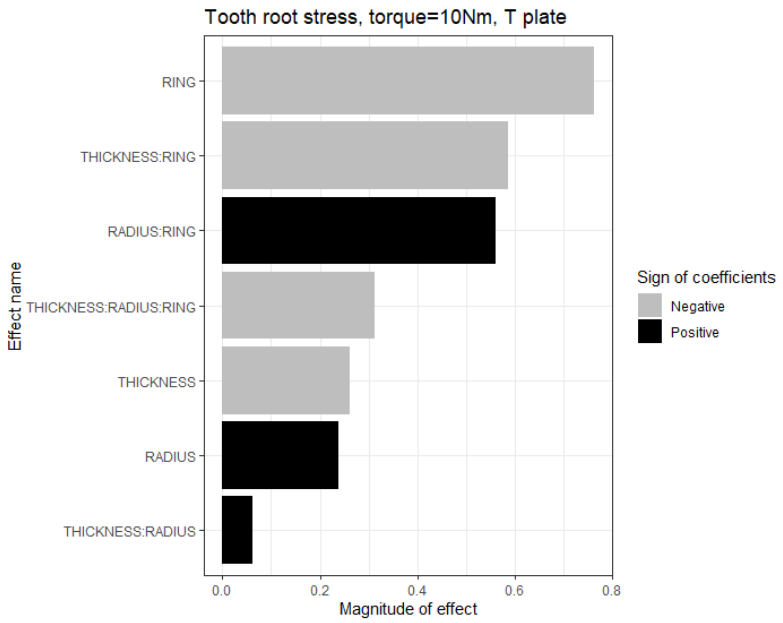

Figure 5.13: Magnitude of effect of geometric variables with T plate type inserts

$$\text{Tooth Root Stress} = 2.96 - 0.26\,x_T + 0.24\,x_{Rd} - 0.76\,x_R + 0.06\,x_T\,x_{Rd} - 0.59\,x_T\,x_R - 0.56\,x_{Rd}\,x_R - 0.31\,x_T\,x_{Rd}\,x_R \quad (5.3)$$

For the T shaped inserts, Figure 5.13, besides the ring effect that remains the biggest factor on high tooth root stress. With this type of T plate inserts, the next biggest influencers on a higher tooth root stress are the combined effects of thickness:ring and radius:ring, being that the thickness effect alone hasn't that much influence on tooth root stress.

The geometric effects have less influence on tooth root stress for the simple plate inserts compared to the T plate inserts.

From this analysis it is concluded that the geometries with simple plate need some improvements, since perhaps the proximity of the insert to the hub (with straight edges) is causing more stress and decreasing load carrying capacity.

Is has also been seen that thinner plater could cause more tooth root stress and if the increase in mass compared with standard polymer gears isn't over 25%, a better solution is the thicker plates insert.

From Figure 5.11 it could be concluded that T shaped insert don't influence or don't factor as much in a higher tooth root stress, being that the difference between simple plate and T plate is due to the combined effect this variable with others. The increase in weight using this type of plate may not justify its difference with simple plate.

For every equation obtained (5.1), (5.2) and (5.3), substituting the variable values for each geometry results in tooth root stress equal to the ones firstly obtained in Figure 5.10, so it can be said that these equations fit exactly for all the values ($R^2 = 1$).

5.6 Equivalent Stress and Strain in polymer/metal interface

There is a concern with the mechanical behaviour of the interface between the insert and polymeric body. The adhesion strength will most likely depend on the manufacturing process, interface temperature, stresses and number of cycles.

In this section the values for the temperature and equivalent stress and strain using the von Mises criteria are evaluated at the polymer/metal interface on the polymer side. It was chosen for this study the geometry PRS2 as an example of a simple plate geometry.

The local maximum values of equivalent stress and strain are displayed in Figure 5.14. In this same Figure it is attributed to each local maximum a reference number point and to each interface a circled number. The number points correspond to a node with the coordinates and equivalent von Mises stress and strain displayed on Table 5.9.

The loading and boundary conditions used for this simulation are displayed in Figure 5.14, with the operating conditions of Table 5.7, having also used for this simulation the considerations of Section 5.4.

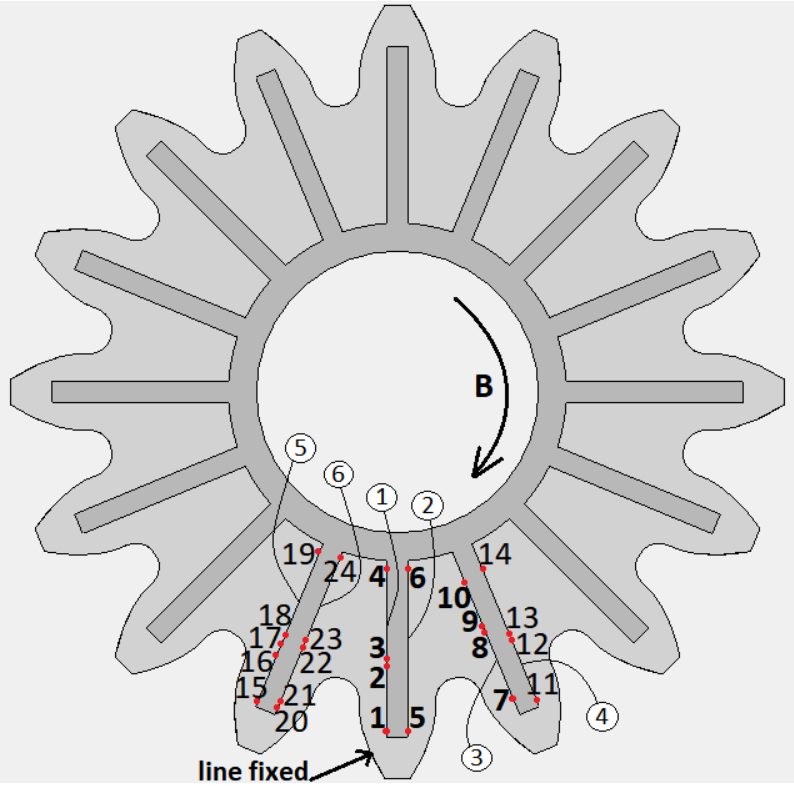

Figure 5.14: Inserts evaluated and their notation, geometry PRS2

The maximum equivalent stress and strain values of Table 5.9 were obtained by plotting for each interface surface the location of the nodes with relation to its equivalent stress and strain values.

It was plotted in Figure 5.15, the temperature and equivalent stress and strain of the interfaces of the insert with the highest stress values which correspond to the interfaces (3) and (4). In this Figure it is represented in colour red the points considered for the maximum stress values and their respective point number.

Table 5.9: Maximum evaluated equivalent stress and strain in the interface using von Mises criteria

Distance from gear tip/ gear module	**Maximum of**	**Equivalent Stress** [MPa]	**Equivalent Strain** [-]	**Coordinates x/y/z [mm]**	**Number Point/ Interface**	
1.13	Stress/strain	**38.3**	0.0158	36.1/1.1/7.0	**1**	
2.75	Stress	**28.8**	0.0059	28.8/1.1/3.9	**2**	(1)
2.83	Strain	**27.1**	0.0100	28.5/1.1/4.4	**3**	
5.03	Stress/Strain	**37.6**	0.0149	18.6/1.1/-7.0	**4**	
1.13	Stress/Strain	62.5	0.0269	36.1/-1.1/7.0	5	(2)
5.03	Stress/Strain	**41.2**	0.0178	18.6/-1.1/7.0	**6**	
1.40	Stress	105.7	0.0145	32.7/-12.3/7.0	7	
3.21	Strain	53.3	0.0221	25.2/-9.2/6.5	8	(3)
3.27	Stress	104.2	0.0131	24.9/-9.1/7.0	9	
4.48	Strain	**47.3**	0.0172	19.9/-7.0/7.0	10	
1.13	Strain	52.1	0.0214	32.9/-14.9/7.0	11	
2.75	Stress	112.0	0.0218	26.2/-12.1/7.0	12	(4)
2.88	Strain	56.4	0.0244	25.7/-11.9/7.0	13	
4.63	Stress	90.5	0.0131	18.4/-8.8/7.0	14	
1.09	Strain	**46.4**	0.0201	33.1/14.9/6.6	**15**	
2.34	Stress	84.4	0.0108	27.9/12.8/-7.0	16	(5)
2.68	Strain	**41.1**	0.0174	26.5/12.2/6.5	17	
2.89	Stress	100.4	0.0142	25.6/11.8/7.0	18	
5.02	Strain	**45.2**	0.0186	16.8/-8.2/7.0	19	
1.13	Stress	94.3	0.0097	33.8/12.8/7.0	20	
1.33	Strain	**37.9**	0.0151	33.0/12.4/6.5	**21**	(6)
2.80	Strain	52.6	0.0216	26.9/9.9/6.5	22	
2.93	Stress	93.4	0.0012	26.3/9.7/6.5	23	
5.05	Strain	**34.6**	0.0137	17.6/5.6/7.0	**24**	

For a better visualization of the results, it was considered in Figure 5.15 the shortest distance from the gear tip to the interface node, having calculated this distance with relation to the module of the gear. When there were nodes with this same distance it is only considered the node with the higher value of stress, strain or temperature.

The whole face of the interface was considered that is both sides and centre of the interface, as can be seen in the z coordinates of the number point of Table 5.9.

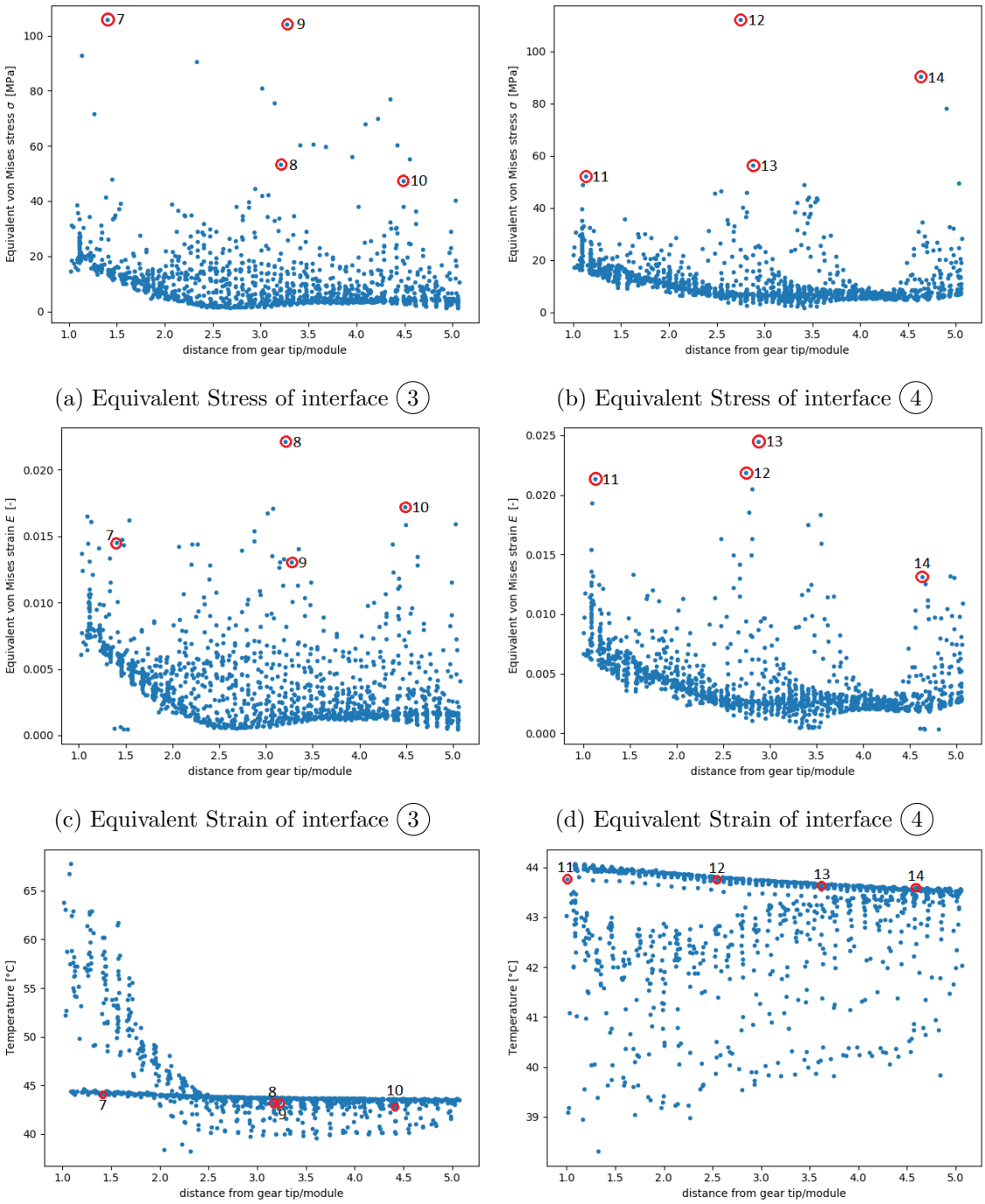

(a) Equivalent Stress of interface (3)

(b) Equivalent Stress of interface (4)

(c) Equivalent Strain of interface (3)

(d) Equivalent Strain of interface (4)

(e) Temperature of interface (3)

(f) Temperature of interface (4)

Figure 5.15: Temperature and Equivalent Stress and Strain of the interfaces **3** and **4** for the loaded thermo-mechanical simulation

As the tip of insert is at the distance of the module from the gear tip the results of Figure 5.15 start in the x axis of each plot at the value one. The distance from the gear tip to the junction between insert and ring, divided with module gear is equal to 5.159 so the results for each interface surface end at this value in the x axis.

The maximum values for temperature of this insert, are located on the interface (3) near the tip, Figure 5.15e, lowering the values and reaching a minimum near the hub. The temperatures are higher in the interface (3) closer to the loaded tooth compared to the other interface in the same insert. The point of maximum temperature 67.7 °C, has an evaluated stress value 15 MPa.

The strain values are also higher in this insert compared to the other insert interfaces, and has it can be seen in Figures 5.15c and 5.15d, the maximum values tend to be in the sides of the gear and in the edges and middle of the length of the insert.

The local stress values where the highest for Point 7 in the interface (3) where the temperature was evaluated at this point as being equal to 44.1 °C. This point is considered to be critical because it is also located in the region near the tip and near stress concentration area of the corner of the insert.

The equation for the fatigue strength under pulsating stress described in the guideline VDI 2736 and displayed in equation (5.4), is going to be used to access the maximum values obtained in this Section. However, in equation (5.4) the temperature is referred in the guideline as being the tooth root temperature, but here is assumed as temperature at other locations also.

$$\sigma_{FlimN} = 26 - 0.0025 \cdot T_{root}^2 + 400 \cdot N_L^{-0.2} \,;\; N_L \in [10^5 \,; 10^8\,] \tag{5.4}$$

Considering the tooth root stress and the tooth root temperature, using equation (5.4), results in fatigue strength for 10^5 cycles equal to 61.8 [MPa] and for 10^8 cycles equal to 31.8 [MPa]. In this manner, the tooth root stress for this geometry PRS2, is under the limit for the fatigue strength and so it is guaranteed to withstand the load.

Using equation (5.4) for the critical maximum von Mises stress seen in this Section for Point 7, with temperature equal to 44.1°C the fatigue strength for 10^5 cycles is equal to 61.1 [MPa] and for 10^8 cycles is equal to 31.2 [MPa], which would result in an excess of stress that could result in failure of the gear.

In Figure 5.16, it is displayed the safety factor for every node of the interface (3) where point 7 is located, by calculating the fatigue strength for 10^5 cycles of equation (5.4) with the temperature of that node and dividing it by the respective stress value.

In Figure 5.16 with the safety factors for each node, it is also indicated in colour red the horizontal line for a safety factor of 1, to help show when the stress of the node is under the fatigue strength calculated for that node and therefore it is critical. As it can be seen there are values that are below this unit value of safety and so there is an issue with stress at the interface.

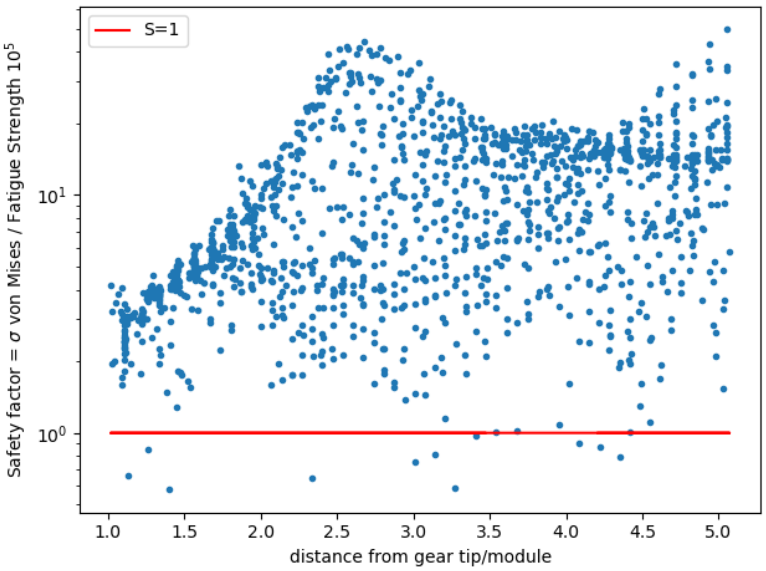

Figure 5.16: Safety factors calculated with fatigue strength on the interface **3**

Thermal Expansion

It is suspected that the tensions in the insert are mainly due to thermal expansion. It was performed the previous simulation but without any loading conditions other than thermal loads.

Considering that the maximum stress and strain are located in the same interface (3) as of what was concluded before, it is plotted in Figure 5.17, the obtained results for this interface with the described simulation.

Taking for instance the maximum equivalent stress value from Figures 5.17a, the load simulation had maximum equivalent stress for 105.7 MPa and 112.0 MPa and the corresponding maximum equivalent stress for the no load simulation was 104.8 MPa and 103.9 MPa.

Other maximum values didn't differ much between the load and no load simulations. It is then concluded that the thermal expansion is causing extra stress and perhaps the materials for this geometry aluminum in the insert and POM in the polymer matrix aren't compatible, at least in what the thermal expansion concerns.

Furthermore, the calculated safety factors in Figure 5.17d still present critical values under the unit value where the stress values at those points are below the fatigue strength for 10^5 cycles using its respective temperature.

The solution for the material of aluminum in the insert should be further analysed.

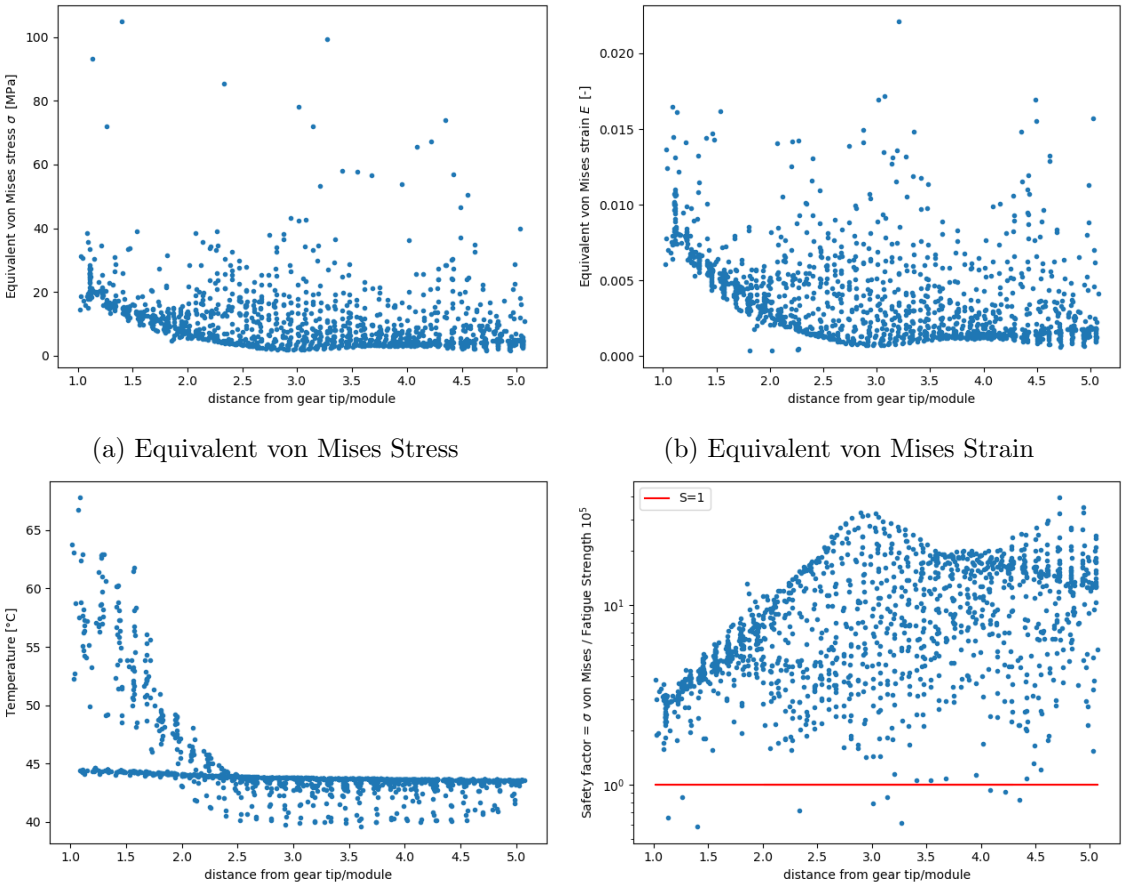

(a) Equivalent von Mises Stress

(b) Equivalent von Mises Strain

(c) Temperature

(d) Safety factor

Figure 5.17: Temperature and Equivalent Stress and Strain of interface **3** for an unloaded thermo-mechanical simulation

5.7 Influence of insert thermal conductivity

In order to verify the conclusions of the work [15] that the aluminum is the best metal material for the insert in what concerns temperature, and to see the influence of the thermal conductivity of metallic inserts in load carrying capacity, it is going to be studied in this Section this influence.

Choosing the best geometry of the simple plate inserts with lower tooth root stress, PRS2, it is going to be repeated the simulation from Section 5.5, but varying the material of the inserts to check the impact of thermal conductivity of the insert on the tooth root stress and tooth root temperature.

It is going to be tested copper, steel and aluminum, with the mechanical and thermal properties listed in Table 5.10, and for the loading conditions represented in Table 5.11. The material aluminum was also tested in this conditions, and it was obtained the following results displayed in Figures 5.18 and 5.19.

Table 5.10: Mechanical and thermal properties of the inserts [14]

Mechanical, Thermal Properties	**Copper**	**Steel**	**Aluminum**
Young's Modulus, E [GPa]	107	206	69
Poisson's ratio, ν [-]	0.36	0.30	0.33
Density, ρ [kg/m^3]	8933	7870	2702
Thermal conductivity, K [$W\,/\,(m\,K)$]	401.0	41.8	237.0
Specific Heat, c_p [$J\,/\,(kg\,K)$]	385	493	903
Coefficient of thermal expansion [$°C^{-1}$]	16.4×10^{-6}	11.7×10^{-6}	22.5×10^{-6}

Table 5.11: Operating conditions tested

Loading conditions	**Torque** of the pinion hub [N·m]	**Rotational Speed**, ω [rpm]	**Ambient Temperature** [°C]
A	7.5	1000	15
B	10.0	1000	15
C	10.75	1000	15

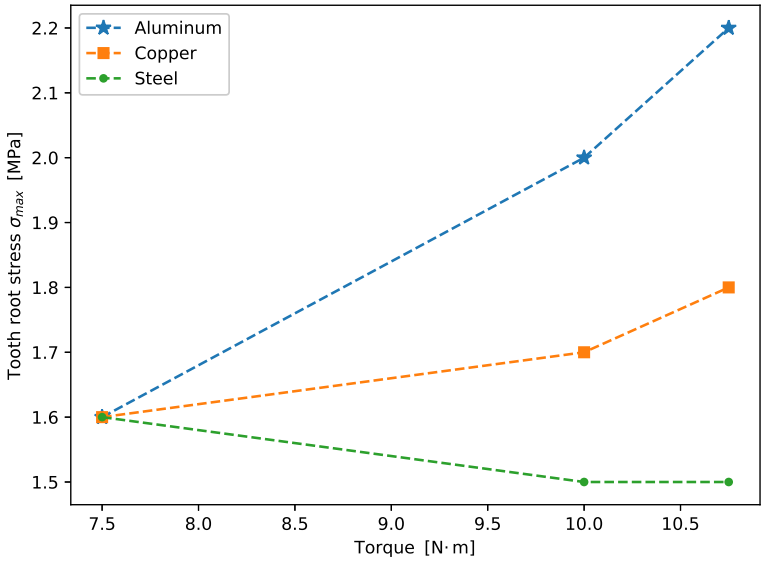

Figure 5.18: Tooth root stress for different material of insert and loading conditions, geometry PRS2

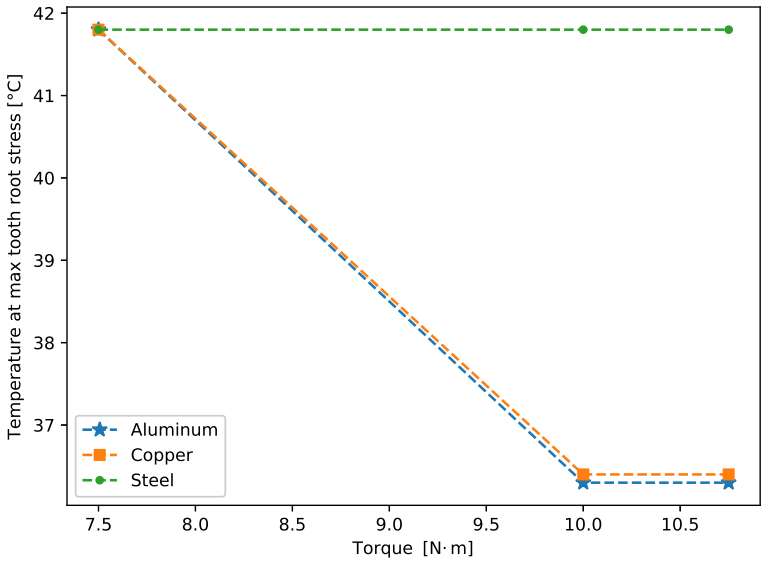

Figure 5.19: Temperature at maximum tooth root stress for different material of insert and loading conditions, geometry PRS2

Figure 5.18 shows that the tooth root stress is higher for the aluminum, followed by copper and then steel. Tt was evaluated higher tooth root stress temperature for steel and a lower values for copper an then aluminum.

Moreover, both steel and copper have a much higher density value than aluminum so if steel and copper should be used, the difference in tooth root stress and its temperature have to compensate the increase of mass of the insert (3.3 times for copper and 2.9 times for steel). In this manner, aluminum is the best metallic material for the insert.

The material of insert being steel could have reached a higher temperature because of the low thermal conductivity, but it had the lowest tooth root stress. Copper had slightly higher temperature than aluminum, but has higher thermal conductivity value than aluminum which suggests that the specific heat could also play a role in the tooth root temperature. Despite this copper had lower tooth root stress than aluminum since probably it has higher Young's Modulus.

5.8 Optimizing position of insert

Following the conclusion of Section 5.5 where it was seen that the floating inserts were causing extra stress, in this Section the length of this insert is going to be shortened in order to study the tooth root stress when the base of the insert isn't in contact with the hub. By doing this procedure it is also decreased the overall weight of the gear set.

As the length of the insert is shortened in the base close to the hub it is expected that the temperature and tooth root temperature increases but the tooth root stress lowers justifying the conclusions of Section 5.5. To this effect, it is going to be studied the tooth root stress and its respective temperature for each optimizing attempt checking if the optimization doesn't worsen the solution by increasing the temperature of the gear.

The distance of the insert to the tooth tip (t) in Figure 5.1 is going to be maintained while increasing the distance of the insert to the hub of the pinion by 0.5, 1.0 and 1.5 times

of the value of the module.

To study a floating geometry it is chosen as of an example geometry PFS2. The resulting geometries are as follows in Figures 5.20, 5.21, 5.22.

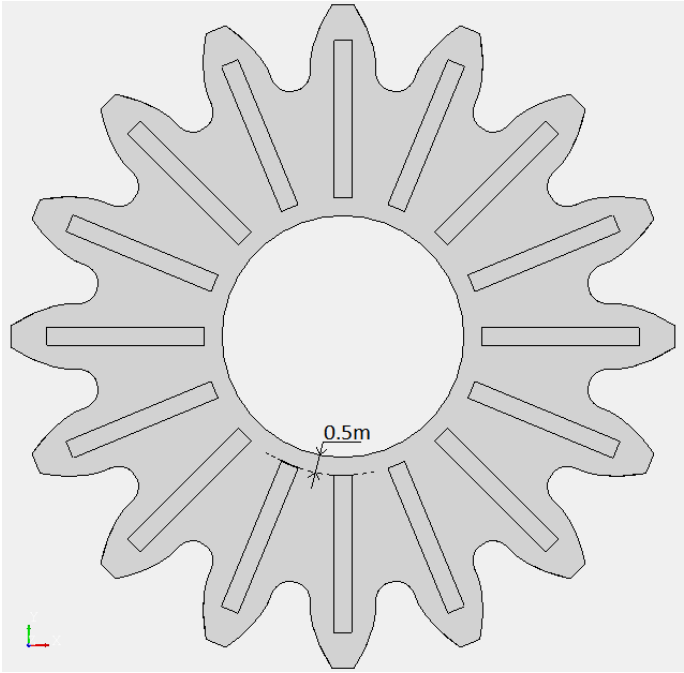

Figure 5.20: Optimization attempt 1, distance from hub and inserts equal to 50% of the module

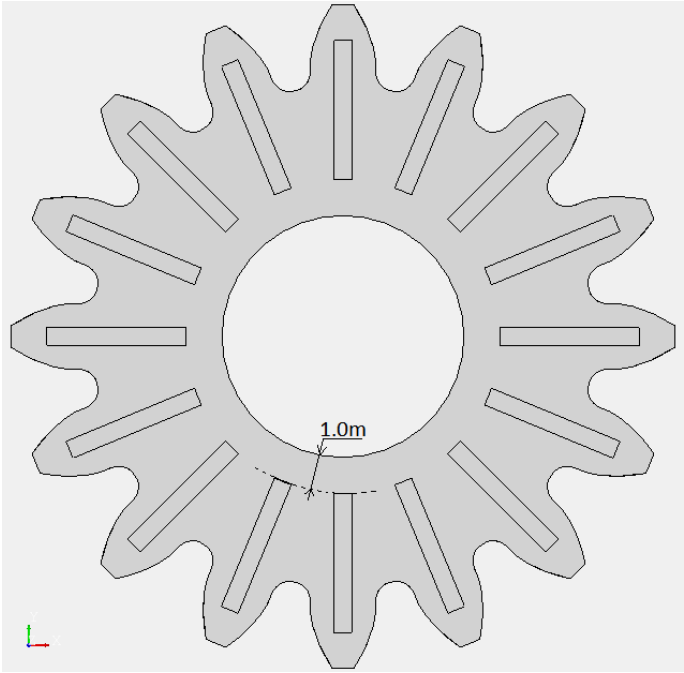

Figure 5.21: Optimization attempt 2, distance from hub and inserts equal to 100% of the module

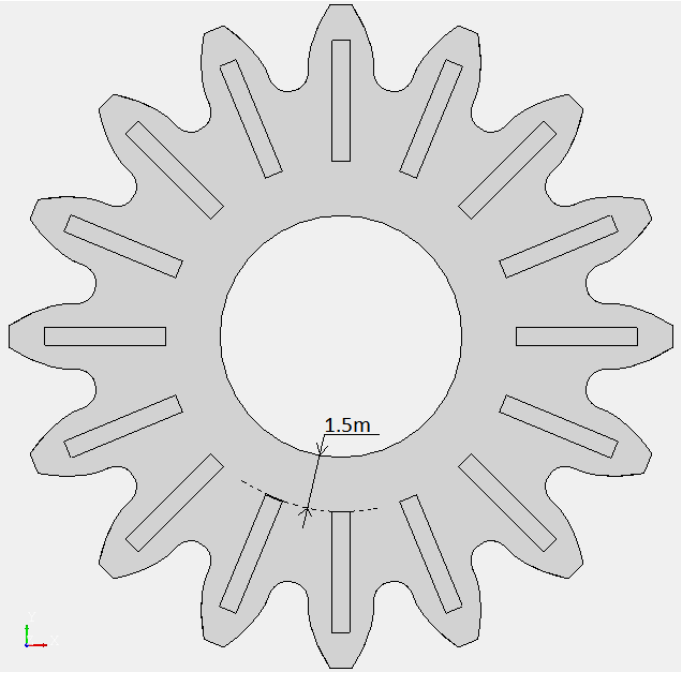

Figure 5.22: Optimization attempt 3, distance from hub and inserts equal to 150% of the module

Using the same procedure for mesh creation it was obtained the following number elements and nodes for each of this three new geometries: for the geometry of Figure 5.20, 229 491 elements and 58 520 nodes; for the geometry of Figure 5.21, 219 286 elements and 55 407 nodes; for the geometry of Figure 5.20, 279 739 elements and 60 560 nodes.

The loading conditions are the same as in Table 5.11, and the results that were obtained for tooth root stress and its temperature are described in Figures 5.23 and 5.24.

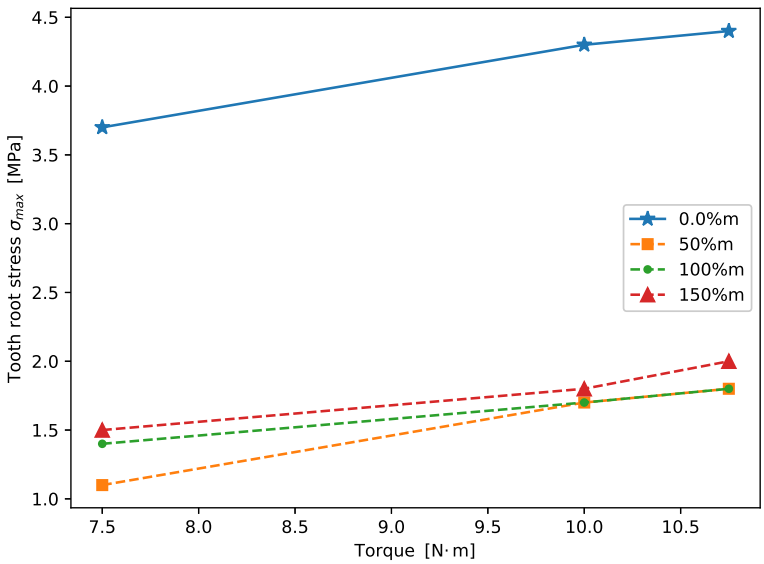

Figure 5.23: Optimization results of tooth root stress for the geometry PFS2

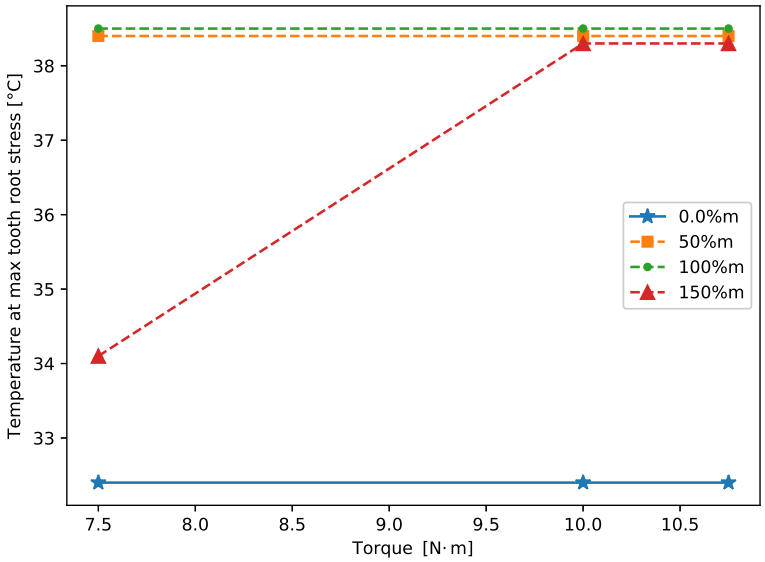

Figure 5.24: Optimization results of temperature at maximum tooth root stress for the geometry PFS2

The results show that increasing the distance from the hub to the base of the inserts decreases the tooth root stress but also increases tooth root temperature. Using the equation for the fatigue strength under pulsating stress described in the guideline VDI 2736 and displayed in equation (5.5), every single result is under the permissible root stress (the lowest is 32.3 MPa for root temperature of 38.5°C and 10^8 cycles).

$$\sigma_{FlimN} = 26 - 0.0025 \cdot T_{root}^2 + 400 \cdot N_L^{-0.2} \,;\, N_L \in [10^5 \,;\, 10^8\,] \tag{5.5}$$

With this decrease in tooth root stress it is expected that the results for tooth root stress for the floating insert geometries would be closer to the fixed insert geometries if there was an increase in the distance from the base of inserts and hub, see also Figure 5.9.

Despite the improvements on tooth root stress, an increase of the root temperature with this correction would also result in a higher tooth root temperature for the floating inserts compared to the fixed inserts.

It is considered that the optimization with a distance equal to the module of the gear is the optimal since it results in a low enough value of tooth root stress without increasing too much the tooth root temperature.

5.9 Proposed solution

Following the conclusions of Section 5.6, where it was seen that the aluminum as insert material, despite improving on tooth root stress and tooth root temperature it is causing high stresses in the interface due to thermal expansion, and the conclusions of Section 5.8 where it was seen improvements in reducing near the hub the length of the floating inserts, in this Section it is introduced a solution using an epoxy silver-filled as the material of the insert with an optimized geometry of PFS2 (distance from hub 100%m).

The reason for choosing an epoxy silver-filled is that it is considered more compatible with POM than aluminum as thermal expansion goes, but it also presents higher thermal conductivity and slightly higher Young's Modulus than POM. The values presented for mechanical and thermal properties of the epoxy are only suggested values because the technical sheet only refers the storage modulus, thermal expansion, density and thermal conductivity of the material.

The epoxy chosen as it is silver-filled has a higher thermal conductivity compared to other epoxy of the EPO-TEK EK kind. The commercial name is EPO-TEK EK 1000-1MP.

To study this solution the tooth root stress is going to be evaluated using the FEM model of Section 5.4, the loading conditions of Table 5.13 and the material properties of epoxy inserts listed in Table 5.12. The geometry that is going to simulated follows Section 5.8 and is the PFS2 with distance 100%m.

Table 5.12: Mechanical and thermal properties of the inserts

Mechanical, Thermal Properties	**Epoxy**
Young's Modulus, E [GPa]	4.2
Poisson's ratio, ν [-]	0.39
Density, ρ [kg/m^3]	3750
Thermal conductivity, K [$W\,/\,(m\,K)$]	22.7
Specific Heat, c [$J\,/\,(kg\,K)$]	1580
Coefficient of thermal expansion [$°C^{-1}$]	101.5×10^{-6}

Table 5.13: Operating conditions tested

Loading conditions	**Torque** of the pinion hub [N·m]	**Rotational Speed**, ω [rpm]	**Ambient Temperature** [°C]
A	7.5	1000	15
B	10.0	1000	15
C	10.75	1000	15

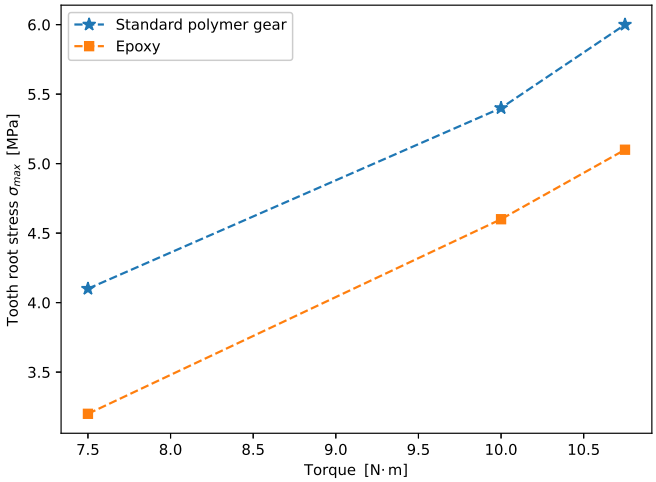

Figure 5.25: Tooth root stress between epoxy insert and standard polymer gear

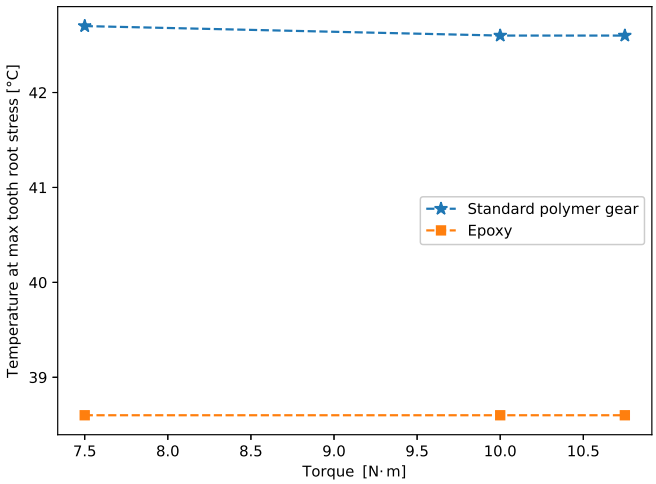

Figure 5.26: Tooth root temperature between epoxy insert and standard polymer gear

In Figure 5.25 it can be seen that the tooth root stress using epoxy as an insert is lower than the case for the standard polymer gear, improving load carrying capacity, but it definitely doesn't have the low tooth root stress value that was evaluated using aluminum as insert material. Adding to that, the tooth root temperature decreased compared to the standard polymer gear.

The temperature and equivalent stress and strain on the interface were also evaluated for the same interface (3) as the one that was seen has critical in Section 5.6, and for a torque value of 10 Nm, having been obtained the results displayed on Figure 5.27.

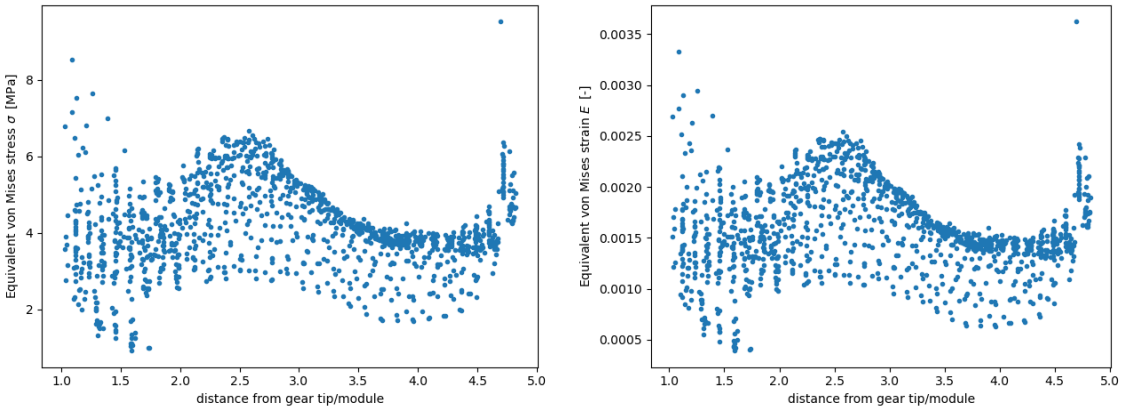

(a) Equivalent von Mises Stress of interface (3) (b) Equivalent con Mises Strain of interface (3)

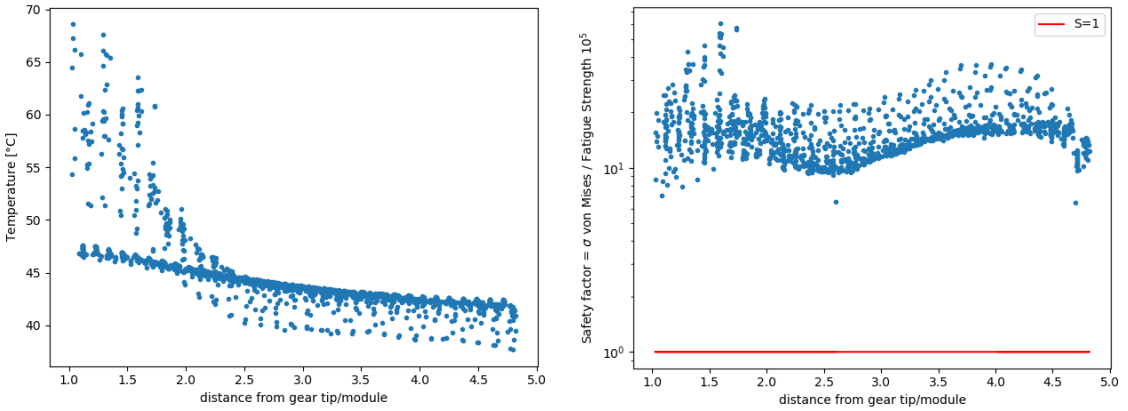

(c) Temperature of interface (3) (d) Safety factor

Figure 5.27: Temperature and Equivalent Stress and Strain of the critical interfaces with Solution Epoxy Case

The calculated safety value used the equivalent stress of the node, divided by the fatigue strength using equation (5.6) with the respective temperature of the node and to 10^5 cycles. As can be seen, there aren't any longer critical stress points which results in an improvement of the interface problem of the aluminum insert.

$$\sigma_{FlimN} = 26 - 0.0025 \cdot T_{root}^2 + 400 \cdot N_L^{-0.2} \,;\, N_L \in [10^5 \,;\, 10^8\,] \tag{5.6}$$

The results for the temperature at the interface in Figure 5.27c continue to be very similar to the ones obtained for the aluminum insert case, but the equivalent stress values lowered significantly, by a factor of more than 10, since in Figure 5.27a the maximum equivalent stress value is of 9.5 MPa. The equivalent strain values also diminished significantly.

The tooth root stress with epoxy diminished by around 14.9% compared to the standard polymer gear for all torque values and the tooth root temperature diminished by 9.7%, improving load carrying capacity.

The results in equivalent von Mises stress are shown in Figure 5.28, for the standard polymer gear, for the aluminum insert before and after optimization, and for the epoxy insert proposed solution.

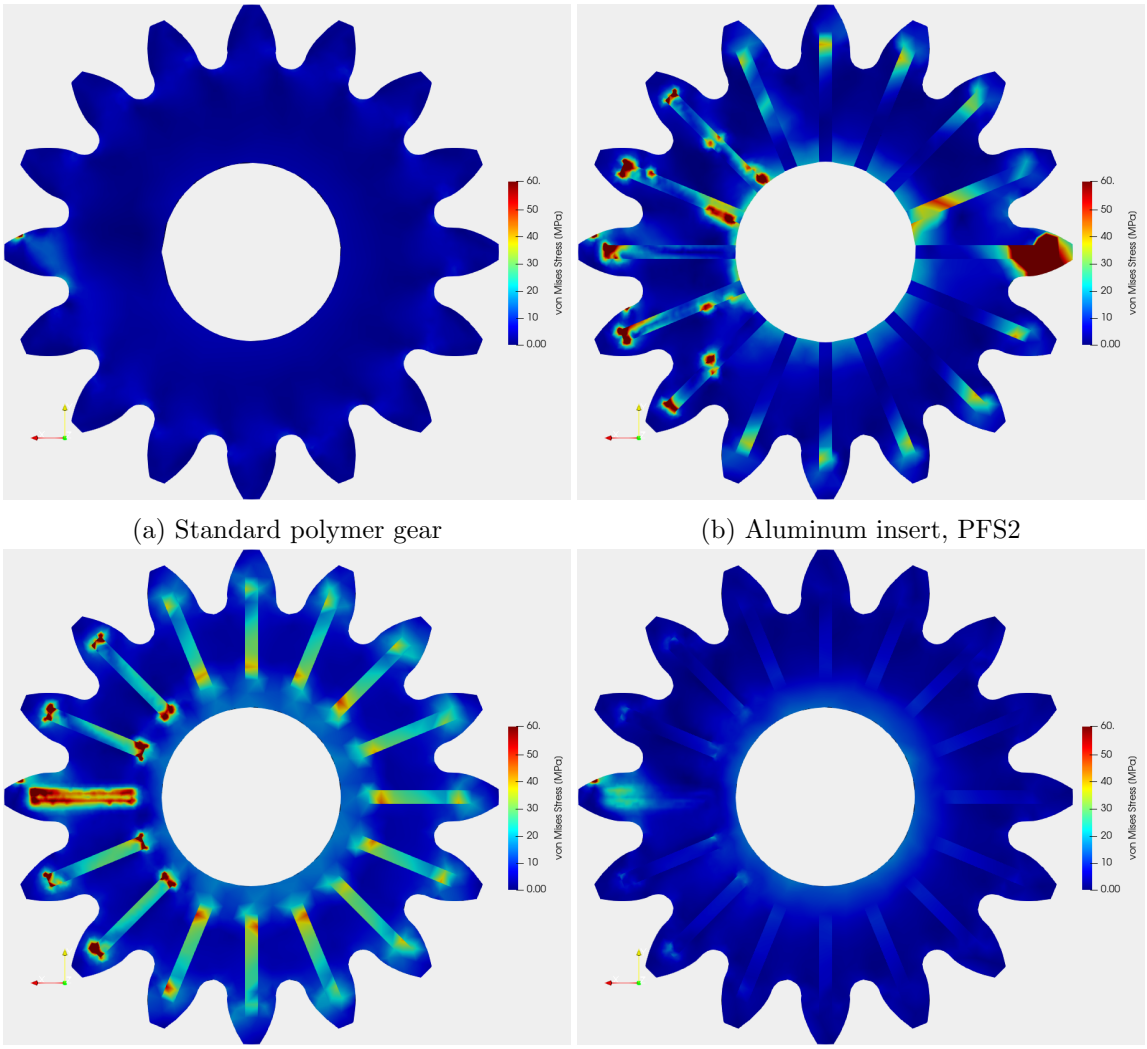

(a) Standard polymer gear

(b) Aluminum insert, PFS2

(c) Optimized Aluminum insert, PFS2 with 100%m distance

(d) Proposed solution Epoxy insert, PFS2 with 100%m distance

Figure 5.28: Equivalent von Mises Stress for some of the cases studied

The results for the safety factor are shown in Figure 5.29, for the standard polymer gear, for the aluminum insert before and after optimization, and for the epoxy insert proposed solution. The safety factor was calculated using the fatigue strength in equation (5.6), for 10^5 cycles and using the temperature and von Mises equivalent stress at each node. In the Figure 5.29, nodes with a safety factor below two, that are critical since they are below two time the value of fatigue strength, are shown in black colour. The inserts are excluded in this Figure.

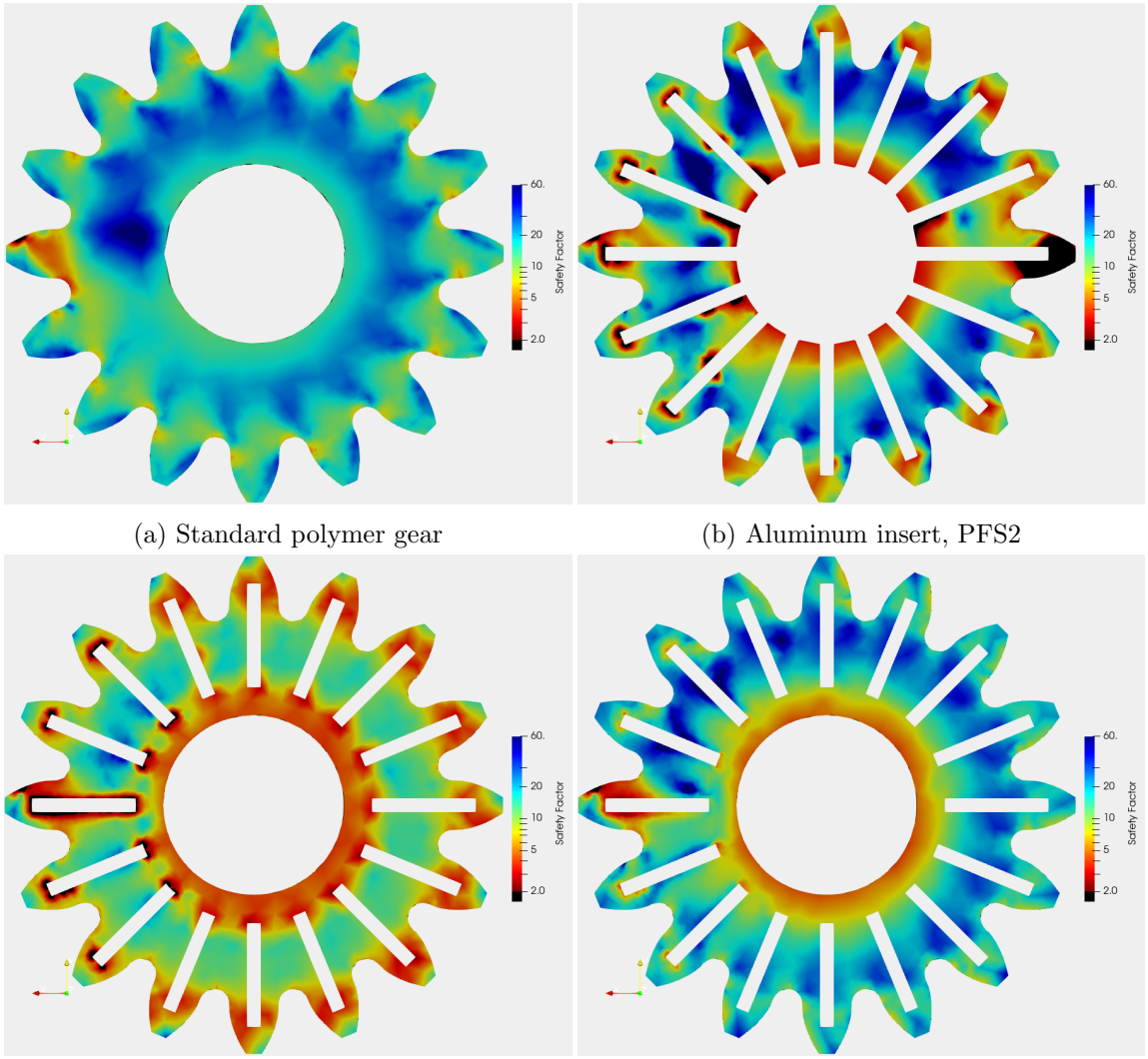

(a) Standard polymer gear

(b) Aluminum insert, PFS2

(c) Optimized Aluminum insert, PFS2 with 100%m distance

(d) Proposed solution Epoxy insert, PFS2 with 100%m distance

Figure 5.29: Safety Factor calculated using Equivalent von Mises Stress and Fatigue strength Eq.(5.6) with 10^5 cycles

5.10 Conclusion

In this Chapter the load carrying capacity of hybrid gears was studied, having been evaluated tooth root stress and temperature but also equivalent stress and strain at the interface of the insert and polymer body.

It was discussed the polymer metal gear solution using different geometries and it was characterized the FEM model that was implemented for the study of this gears, describing the boundary conditions, mesh generated for these gear and the material's properties of the inserts.

The influence of geometry variables was analysed having been identified the geometric variables and factors/effects that lead to higher tooth stress. The floating geometries were flagged as having more stress because of the proximity of the hub to the base of the inserts. Regardless of this annotation, it was concluded that every hybrid gear geometry with aluminum inserts presented improvements on the load carrying capacity compared to the standard gear and with lower temperatures.

The material of the insert aluminum was then compared to other metals but there wasn't any further significant advantage on load carrying capacity when using these type of insert material, even more so because of the added overall weight.

The insert interface was then evaluated on the polymer side for temperature and equivalent stress and strain, having concluded the critical insert location, identified the evolution of stress, strain and temperature along the length of the insert and it was verified that using the aluminum insert can result in possible failure of the gear because of excess stress in the polymer metal interface. It was then analysed the hypothesis that this excess stress could be the result of thermal expansion and that hypothesis was verified.

Following the conclusions of the higher stress values due to proximity of the hub of the floating inserts and the thermal expansion issue it was then attempted optimizations and solutions for this problems. As for the floating inserts it was successively increased the distance from the base of insert to the hub which lead to a lower tooth root stress, nearing this solution to the fixed inserts but it also lead to a higher tooth root temperature.

In regards to the interface stress issue it was attempted a replacement of insert material to an epoxy silver-filled since it is more related in terms of properties to POM but with higher thermal conductivity. It was seen that the tooth root stress is lower than that of the standard polymer gear, improving load carrying capacity, and it also resulted in lower and not critical interface stress and strain and lower tooth root temperature.

Chapter 6

Conclusion

In this dissertation, the stress and temperature of steel, polymeric and hybrid gears were evaluated using mechanical and thermo-mechanical Finite Element models. The load carrying capacity of gears could be accessed, including the study of polymeric gears with metallic inserts which was the main objective of this work.

A study of polymer gears' materials and properties, attempts to improve polymer gears and which standards, guidelines and Finite Elements Methods exist, was conducted to further introduce the need for a hybrid gear solution.

Using as a basis a thermal and a gear power loss model already validated in the literature, it was described Finite Element mechanical models that couple these other models creating an uncoupled Thermo-mechanical Finite Element model. This thermo-mechanical model was also validated simulating polymer gears and comparing with standards.

After validation, a study of the load carrying capacity using tooth root stress for the polymer gears with metallic inserts was conducted. It was seen the influence of geometric variables, such as insert shape and type, filleting and thickness, having concluded that fixed inserts improve significantly the standard polymer gear by increasing load carrying capacity and lowering temperature of the gear. However, the relative increase in weight could be an issue for this solution.

It was then described the influence in the metal material of inserts considering three materials with different values of thermal conductivity and density, having concluded that aluminium is still the best solution with a good compromise of value of thermal conductivity, good mechanical resistance, low density and low price of material. The interface between aluminum and the polymer was then studied keeping in mind the adhesion of this two materials when in operation and having concluded an issue with critical stress values in the interface on the polymer side due to thermal expansion.

An optimization of the floating inserts was conducted by increasing the distance from the hub to the base of the inserts and it was seen that the load carrying capacity was increased and was now with similar tooth root stress values compared to the fixed inserts, but it also lead to an increase in tooth root temperature.

In continuation of the study of the interface and of the optimization of the aluminium insert, an optimized geometry using epoxy silver-filled insert material with similar properties of the POM regarding more compatible thermal expansion value of the polymer, was evaluated and it was concluded that the tooth root stress and temperature was lower, increasing load carrying capacity of the standard polymer gear and the stress and strain at the interface was no longer critical.

6.1 Future Works

- Develop a study considering friction in the mechanical model besides friction in the thermal model
- Verify that the uncoupled and coupled thermo-mechanical models lead to similar results for the application described in this work
- Comparing with more standards the validation cases
- Trying to combine the higher load carrying capacity of aluminum inserts with the interface stress and strain values of the epoxy inserts, by considering an epoxy coating of the aluminum, where the POM is joined to the aluminum by epoxy
- Manufacture the proposed solution using 3D printing
- Experimentally validate the proposed hybrid gear geometries

Bibliography

[1] VDI. 2016. VDI 2736: Part 1. 2016. Thermoplastic gear wheels - Materials, material selection, production methods, production tolerances, form design.

[2] Prashant Kumar Singh, Siddhartha, and Akant Kumar Singh. An investigation on the effects of the various techniques over the performance and durability of polymer gears. *Materials Today: Proceedings*, 4(2):1606–1614, 2017. ISSN 22147853. doi: 10.1016/j.matpr.2017.01.184. URL http://dx.doi.org/10.1016/j.matpr.2017.01.184.

[3] V. Roda-Casanova, F. Sanchez-Marin, and A. Porras-Vazquez. A Fast Finite Element Based Methology To Predict The Temperature Field In A Thermoplastic Spur Gear Drive. *DETC2017-67724*, pages 1–10, 2018.

[4] S.M. M Evans and P.S. S Keogh. Efficiency and running temperature of a polymer–steel spur gear pair from slip/roll ratio fundamentals. *Tribology International*, 97:379–389, may 2016. ISSN 0301679X. doi: 10.1016/j.triboint.2016.01.052. URL http://www.sciencedirect.com/science/article/pii/S0301679X16000827.

[5] M. Kalin and A. Kupec. The dominant effect of temperature on the fatigue behaviour of polymer gears. *Wear*, 376-377:1339–1346, 2017. ISSN 00431648. doi: 10.1016/j.wear.2017.02.003. URL http://dx.doi.org/10.1016/j.wear.2017.02.003.

[6] Naohisa Tsukamoto. Argument on Plastic Gears for Power Transmission. *JSME international journal. Ser. C, Dynamics, control, robotics, design and manufacturing*, 38(1):1–8, 1995. ISSN 1340-8062. doi: 10.1299/jsmec1993.38.1.

[7] Aljaž Pogačnik and Jože Tavčar. An accelerated multilevel test and design procedure for polymer gears. *Materials & Design*, 65:961–973, 2015. ISSN 02613069. doi: 10.1016/j.matdes.2014.10.016. URL http://linkinghub.elsevier.com/retrieve/pii/S0261306914008036.

[8] Julien Cathelin, Eric Letzelter, Michele Guingand, Jean-Pierre de Vaujany, and Laurent Chazeau. Experimental and Numerical Study of a Loaded Cylindrical PA66 Gear. *Journal of Mechanical Design*, 135(4):41007, 2013. ISSN 1050-0472. doi: 10.1115/1.4023634. URL http://mechanicaldesign.asmedigitalcollection.asme.org/article.aspx?doi=10.1115/1.4023634.

[9] N.A A Wright and S.N N Kukureka. Wear testing and measurement techniques for polymer composite gears. *Wear*, 251(1-12):1567–1578, oct 2001. ISSN 00431648. doi: 10.1016/S0043-1648(01)00793-1. URL http://www.sciencedirect.com/science/article/pii/S0043164801007931.

[10] Jun-ichi Nozawa, Tadashi Komoto, Takahiko Kawai, and Hiroyuki Kumehara. Tribological properties of polymer-sheet-adhered metal hybrid gear. *Wear*, 266(9-10):893–897, apr 2009. ISSN 00431648. doi: 10.1016/j.wear.2008.12.008. URL http://linkinghub.elsevier.com/retrieve/pii/S0043164808004274.

[11] Boštjan Trobentar, Srečko Glodež, Jože Flašker, and Boštjan Zafošnik. The influence of surface coatings on the tooth tip deflection of polymer gears. *Materiali in Tehnologije*, 50(4):517–522, 2016. ISSN 15803414. doi: 10.17222/mit.2015.056.

[12] a. J. Mertens and S. Senthilvelan. Durability enhancement of polymer gear using compressed air cooling. *Proceedings of the Institution of Mechanical Engineers, Part L: Journal of Materials: Design and Applications*, 230(2):515–525, apr 2016. ISSN 1464-4207. doi: 10.1177/1464420715581195. URL `http://pil.sagepub.com/lookup/doi/10.1177/1464420715581195`.

[13] Jože Duhovnik, Damijan Zorko, and Luka Sedej. The effect of the teeth profile shape on polymer gear pair properties. *Tehnicki vjesnik - Technical Gazette*, 23(1):199–207, 2016. ISSN 13303651. doi: 10.17559/TV-20151028072528. URL `http://hrcak.srce.hr/index.php?show=clanak{&}id{_}clanak{_}jezik=225587{&}lang=en`.

[14] Carlos M. C. G. Fernandes, Diogo M. P. Rocha, Ramiro C. Martins, Luís Magalhães, and Jorge H. O. Seabra. Hybrid Polymer Gear Concepts to Improve Thermal Behavior. *Journal of Tribology*, 141(3):032201, 2019. ISSN 0742-4787. doi: 10.1115/1.4041461. URL `http://tribology.asmedigitalcollection.asme.org/article.aspx?doi=10.1115/1.4041461`.

[15] Diogo Rocha. Bulk Temperature In Polymer-Metal Hybrid Gears. 2017.

[16] VDI. 2014. VDI 2736: Part 2. 2014. Thermoplastic gear wheels - Calculation of the load-carrying capacity of cylindrical gears. (June), 2014.

[17] I. Moriwaki, A. Ueda, M. Nakamura, K. Yoneda, and D. Iba. *New Japanese Standard JIS B 1759 on load capacity of plastic gears*. Woodhead Publishing Limited, 2014. doi: 10.1533/9781782421955.1172. URL `http://dx.doi.org/10.1533/9781782421955.1172`.

[18] Borut Černe, Jože Duhovnik, and Jože Tavčar. Semi-analytical flash temperature model for thermoplastic polymer spur gears with consideration of linear thermomechanical material characteristics. *Journal of Computational Design and Engineering*, 6(4):617–628, 2019. ISSN 22885048. doi: 10.1016/j.jcde.2019.03.001.

[19] P. Wriggers. *Computational contact mechanics, second ed., Springer*. 2006. ISBN 9783540326083. doi: 10.1007/978-3-540-32609-0.

[20] Guido Dhondt. *The Finite Element Method for Three-dimensional Thermomechanical Applications*. 2004. ISBN 0470857528.

[21] Rhys Gareth Jones. The Mathematical Modelling of Gearbox Vibration under Applied Lateral Misalignment. 2012.

[22] M. Karimpour, K. D. Dearn, and D. Walton. A kinematic analysis of meshing polymer gear teeth. *Proceedings of the Institution of Mechanical Engineers, Part L: Journal of Materials Design and Applications*, 2010. ISSN 1464-4207. doi: 10.1243/14644207JMDA315.

[23] V Rajaprabakaran and Mr R Ashokraj. Spur Gear Tooth Stress Analysis And Stress Reduction. *IOSR Journal of Mechanical and Civil Engineering*, 3(1):38–48, 2011.

[24] C.M.C.G. Carlos M C G Fernandes, D M P Diogo M P Rocha, Ramiro C R C Martins, Luis Magalhães, and Jorge H O J H O Seabra. Finite element method model to predict bulk and flash temperatures on polymer gears. *Tribology International*, 120: 255–268, 2018. ISSN 0301679X. doi: 10.1016/j.triboint.2017.12.027. URL `https://doi.org/10.1016/j.triboint.2017.12.027`.

[25] ISO 6336-3:2006: Calculation of load capacity of spur and helical gears - Part 3: Calculation of tooth bending strength. *International Organization for Standardization*, 3, 2006. URL `http://upload.engineer365.cn/uploads/questions/2013/12/19/e36566045131609484.pdf`.

[26] ISO 6336-2:2006: Calculation of load capacity of spur and helical gears - Part 2: Calculation of surface durability (pitting). *International Organization for Standardization*, 2:2–11, 2006.

[27] ISO 6336-4:2006: Calculation of load capacity of spur and helical gears - Part 4: Calculation of tooth flank fracture load capacity. *International Organization for Standardization*, 4, 2019.

Appendix A

Friction heat flux routine

```
!
!     CalculiX - A 3-dimensional finite element program
!              Copyright (C) 1998-2019 Guido Dhondt
!
!     This program is free software; you can redistribute it and/or
!     modify it under the terms of the GNU General Public License as
!     published by the Free Software Foundation(version 2);
!
!
!     This program is distributed in the hope that it will be useful,
!     but WITHOUT ANY WARRANTY; without even the implied warranty of
!     MERCHANTABILITY or FITNESS FOR A PARTICULAR PURPOSE. See the
!     GNU General Public License for more details.
!
!     You should have received a copy of the GNU General Public License
!     along with this program; if not, write to the Free Software
!     Foundation, Inc., 675 Mass Ave, Cambridge, MA 02139, USA.
!
      subroutine dflux(flux,sol,kstep,kinc,time,noel,npt,coords,
     &     jltyp,temp,press,loadtype,area,vold,co,lakonl,konl,
     &     ipompc,nodempc,coefmpc,nmpc,ikmpc,ilmpc,iscale,mi,
     &     sti,xstateini,xstate,nstate_,dtime)
!
!     user subroutine dflux
!
!
!     INPUT:
!
!     sol                 current temperature value
!     kstep               step number
!     kinc                increment number
!     time(1)             current step time
!     time(2)             current total time
!     noel                element number
!     npt                 integration point number
!     coords(1..3)        global coordinates of the integration point
!     jltyp               loading face kode:
!                         1  = body flux
!                         11 = face 1
!                         12 = face 2
!                         13 = face 3
!                         14 = face 4
!                         15 = face 5
!                         16 = face 6
!     temp                currently not used
!     press               currently not used
!     loadtype            load type label
!     area                for surface flux: area covered by the
!                             integration point
!                         for body flux: volume covered by the
!                             integration point
!     vold(0..4,1..nk)    solution field in all nodes
!                         0: temperature
```

```
54  !                          1: displacement in global x-direction
55  !                          2: displacement in global y-direction
56  !                          3: displacement in global z-direction
57  !                          4: static pressure
58  !     co(3,1..nk)          coordinates of all nodes
59  !                          1: coordinate in global x-direction
60  !                          2: coordinate in global y-direction
61  !                          3: coordinate in global z-direction
62  !     lakonl               element label
63  !     konl(1..20)          nodes belonging to the element
64  !     ipompc(1..nmpc))     ipompc(i) points to the first term of
65  !                          MPC i in field nodempc
66  !     nodempc(1,*)         node number of a MPC term
67  !     nodempc(2,*)         coordinate direction of a MPC term
68  !     nodempc(3,*)         if not 0: points towards the next term
69  !                                    of the MPC in field nodempc
70  !                          if 0: MPC definition is finished
71  !     coefmpc(*)           coefficient of a MPC term
72  !     nmpc                 number of MPC's
73  !     ikmpc(1..nmpc)       ordered global degrees of freedom of the MPC's
74  !                          the global degree of freedom is
75  !                          8*(node-1)+direction of the dependent term of
76  !                          the MPC (direction = 0: temperature;
77  !                          1-3: displacements; 4: static pressure;
78  !                          5-7: rotations)
79  !     ilmpc(1..nmpc)       ilmpc(i) is the MPC number corresponding
80  !                          to the reference number in ikmpc(i)
81  !     mi(1)                max # of integration points per element (max
82  !                          over all elements)
83  !     mi(2)                max degree of freedomm per node (max over all
84  !                          nodes) in fields like v(0:mi(2))...
85  !     sti(i,j,k)           actual Cauchy stress component i at integration
86  !                          point j in element k. The components are
87  !                          in the order xx,yy,zz,xy,xz,yz
88  !     xstateini(i,j,k)     value of the state variable i at integration
89  !                          point j in element k at the beginning of the
90  !                          present increment
91  !     xstate(i,j,k)    value of the state variable i at integration
92  !                          point j in element k at the end of the
93  !                          present increment
94  !     nstate_              number of state variables
95  !     dtime                time length of the increment
96  !
97  !
98  !     OUTPUT:
99  !
100 !     flux(1)              magnitude of the flux
101 !     flux(2)              not used; please do NOT assign any value
102 !     iscale               determines whether the flux has to be
103 !                          scaled for increments smaller than the
104 !                          step time in static calculations
105 !                          0: no scaling
106 !                          1: scaling (default)
107 !
108       implicit none
109 !
110       character*8 lakonl
111       character*20 loadtype
112 !
113       integer kstep,kinc,noel,npt,jltyp,konl(20),ipompc(*),nstate_,i,
```

```
      &  nodempc(3,*),nmpc,ikmpc(*),ilmpc(*),node,idof,id,iscale,mi(*)
!
       real*8 flux(2),time(2),coords(3),sol,temp,press,vold(0:mi(2),*),
      &  area,co(3,*),coefmpc(*),sti(6,mi(1),*),xstate(nstate_,mi(1),*),
      &  xstateini(nstate_,mi(1),*),dtime
!
       intent(in) sol,kstep,kinc,time,noel,npt,coords,
      &     jltyp,temp,press,loadtype,area,vold,co,lakonl,konl,
      &     ipompc,nodempc,coefmpc,nmpc,ikmpc,ilmpc,mi,sti,
      &     xstateini,xstate,nstate_,dtime
!
       intent(out) flux,iscale
!
       real*8 rconp, rconw, rbasep, rbasew, rAp, rBp, rDp, rAw, rBw, rDw,
      & kp, kg, cpp, cpg, rohp, rohg, ur, pi, np, nr, al, b, betab, fbn,
      & alpha_tw, beta_kp, beta_kw, RCPp, RCPw, FACT, torquep, COF
!     operating conditions
       parameter(b=14)
!     properties of the materials
       parameter(kp=0.3, rohp=1415, cpp=1465)
       parameter(kg=0.3, rohg=1415, cpg=1465)
!     gear geometric properties
       parameter(rbasep=33.829, rAp=34.123, rBp=35.357, rDp=38.204)
       parameter(rbasew=50.743, rAw=51.999, rBw=53.571, rDw=56.411)
       parameter(ur=1.5, al=91.5, alpha_tw=0.391633)
!     read input
       read(loadtype(8:11), *) COF
       read(loadtype(13:15), *) torquep
       read(loadtype(17:20), *) np
!     constant PI
       pi=4.D0*DATAN(1.D0)
       nr=np/ur
       betab=0
       fbn=(1000*torquep/rbasep)/cos(betab)
       FACT=1000*COF*np*fbn/(120*b)
       if (loadtype(5:6).eq.'G1') then
         rconp=1000*(coords(1)**2+coords(2)**2)**0.5
         RCPp=(rconp**2-rbasep**2)**0.5
         beta_kp=(kp*cpp*rohp*pi*np*RCPp)**0.5/((kp*cpp*rohp*pi*np*
      & RCPp)**0.5+(kg*cpg*rohg*pi*nr*(al*sin(alpha_tw)-RCPp))**0.5)
         if (rconp.LT.rAp) then
           flux(1)=0
         elseif ((rconp.LE.rBp).OR.(rconp.GT.rDp)) then
           flux(1)=FACT*0.5*beta_kp*abs(al*sin(alpha_tw)-
      & (1+ur)*RCPp)/RCPp
         else
           flux(1)=FACT*beta_kp*abs(al*sin(alpha_tw)-
      & (1+ur)*RCPp)/RCPp
         endif
       endif
       if (loadtype(5:6).eq.'G2') then
         rconw=1000*((coords(1)-0.0915)**2+coords(2)**2)**0.5
         RCPw=(rconw**2-rbasew**2)**0.5
         beta_kw=(kg*cpg*rohg*pi*nr*RCPw)**0.5/
      & ((kg*cpg*rohg*pi*nr*RCPw)**0.5+
      & (kp*cpp*rohp*pi*np*(al*sin(alpha_tw)-RCPw))**0.5)
         if (rconw.LT.rAw) then
           flux(1)=0
         elseif ((rconw.LE.rBw).OR.(rconw.GT.rDw)) then
           flux(1)=FACT*0.5*beta_kw*abs((al*sin(alpha_tw)-
```

```
174       & RCPw)*ur-RCPw)/RCPw
175          else
176            flux(1)=FACT*beta_kw*abs((al*sin(alpha_tw)-
177       & RCPw)*ur-RCPw)/RCPw
178          endif
179        endif
180        return
181        end
```

Appendix B

Validation code for the Steel Gears

B.1 Step 1 and 2, Rotational approach and Torque in hub pinion CCX code

```
*INCLUDE, INPUT=allinone.inp

*MATERIAL,NAME=steel
*ELASTIC
206.00E+09,0.3

*DENSITY
7830.0E+0

*SOLID SECTION,MATERIAL=steel,ELSET=Eall

*CONTACT PAIR,INTERACTION=SI1,TYPE=SURFACE TO SURFACE
slave,master
*SURFACE INTERACTION,NAME=SI1
*SURFACE BEHAVIOR,PRESSURE-OVERCLOSURE=Linear
1030000.00E+09

*Nset, Nset=RP1F
1070000
*Nset, Nset=RP1M
1070001
*Nset, Nset=RP2F
1070002
*Nset, Nset=RP2M
1070003

*RIGID BODY,NSET=hub_slv,REF NODE=1070000,ROT NODE=1070001
*RIGID BODY,NSET=hub_mst,REF NODE=1070002,ROT NODE=1070003

**********************************************
**********************************************
*STEP
*STATIC
**
*BOUNDARY
1070000,1,1,0
1070000,2,2,0
1070000,3,3,0
1070001,1,1,0
1070001,2,2,0
1070001,3,3,0.005

*BOUNDARY
1070002,1,1,0
1070002,2,2,0
1070002,3,3,0
1070003,1,1,0
1070003,2,2,0
```

```
1070003,3,3,0

  *NODE FILE
U,RF,
  *EL FILE
S,E,
*NODE PRINT, NSET=RP1F
RF
*NODE PRINT, NSET=RP1M
RF
*NODE PRINT, NSET=RP2F
RF
*NODE PRINT, NSET=RP2M
RF
*SECTION PRINT, SURFACE=hub_slv, NAME=SP1
SOF,SOM
*CONTACT FILE
CDIS,CSTR
*END STEP
**********************************************
**********************************************
*STEP
*STATIC
**
*BOUNDARY, OP=NEW
1070000,1,1,0
1070000,2,2,0
1070000,3,3,0
1070001,1,1,0
1070001,2,2,0
1070002,1,1,0
1070002,2,2,0
1070002,3,3,0
1070003,1,1,0
1070003,2,2,0
1070003,3,3,0

*CLOAD,OP=NEW
1070001,3,250.0

  *NODE FILE
U,RF,
  *EL FILE
S,E,
*NODE PRINT, NSET=RP1F
RF
*NODE PRINT, NSET=RP1M
RF
*NODE PRINT, NSET=RP2F
RF
*NODE PRINT, NSET=RP2M
RF
*SECTION PRINT, SURFACE=hub_slv, NAME=SP2
SOF,SOM
*CONTACT FILE
CDIS,CSTR
*END STEP
```

B.2 Step 3, Mesh Stiffness

B.2.1 Python code running CCX

```
import numpy as np
import math
import matplotlib.pyplot as plt
import os
import shutil

t = np.linspace(0.02 , 1,  50)
u = 1.5
theta = np.pi/4.5

#####################################
# Alter the variable m as being the gamma_t, twist, to simulate. each ... twist should be like this:'0.5'.#
# in case of wanting to test only one twist:m=['0.5'] #
#####################################
m=['0.4','0.5','0.6']
mm=0

for ii in range(0,np.size(m)):
 mm+=1
 theta_t = float(m[ii])*np.pi/180

 theta_p = t*theta
 theta_w = -t*theta/u + theta_t

 array_r = np.around(np.array([t,theta_p]), decimals = 12).T
 array_r2 = np.around(np.array([t,theta_w]), decimals = 12).T

 np.savetxt('out_p.inp',array_r,fmt='%9f',delimiter=', ',newline=','+'\n')
 np.savetxt('out_w.inp',array_r2,fmt='%9f',delimiter=', ',newline=','+'\n')

 #Alter here the way to run CCX in your terminal, depends on operating ... system
 #The CCX code has the name _main_combined, alter accordingly
 os.system('ccx212 _main_combined')

 shutil.copy('_main_combined.dat','_main_combined'+m[ii]+'.dat')

 filepath = '_main_combined.dat'
 i = 0
 j = 0
 k = 0
 data = []
 data2 = []
 aux = 1/((0.036*math.cos(20*np.pi/180))**2)
 with open(filepath,'r') as fp:
    line = fp.readline()
    cnt = 1
    while line:
        if not line.strip()and i == 0:
         i += 1
        elif i == 1:
         k += 1
```

```
52            if k == 3:
53             text_file = open(line.rstrip('\n')+".txt", "w")
54            if k == 7:
55             text_file = open(line.rstrip('\n')+".txt", "w")
56             k = 3
57            data.append(line.rstrip('\n')+".txt")
58            j += 1
59            print(line.rstrip('\n')+".txt")
60            i += 1
61           elif not line.strip() and i == 3:
62            i = 1
63            if k == 3:
64             text_file.close()
65             a = np.loadtxt(data[np.size(data)-1])
66             aux3=a[3]*aux/(float(m[ii])*np.pi/180)
67             data2.append(aux3)
68             os.remove(data[np.size(data)-1])
69            if k == 7:
70             text_file.close()
71             a = np.loadtxt(data[np.size(data)-1])
72             aux3=a[3]*aux/(float(m[ii])*np.pi/180)
73             data2.append(aux3)
74             os.remove(data[np.size(data)-1])
75           else:
76            if not line.strip():
77             i += 1
78            else:
79             if k == 3:
80              text_file.write(line)
81             if k == 7:
82              text_file.write(line)
83           line = fp.readline()
84           cnt += 1
85
86  array_x=np.linspace(0.013963*180/np.pi,0.698132*np.size(data2)*3.6/np.pi,\
87  np.size(data2)).T
88  array_y=data2
89  #Plots and save results in a text file as for instance for twist 0.5, ...
        a text file as x05.txt
90  np.savetxt('x'+m[ii]+'.txt',array_x,fmt='%12f',newline='\n')
91  np.savetxt('y'+m[ii]+'.txt',array_y,fmt='%12f',newline='\n')
92  plt.figure(mm)
93  plt.title(r'Mesh Stiffness, $\gamma_t\,=\,$'+m[ii])
94  locals()['x'+chr(int(m[ii][0])+97)+chr(int(m[ii][2])+97)]=\
95  np.loadtxt('x'+m[ii]+'.txt')
96  locals()['y'+chr(int(m[ii][0])+97)+chr(int(m[ii][2])+97)]=\
97  np.loadtxt('y'+m[ii]+'.txt')
98  plt.plot(locals()['x'+chr(int(m[ii][0])+97)+chr(int(m[ii][2])+97)],\
99  locals()['y'+chr(int(m[ii][0])+97)+chr(int(m[ii][2])+97)],marker=".")
100 plt.tight_layout()
101 plt.show(block=False)
102
103 mm+=1
104 plt.figure(mm)
105 locals()['By'+chr(int(m[ii][0])+97)+chr(int(m[ii][2])+97)]=\
106 np.true_divide(locals()['y'+chr(int(m[ii][0])+97)+chr(int(m[ii][2])+97)],\
107 aux/(float(m[ii])*np.pi/180))
108 plt.title(r'Torque, $\gamma_t\,=\,$'+m[ii])
109 plt.plot(locals()['x'+chr(int(m[ii][0])+97)+chr(int(m[ii][2])+97)],\
110 locals()['By'+chr(int(m[ii][0])+97)+chr(int(m[ii][2])+97)],marker=".")
```

```
111  plt.tight_layout()
112  plt.show(block=False)
113
114 #Plots for all the twist tested, just in case there is more than one.
115 #Deletes all the previous plots
116 if np.size(m)>1:
117  plt.close('all')
118  plt.figure(1)
119  for ii in range(0,np.size(m)):
120   plt.plot(locals()['x'+chr(int(m[ii][0])+97)+chr(int(m[ii][2])+97)],\
121   np.true_divide(locals()['y'+chr(int(m[ii][0])+97)+chr(int(m[ii][2])+97)],\
122   1e6),marker=".",label=m[ii])
123  plt.title(r'Mesh Stiffness')
124  plt.legend(loc='best')
125  plt.tight_layout()
126  plt.savefig('meshstiff.eps')
127  plt.figure(2)
128  for ii in range(0,np.size(m)):
129   plt.plot(locals()['x'+chr(int(m[ii][0])+97)+chr(int(m[ii][2])+97)],\
130   locals()['By'+chr(int(m[ii][0])+97)+chr(int(m[ii][2])+97)],marker=".",\
131   label=m[ii])
132  plt.title(r'Torque')
133  plt.legend(loc='best')
134  plt.tight_layout()
135  plt.savefig('torque.eps')
```

B.2.2 Step 3, Mesh Stiffness CCX code

```
1  *INCLUDE, INPUT=allinone.inp
2
3  *MATERIAL,NAME=steel
4  *ELASTIC
5  206.0E+09,0.3
6
7  *DENSITY
8  7830.0E+00
9
10 *SOLID SECTION,MATERIAL=steel,ELSET=Eall
11
12 *CONTACT PAIR,INTERACTION=SI1,TYPE=SURFACE TO SURFACE
13 Sslave,Smaster
14 *SURFACE INTERACTION,NAME=SI1
15 *SURFACE BEHAVIOR,PRESSURE-OVERCLOSURE=Linear
16 1030000.0E+09
17
18 *AMPLITUDE,NAME=Amp0
19 0,0,1,1
20 **
21 *AMPLITUDE,NAME=Graph1
22 *INCLUDE, INPUT=out_p.inp
23
24 *AMPLITUDE,NAME=Graph2
25 *INCLUDE, INPUT=out_w.inp
26
27 *Nset, Nset=RP1F
28 1070000
29 *Nset, Nset=RP1M
```

```
1070001
*Nset, Nset=RP2F
1070002
*Nset, Nset=RP2M
1070003

*RIGID BODY,NSET=hub_slv,REF NODE=1070000,ROT NODE=1070001

*RIGID BODY,NSET=hub_mst,REF NODE=1070002,ROT NODE=1070003

*TIME POINTS,NAME=T1,GENERATE
0.02,1.0,2.0000E-02

**********
**********
*STEP
*STATIC
**
*BOUNDARY
1070000,1,1,0
1070000,2,2,0
1070000,3,3,0
1070001,1,1,0
1070001,2,2,0
1070001,3,3,0.005
**
*BOUNDARY
1070002,1,1,0
1070002,2,2,0
1070002,3,3,0
1070003,1,1,0
1070003,2,2,0
1070003,3,3,0

  *NODE FILE
U,RF,
  *EL FILE
S,E,
*CONTACT FILE
CSTR
*END STEP

**********
**********
*STEP
*STATIC
**
*BOUNDARY,OP=NEW
1070000,1,1,0
1070000,2,2,0
1070000,3,3,0
1070001,1,1,0
1070001,2,2,0
1070002,1,1,0
1070002,2,2,0
1070002,3,3,0
1070003,1,1,0
1070003,2,2,0
1070003,3,3,0

```

```
*CLOAD,OP=NEW
1070001,3,215.513

  *NODE FILE
U,RF,
  *EL FILE
S,E,
*CONTACT FILE
CSTR
*END STEP

**********************************
**********************************
*STEP,NLGEOM,INC=200
*STATIC
2.e-2,1.0
**
*BOUNDARY,AMPLITUDE=graph1,TIME DELAY=0
1070000,1,1,0
1070000,2,2,0
1070000,3,3,0
1070001,1,1,0
1070001,2,2,0
1070001,3,3,1
**
*BOUNDARY,AMPLITUDE=graph2,TIME DELAY=0
1070002,1,1,0
1070002,2,2,0
1070002,3,3,0
1070003,1,1,0
1070003,2,2,0
1070003,3,3,1

  *NODE FILE,TIME POINTS=T1
U,RF,
  *EL FILE,TIME POINTS=T1
S,E,
*NODE PRINT,NSET=hub_mst,TIME POINTS=T1
RF
*NODE PRINT,NSET=hub_slv,TIME POINTS=T1
RF
*NODE PRINT,NSET=RP1M,TIME POINTS=T1
RF
*NODE PRINT,NSET=RP2M,TIME POINTS=T1
RF
*CONTACT FILE,TIME POINTS=T1
CSTR
*END STEP
```

B.3 Contactless Model CCX code

```
1  *INCLUDE, INPUT=allinone.inp
2
3  *MATERIAL,NAME=steel
4  *ELASTIC
5  206.00E+09,0.3
6
7  *DENSITY
8  7830.0E+0
9
10 *SOLID SECTION,MATERIAL=steel,ELSET=Eall
11
12 *NODE
13 1070002, 0.0915, 0, 0
14 1070003, 0.0915, 0, 0
15
16 *Nset, Nset=RP1F
17 1070000
18 *Nset, Nset=RP1M
19 1070001
20
21 *RIGID BODY,NSET=hub_slv,REF NODE=1070000,ROT NODE=1070001
22
23 ************************************************
24 ************************************************
25 *STEP
26 *STATIC
27 **
28 *BOUNDARY, OP=NEW
29 1070000,1,1,0
30 1070000,2,2,0
31 1070000,3,3,0
32 1070001,1,1,0
33 1070001,2,2,0
34 forc1,1,3,0
35 **Forc1 represents contact in two teeth, in the inner and outer most ...
       points of contact D+A
36 **Forc21 is the line with contact A, that is inner most point of ...
       contact, in one tooth
37 **Forc22 is the line with contact D, that is outer most point of ...
       contact, in one tooth
38
39 *CLOAD, OP=NEW
40 1070001,3,340.4254392
41
42   *NODE FILE
43 U,RF,
44   *EL FILE
45 S,E,
46 *NODE PRINT,NSET=hub_slv
47 RF
48 *NODE PRINT,NSET=RP-1_ref_1070000
49 RF
50 *NODE PRINT,NSET=RP-1_rot_1070001
51 RF
52 *SECTION PRINT, SURFACE=hub_slv, NAME=SP2
```

```
53 SOF,SOM
54 *CONTACT FILE
55 CDIS,CSTR
56 *END STEP
```

Appendix C

Validation code for the Polymer Gears

C.1 Step 1 and 2, Rotational approach and Torque in hub pinion CCX code

```
*INCLUDE, INPUT=allinone.inp

*PHYSICAL CONSTANTS, ABSOLUTE ZERO=0, STEFAN BOLTZMANN=5.669E-8
**line below only makes sense for trasient analysis
*INITIAL CONDITIONS,TYPE=TEMPERATURE
Nall,288.15

*MATERIAL,NAME=POM
*ELASTIC
3.10E+09,0.43,273.15
2.90E+09,0.44,293.15
2.60E+09,0.44,313.15
2.40E+09,0.45,333.15
2.10E+09,0.45,353.15
1.80E+09,0.46,373.15
1.50E+09,0.47,393.15
1.10E+09,0.48,413.15
0.50E+09,0.49,433.15

***EXPANSION, ZERO=288.15
**12.200E-05,273.15
**13.400E-05,293.15
**15.000E-05,313.15
**17.000E-05,333.15
**19.000E-05,353.15
**21.500E-05,373.15
**24.100E-05,393.15
**31.300E-05,413.15
**70.200E-05,433.15
*EXPANSION
13.800E-05

*CONDUCTIVITY
3.0000E-01
*SPECIFIC HEAT
1470.0
*DENSITY
1.4100E+03

*SOLID SECTION,MATERIAL=POM,ELSET=Eall

*CONTACT PAIR,INTERACTION=SI1,TYPE=SURFACE TO SURFACE
slave,master
*SURFACE INTERACTION,NAME=SI1
*SURFACE BEHAVIOR,PRESSURE-OVERCLOSURE=Linear
1000.0E+09
*GAP CONDUCTANCE
17563.08,,273
```

```
49
50 *NODE
51 1070000, 0, 0, 0
52 1070001, 0, 0, 0
53 1070002, 0.0915, 0, 0
54 1070003, 0.0915, 0, 0
55
56 *Nset, Nset=RP1F
57 1070000
58 *Nset, Nset=RP1M
59 1070001
60 *Nset, Nset=RP2F
61 1070002
62 *Nset, Nset=RP2M
63 1070003
64
65 *RIGID BODY,NSET=hub_slv,REF NODE=1070000,ROT NODE=1070001
66 *RIGID BODY,NSET=hub_mst,REF NODE=1070002,ROT NODE=1070003
67
68 **********************************************
69 **********************************************
70 *STEP, NLGEOM
71 *UNCOUPLED TEMPERATURE-DISPLACEMENT,STEADY STATE
72
73 *FILM
74 ar, F0, 288.15, 43.6215
75 *DFLUX
76 fl_p, S0NUGEAR1, 1.0
77 *DFLUX
78 fl_w, S0NUGEAR2, 1.0
79
80 *BOUNDARY
81 1070000,1,1,0
82 1070000,2,2,0
83 1070000,3,3,0
84 1070001,1,1,0
85 1070001,2,2,0
86 1070001,3,3,0.005
87
88 *BOUNDARY
89 1070002,1,1,0
90 1070002,2,2,0
91 1070002,3,3,0
92 1070003,1,1,0
93 1070003,2,2,0
94 1070003,3,3,0
95
96 *NODE FILE
97 NT, U, RF
98 *EL FILE
99 HFL, S, E
100 *CONTACT FILE
101 CDIS,CSTR
102 *NODE PRINT, NSET=RP1F
103 RF
104 *NODE PRINT, NSET=RP1M
105 RF
106 *NODE PRINT, NSET=RP2F
107 RF
108 *NODE PRINT, NSET=RP2M
```

```
RF
*SECTION PRINT, SURFACE=hub_slv, NAME=SP1
SOF,SOM
*END STEP

**********************************************
**********************************************
*STEP, NLGEOM
*UNCOUPLED TEMPERATURE-DISPLACEMENT,STEADY STATE

*FILM
ar, F0, 288.15, 43.6215
*DFLUX
fl_p, S0NUGEAR1, 1.0
*DFLUX
fl_w, S0NUGEAR2, 1.0

*BOUNDARY, OP=NEW
1070000,1,1,0
1070000,2,2,0
1070000,3,3,0
1070001,1,1,0
1070001,2,2,0
1070002,1,1,0
1070002,2,2,0
1070002,3,3,0
1070003,1,1,0
1070003,2,2,0
1070003,3,3,0

*CLOAD, OP=NEW
1070001,3,10.0

*NODE FILE
NT, U, RF
*EL FILE
HFL, S, E
*CONTACT FILE
CDIS,CSTR
*EL PRINT, ELSET=toothroot
S
*NODE PRINT, NSET=RP1F
RF
*NODE PRINT, NSET=RP1M
RF
*NODE PRINT, NSET=RP2F
RF
*NODE PRINT, NSET=RP2M
RF
*SECTION PRINT, SURFACE=hub_slv, NAME=SP2
SOF,SOM
*END STEP
```

C.2 Step 3, Mesh Stiffness CCX code

In order for the CCX code to calculate the mesh stiffness of the standard polymer gear it was also needed a Python program to process and store the information from various simulations. The python program described in Appendix B.2.1 was used, but calling a different CCX code that is now described in this Appendix Section.

```
*INCLUDE, INPUT=allinone.inp

*PHYSICAL CONSTANTS, ABSOLUTE ZERO=0, STEFAN BOLTZMANN=5.669E-8
**line below only makes sense for trasient analysis
*INITIAL CONDITIONS,TYPE=TEMPERATURE
Nall,288.15

*MATERIAL,NAME=POM
*ELASTIC
3.10E+09,0.43,273.15
2.90E+09,0.44,293.15
2.60E+09,0.44,313.15
2.40E+09,0.45,333.15
2.10E+09,0.45,353.15
1.80E+09,0.46,373.15
1.50E+09,0.47,393.15
1.10E+09,0.48,413.15
0.50E+09,0.49,433.15

***EXPANSION, ZERO=288.15
**12.200E-05,273.15
**13.400E-05,293.15
**15.000E-05,313.15
**17.000E-05,333.15
**19.000E-05,353.15
**21.500E-05,373.15
**24.100E-05,393.15
**31.300E-05,413.15
**70.200E-05,433.15
*EXPANSION
13.800E-05

*CONDUCTIVITY
3.0000E-01
*SPECIFIC HEAT
1470.0
*DENSITY
1.4100E+03

*SOLID SECTION,MATERIAL=POM,ELSET=Eall

*CONTACT PAIR,INTERACTION=SI1,TYPE=SURFACE TO SURFACE
Sslave1,Smaster1
*SURFACE INTERACTION,NAME=SI1
*SURFACE BEHAVIOR,PRESSURE-OVERCLOSURE=Linear
75.0E+09
*GAP CONDUCTANCE
17563.08,,273

*AMPLITUDE,NAME=Amp0
```

```
0,0,1,1
**
*AMPLITUDE,NAME=Graph1
*INCLUDE, INPUT=out_p.inp

*AMPLITUDE,NAME=Graph2
*INCLUDE, INPUT=out_w.inp

*NODE
1070000, 0, 0, 0
1070001, 0, 0, 0
1070002, 0.0915, 0, 0
1070003, 0.0915, 0, 0

*Nset, Nset=RP1F
1070000
*Nset, Nset=RP1M
1070001
*Nset, Nset=RP2F
1070002
*Nset, Nset=RP2M
1070003

*RIGID BODY,NSET=hub_slv,REF NODE=1070000,ROT NODE=1070001
*RIGID BODY,NSET=hub_mst,REF NODE=1070002,ROT NODE=1070003

*TIME POINTS,NAME=T1,GENERATE
0.02,1.0,2.0000E-02

**********************************************
**********************************************
*STEP, NLGEOM
*UNCOUPLED TEMPERATURE-DISPLACEMENT,STEADY STATE

*FILM
ar, F0, 288.15, 43.6215
*DFLUX
fl_p, S0NUGEAR1, 1.0
*DFLUX
fl_w, S0NUGEAR2, 1.0

*BOUNDARY
1070000,1,1,0
1070000,2,2,0
1070000,3,3,0
1070001,1,1,0
1070001,2,2,0
1070001,3,3,0.005

*BOUNDARY
1070002,1,1,0
1070002,2,2,0
1070002,3,3,0
1070003,1,1,0
1070003,2,2,0
1070003,3,3,0

  *NODE FILE
U,
  *EL FILE
```

```
S,E,
*CONTACT FILE
CSTR
*END STEP

**********************************************
**********************************************
*STEP, NLGEOM
*UNCOUPLED TEMPERATURE-DISPLACEMENT,STEADY STATE

*FILM
ar, F0, 288.15, 43.6215
*DFLUX
fl_p, S0NUGEAR1, 1.0
*DFLUX
fl_w, S0NUGEAR2, 1.0

*BOUNDARY, OP=NEW
1070000,1,1,0
1070000,2,2,0
1070000,3,3,0
1070001,1,1,0
1070001,2,2,0
1070002,1,1,0
1070002,2,2,0
1070002,3,3,0
1070003,1,1,0
1070003,2,2,0
1070003,3,3,0

*CLOAD, OP=NEW
1070001,3,10.0

  *NODE FILE
U,
  *EL FILE
S,E,
*CONTACT FILE
CSTR
*END STEP

**********************************************
**********************************************
*STEP, NLGEOM
*UNCOUPLED TEMPERATURE-DISPLACEMENT,STEADY STATE
2.e-2,1.0

*FILM
ar, F0, 288.15, 43.6215
*DFLUX
fl_p, S0NUGEAR1, 1.0
*DFLUX
fl_w, S0NUGEAR2, 1.0

*BOUNDARY,AMPLITUDE=graph1,TIME DELAY=0
1070000,1,1,0
1070000,2,2,0
1070000,3,3,0
1070001,1,1,0
1070001,2,2,0
```

```
171 1070001,3,3,1
172 **
173 *BOUNDARY,AMPLITUDE=graph2,TIME DELAY=0
174 1070002,1,1,0
175 1070002,2,2,0
176 1070002,3,3,0
177 1070003,1,1,0
178 1070003,2,2,0
179 1070003,3,3,1
180
181 *CLOAD, OP=NEW
182 1070001,3,10.0
183
184   *NODE FILE,TIME POINTS=T1
185 U,
186   *EL FILE,TIME POINTS=T1
187 S,E,
188 *NODE PRINT,NSET=hub_mst,TIME POINTS=T1
189 RF
190 *NODE PRINT,NSET=hub_slv,TIME POINTS=T1
191 RF
192 *NODE PRINT,NSET=RP1M,TIME POINTS=T1
193 RF
194 *NODE PRINT,NSET=RP2M,TIME POINTS=T1
195 RF
196 *CONTACT FILE,TIME POINTS=T1
197 CSTR
198 *END STEP
```

C.3 Thermo-contactless CCX code

```
*INCLUDE, INPUT=allinone.inp

*PHYSICAL CONSTANTS, ABSOLUTE ZERO=0, STEFAN BOLTZMANN=5.669E-8
**line below only makes sense for trasient analysis
*INITIAL CONDITIONS,TYPE=TEMPERATURE
Nall,288.15

*MATERIAL,NAME=POM
*ELASTIC
3.10E+09,0.43,273.15
2.90E+09,0.44,293.15
2.60E+09,0.44,313.15
2.40E+09,0.45,333.15
2.10E+09,0.45,353.15
1.80E+09,0.46,373.15
1.50E+09,0.47,393.15
1.10E+09,0.48,413.15
0.50E+09,0.49,433.15

***EXPANSION, ZERO=288.15
**12.200E-05,273.15
**13.400E-05,293.15
**15.000E-05,313.15
**17.000E-05,333.15
**19.000E-05,353.15
**21.500E-05,373.15
**24.100E-05,393.15
**31.300E-05,413.15
**70.200E-05,433.15
*EXPANSION
13.800E-05

*CONDUCTIVITY
3.0000E-01
*SPECIFIC HEAT
1470.0
*DENSITY
1.4100E+03

*SOLID SECTION,MATERIAL=POM,ELSET=Eall

*NODE
1070000, 0, 0, 0
1070001, 0, 0, 0
1070002, 0.0915, 0, 0
1070003, 0.0915, 0, 0

*Nset, Nset=RP1F
1070000
*Nset, Nset=RP1M
1070001
*Nset, Nset=RP2F
1070002
*Nset, Nset=RP2M
1070003
```

```
56
57 *RIGID BODY,NSET=hub_slv,REF NODE=1070000,ROT NODE=1070001
58
59 **********************************************
60 **********************************************
61 *STEP, NLGEOM
62 *UNCOUPLED TEMPERATURE-DISPLACEMENT,STEADY STATE
63
64 *FILM
65 ar_p, F0, 288.15, 43.6215
66 *DFLUX
67 fl_p, S0NUGEAR1, 1.378
68
69 *BOUNDARY, OP=NEW
70 1070000,1,1,0
71 1070000,2,2,0
72 1070000,3,3,0
73 1070001,1,1,0
74 1070001,2,2,0
75 forc22,1,3,0
76 **forc21,1,3,0
77
78 *CLOAD, OP=NEW
79 1070001,3,13.78
80
81 *NODE FILE
82 NT, U, RF
83 *EL FILE
84 HFL, S, E
85 *CONTACT FILE
86 CDIS,CSTR
87 *NODE PRINT, NSET=RP1F
88 RF
89 *NODE PRINT, NSET=RP1M
90 RF
91 *NODE PRINT, NSET=RP2F
92 RF
93 *NODE PRINT, NSET=RP2M
94 RF
95 *SECTION PRINT, SURFACE=hub_slv, NAME=SP2
96 SOF,SOM
97 *END STEP
```

Appendix D

Hybrid gears

D.1 Thermo-Contactless CCX Code

```
*INCLUDE, INPUT=allinone.inp

*PHYSICAL CONSTANTS, ABSOLUTE ZERO=0, STEFAN BOLTZMANN=5.669E-8

*INITIAL CONDITIONS,TYPE=TEMPERATURE
Nall,288.15

*MATERIAL,NAME=POM
*ELASTIC
3.10E+09,0.43,273.15
2.90E+09,0.44,293.15
2.60E+09,0.44,313.15
2.40E+09,0.45,333.15
2.10E+09,0.45,353.15
1.80E+09,0.46,373.15
1.50E+09,0.47,393.15
1.10E+09,0.48,413.15
0.50E+09,0.49,433.15

***EXPANSION, ZERO=288.15
**12.200E-05,273.15
**13.400E-05,293.15
**15.000E-05,313.15
**17.000E-05,333.15
**19.000E-05,353.15
**21.500E-05,373.15
**24.100E-05,393.15
**31.300E-05,413.15
**70.200E-05,433.15
*EXPANSION
13.800E-05
*CONDUCTIVITY
3.0000E-01
*SPECIFIC HEAT
1470.0
*DENSITY
1.4100E+03

*MATERIAL,NAME=steel
*ELASTIC
206.00E+09,0.30
*EXPANSION, ZERO=288.15
11.700E-06
*CONDUCTIVITY
41.8
*SPECIFIC HEAT
493.0
*DENSITY
7870.0E+0

```

```
51 *MATERIAL,NAME=copper
52 *ELASTIC
53 107.00E+09,0.36
54 *EXPANSION, ZERO=288.15
55 16.400E-06
56 *CONDUCTIVITY
57 401.0
58 *SPECIFIC HEAT
59 385.0
60 *DENSITY
61 8933.0E+0
62
63 *MATERIAL,NAME=aluminum
64 *ELASTIC
65 69.00E+09,0.33
66 *EXPANSION, ZERO=288.15
67 22.500E-06
68 *CONDUCTIVITY
69 237.0
70 *SPECIFIC HEAT
71 903.0
72 *DENSITY
73 2702.0E+0
74
75 ***SOLID SECTION,MATERIAL=aluminum,ELSET=inserto_slv
76 *INCLUDE, INPUT=solid.inp
77 *SOLID SECTION,MATERIAL=POM,ELSET=pinhao
78
79 *CONTACT PAIR,INTERACTION=SI3,TYPE=SURFACE TO SURFACE
80 slave1_16ins,master1_16ins
81 *SURFACE INTERACTION,NAME=SI3
82 *SURFACE BEHAVIOR,PRESSURE-OVERCLOSURE=Tied
83 *INCLUDE, INPUT=penalty.inp
84 **11000.00E+09
85 **4738.00E+09
86 *FRICTION
87 0.2,5000.
88 *GAP CONDUCTANCE
89 17563.08,,273
90
91 *NODE
92 1070000, 0, 0, 0
93 1070001, 0, 0, 0
94 1070002, 0.0915, 0, 0
95 1070003, 0.0915, 0, 0
96
97 *Nset, Nset=RP-1_ref_1070000
98 1070000
99 *Nset, Nset=RP-1_rot_1070001
100 1070001
101
102 *RIGID BODY,NSET=hub_slv,REF NODE=1070000,ROT NODE=1070001
103
104 ************************************************
105 ************************************************
106
107 ***STEP, NLGEOM
108 ***UNCOUPLED TEMPERATURE-DISPLACEMENT,STEADY STATE
109 **
110 ***FILM
```

```
**ar_p, F0, 288.15, 43.6215
***FILM
**ar_ins, F0, 288.15, 43.6215
***DFLUX
**fl_p, S0NUGEAR1, 1.
**
***BOUNDARY
**1070000,1,1,0
**1070000,2,2,0
**1070000,3,3,0
**1070001,1,1,0
**1070001,2,2,0
**1070001,3,3,0.005
**forc1,1,1,0
**forc1,2,2,0
**forc1,3,3,0
**
**  *NODE FILE
**NT, U, RF
**  *EL FILE
**HFL, S, E
***NODE PRINT,NSET=RP-1_ref_1070000
**RF
***NODE PRINT,NSET=RP-1_rot_1070001
**RF
***SECTION PRINT, SURFACE=hub_slv, NAME=SP1
**SOF,SOM
***CONTACT FILE
**CSTR
***END STEP

**********************************************
**********************************************
*STEP, NLGEOM
*UNCOUPLED TEMPERATURE-DISPLACEMENT,STEADY STATE

*FILM
ar_p, F0, 288.15, 43.6215
*FILM
ar_ins, F0, 288.15, 43.6215
*DFLUX
fl_p, S0NUGEAR1, 1.

*BOUNDARY, OP=NEW
1070000,1,1,0
1070000,2,2,0
1070000,3,3,0
1070001,1,1,0
1070001,2,2,0
forc22,1,3,0

*CLOAD
*INCLUDE, INPUT=cload.inp

  *NODE FILE
NT, U, RF
  *EL FILE
HFL, S, E
*NODE PRINT,NSET=RP-1_ref_1070000
RF
```

```
*NODE PRINT,NSET=RP-1_rot_1070001
RF
*SECTION PRINT, SURFACE=hub_slv, NAME=SP2
SOF,SOM
*CONTACT FILE
CSTR
*END STEP
```

D.2 Influence of geometric variables

```
THICKNESS <- RADIUS <- RING <- PLATE <- c(-1,+1)
design <- expand.grid(THICKNESS=THICKNESS, RADIUS=RADIUS, RING=RING, ...
    PLATE=PLATE)
THICKNESS <- design$THICKNESS
RADIUS <- design$RADIUS
RING <- design$RING
PLATE <- design$PLATE

#Tooth root stress 10 Nm
Sd <- c(7.0,4.3,6.0,4.5,2.1,2.0,5.4,2.1,4.1,4.0,2.7,4.1,2.0,0.8,4.1,1.9)
#Tooth root stress simple plate torque 7.5 Nm
Sd75 <- c(6.7,3.8,5.9,3.9,2.1,2.3,5.1,2.7)
#Tooth root stress T plate torque 7.5 Nm
Sd75T <- c(4.1,3.9,3.3,3.7,2.2,1.0,4.2,1.7)
#Tooth root stress T plate torque 10.75 Nm
Sd1075 <- c(6.7,3.8,5.9,3.9,2.1,2.3,5.1,2.7)
#Tooth root stress T plate torque 10.75 Nm
Sd1075T <- c(4.1,3.9,3.3,3.7,2.2,1.0,4.2,1.7)

stress2 <- lm(Sd ~ THICKNESS*RADIUS*RING*PLATE)

library(pid)
dev.off()
cex.axis=1.5
cex.label=1.5
cex.main=1.5
paretoPlot(stress2,main='Tooth root stress, torque=10Nm')
```

D.3 Influence of geometric variables, simple and T plates

```
THICKNESS <- RADIUS <- RING <- c(-1,+1)
design <- expand.grid(THICKNESS=THICKNESS, RADIUS=RADIUS, RING=RING)
THICKNESS <- design$THICKNESS
RADIUS <- design$RADIUS
RING <- design$RING

#Tooth root stress simple plate torque 10 Nm
Sd <- c(7.0,4.3,6.0,4.5,2.1,2.0,5.4,2.1)
#Tooth root stress T plate torque 10 Nm
SdT <- c(4.1,4.0,2.7,4.1,2.0,0.8,4.1,1.9)
#Tooth root stress simple plate torque 7.5 Nm
Sd75 <- c(6.7,3.8,5.9,3.9,2.1,2.3,5.1,2.7)
```

```
#Tooth root stress T plate torque 7.5 Nm
Sd75T <- c(4.1,3.9,3.3,3.7,2.2,1.0,4.2,1.7)
#Tooth root stress T plate torque 10.75 Nm
Sd1075 <- c(6.7,3.8,5.9,3.9,2.1,2.3,5.1,2.7)
#Tooth root stress T plate torque 10.75 Nm
Sd1075T <- c(4.1,3.9,3.3,3.7,2.2,1.0,4.2,1.7)

stress2 <- lm(Sd ¬ THICKNESS*RADIUS*RING)
stress2T <- lm(SdT ¬ THICKNESS*RADIUS*RING)

library(pid)
dev.off()

paretoPlot(stress2,main='Tooth root stress, torque=10Nm, simple plate')
paretoPlot(stress2T,main='Tooth root stress, torque=10Nm, T plate')
```